17.9.69

UNIVERSITY OF ADELAIDE

PHYSICS DEPARTMENT

REFRACTION IN THE LOWER ATMOSPHERE

by

Malcolm Stewart Brown, B.Sc.

(WEAPONS RESEARCH ESTABLISHMENT, SALISBURY, S.A.)

THESIS SUBMITTED FOR THE

M.Sc. DEGREE

1969

TABLE OF CONTENTS

LIST OF APPENDICES

S U M M A R Y

A years survey of atmospheric refraction over a fixed sightline at Woomera in South Australia has been conducted. The results show that there is little seasonal variation in the diurnal refraction cycle.

The refraction angle on a sightline may be calculated providing the vertical refractive index gradient is known. Two methods of determining the gradient are tested. The gradient is measured directly with an optical refractometer and indirectly by measuring the air temperature gradient. Measured refraction angles are compared with the refraction predicted from the gradient measurements and the relative merits of the two methods of measuring the gradients are discussed.

S T A T E M E N T

I herewith state that this thesis does not contain any material which has been accepted for the award of any other degree or diploma in any University and that, to the best of my knowledge and belief, the thesis contains no material previously published or written by another person, except when due reference is made in the text of the thesis.

1. INTRODUCTION

This thesis presents the results of an investigation into optical refraction in the lower atmosphere.

Atmospheric refraction occurs when light passes through air which has a density gradient normal to the direction of propagation. In the earth's atmosphere under normal conditions the air density decreases with height and causes light to be deviated towards the earth's surface. This direction of bending is defined as positive refraction and causes distant objects to appear higher above ground than they really are. Under conditions of high insolation when the lowest layers of the atmosphere become heated, negative refraction angles are measured.

The first part of this thesis describes the construction of a refraction monitor and a year's survey of atmospheric refraction angles on a fixed sightline at Woomera in South Australia. From these measurements the diurnal variation in the refraction angle throughout the year was derived.

The second part of the work deals with the construction and use of thermoelectric equipment to measure the air temperature gradient. From the results obtained, the refraction angle on selected sightlines was calculated and the correlation between measured and calculated refraction angles is discussed.

The final part deals with the construction of a refractometer which was used to measure directly the refractive index gradient.

Measurements made with the instrument are used to calculate the refraction angle by two methods.

2. THE CAUSES OF REFRACTION IN THE EARTH'S ATMOSPHERE

For the purpose of this discussion we will assume that a beam of electromagnetic radiation propagates in a straight line in a homogeneous medium, and any effects due to the particle nature of the radiation may be ignored. In particular we are interested in the visible region of the spectrum and the manner in which light travels through the earth's atmosphere.

2.1 Variation of Air Density With Height

The atmosphere is a mixture of gases with a vertical gradient of density and pressure* approximately as shown in figure 1.

The density ρ is related to the pressure P and absolute air temperature T by:

$$\rho = c\frac{P}{T}$$

where c is constant.

Variations in the air temperature have the effect of modifying the steady decrease in density, especially in the lower atmosphere.

In the lowest 5,000 to 10,000 feet of the earth's atmosphere there is a basic adiabatic temperature gradient of $-.003^{\circ}$C/foot, and superimposed on it a diurnal variation caused by heat transfer to and from the earth's surface.

* See for example reference 1.

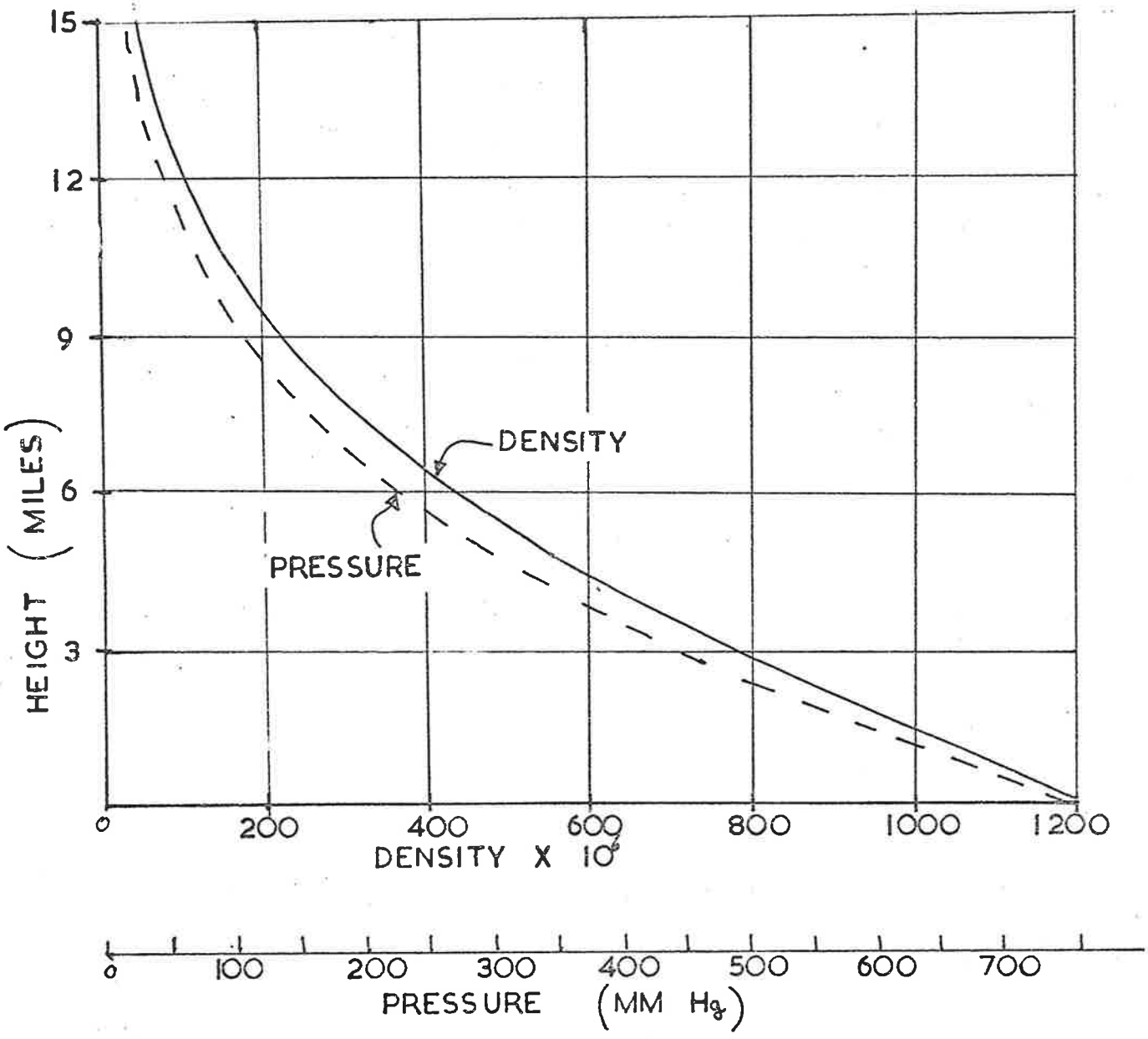

FIGURE 1. DENSITY AND PRESSURE OF THE EARTH'S ATMOSPHERE

The general pattern of the diurnal temperature cycle (2) is outlined below.

Figure (2) shows a typical set of temperature measurements which illustrate the cycle. During the day, the earth's surface is heated by solar radiation and the lowest layers of the atmosphere become warmer. Near the ground, the temperature is higher and the temperature gradient becomes very large (known as super adiabatic). Gradients as high as $-0.5^{\circ}C$/foot have been measured 1 foot above the ground. Air near the ground becomes less dense than the air above it and the air mass becomes unstable. Convective plumes of warm air rise from near the ground and are replaced by a steady downward flow of cooler air (3).

As the sun goes down in the evening, the ground loses heat by radiation and its temperature falls below the air temperature. The air is then cooled from the bottom, and near the ground the temperature increases with height. By sunrise this stable condition may have spread to a height of a thousand feet or more. In the morning as the sun rises, the ground is heated once more. Shortly after dawn, the air near the ground is warmed and convection processes destroy the stable night time conditions. As the day progresses, a decrease of temperature with height is

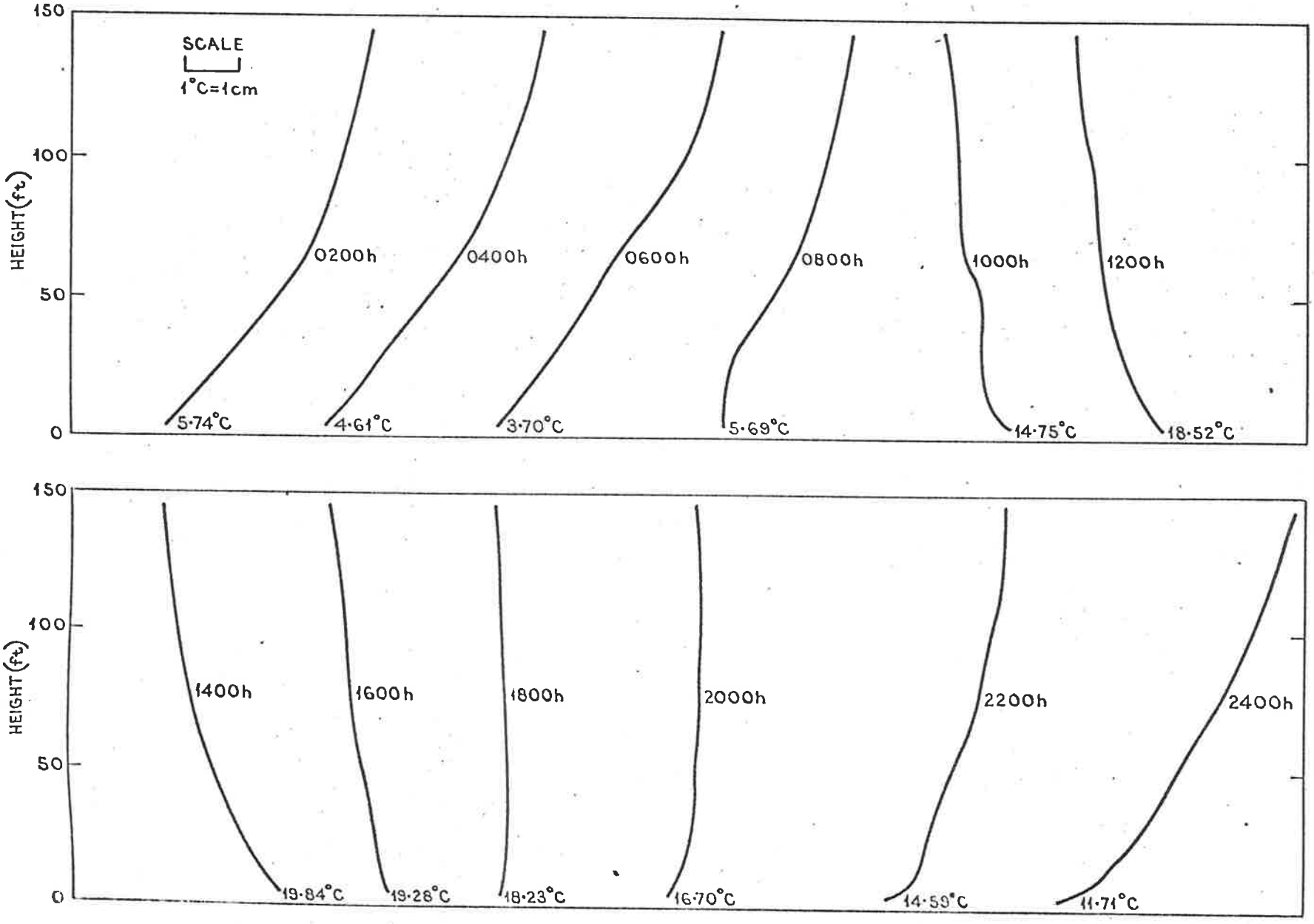

FIGURE 2 TEMPERATURE GRADIENTS FOR A 24 HOUR PERIOD AT WOOMERA - 17.8.67

established, which continues throughout the day.

The diurnal temperature gradient cycle has the effect of reducing the density gradient during the day, and increasing it at night. The refractive index of the air n is related to its density by (4):

$$n - 1 = K.\rho$$

$(n - 1)$ is often referred to as the refractivity N and is proportional to the density.

2.2 Curvature of the Ray Path

Referring to figure 3, Snell's law tells us that when the ray travelling to the observer at P crosses the radius $(R + h_1)$

$$n_1 \cos \alpha_1 = n_2 \cos \beta_1 \qquad (1)$$

where α_1 is the incident elevation angle and

β_1 is the refracted angle of the ray

R is the radius of the earth

h is the height above the earth's surface

also, in the triangle formed by the radii

$(R + h_1)$, $(R + h_2)$, and SQ,

$$(R + h_2) \cos\alpha_2 = (R + h_1) \cos\beta_1$$

$$\text{or } \cos\beta_1 = \frac{(R + h_2)}{(R + h_1)} \cos\alpha_2$$

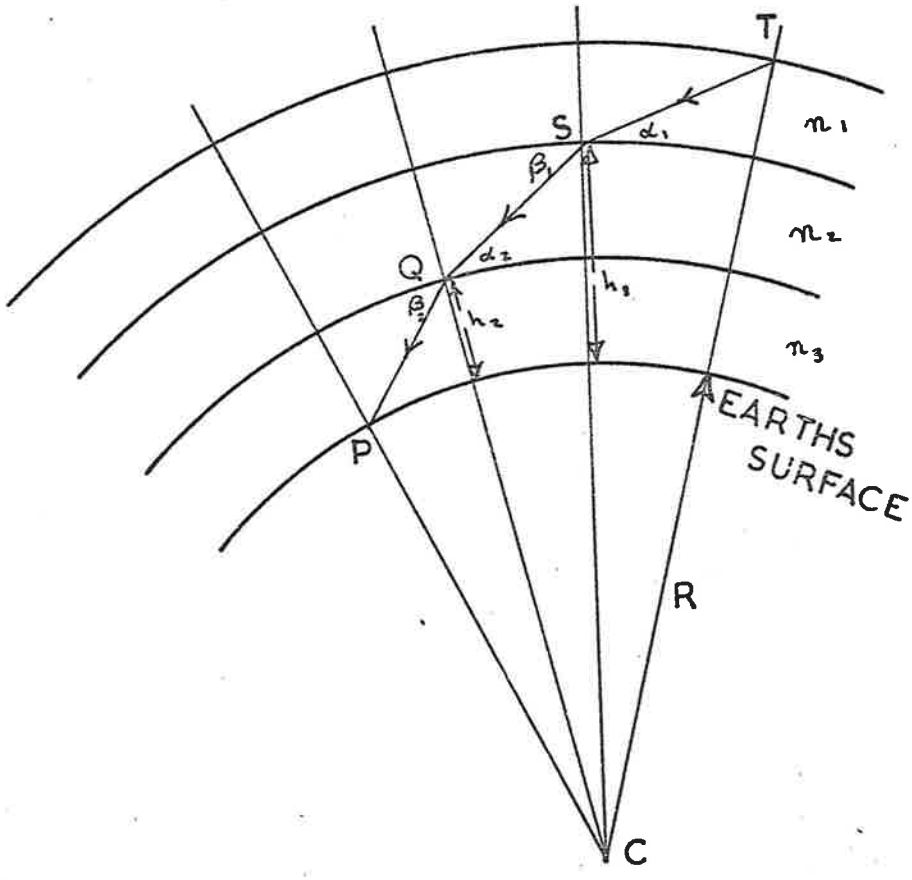
T
S
Q
P
C
R
α_1
β_1
α_2
β_2
h_2
h_3
n_1
n_2
n_3
EARTHS
SURFACE

FIGURE 3.

substituting in equation (1)

$$n_1 \cos\alpha_1 = n_2 \cos\alpha_2 \frac{(R + h_2)}{(R + h_1)}$$

$$\therefore (R + h_1)n_1 \cos\alpha_1 = (R + h_2)n_2 \cos\alpha_2$$

or in general

$$(R + h)\, n \cos\alpha = \text{CONSTANT} \qquad (2)$$

As the ray of light passes through the atmosphere, it follows a curved path as in figure 4.

The curvature may be expressed in terms of the change in direction (ψ) of the tangent to the ray.

$\psi = \theta - \alpha$

θ is the angle at the centre

α is the angle at which the ray crosses the surfaces of equal refractive index.

Then the curvature of the ray is defined by

$$\frac{1}{\sigma} = \frac{d\psi}{ds}$$

S is the distance along the ray path.

In figure 4:

$$ds = d\ell \sec\alpha$$

$$\text{so } \frac{1}{\sigma} = \frac{d(\theta - \alpha)}{d\ell \sec\alpha}$$

also from figure 4:

$$d\theta = \frac{d\ell}{R + h}$$

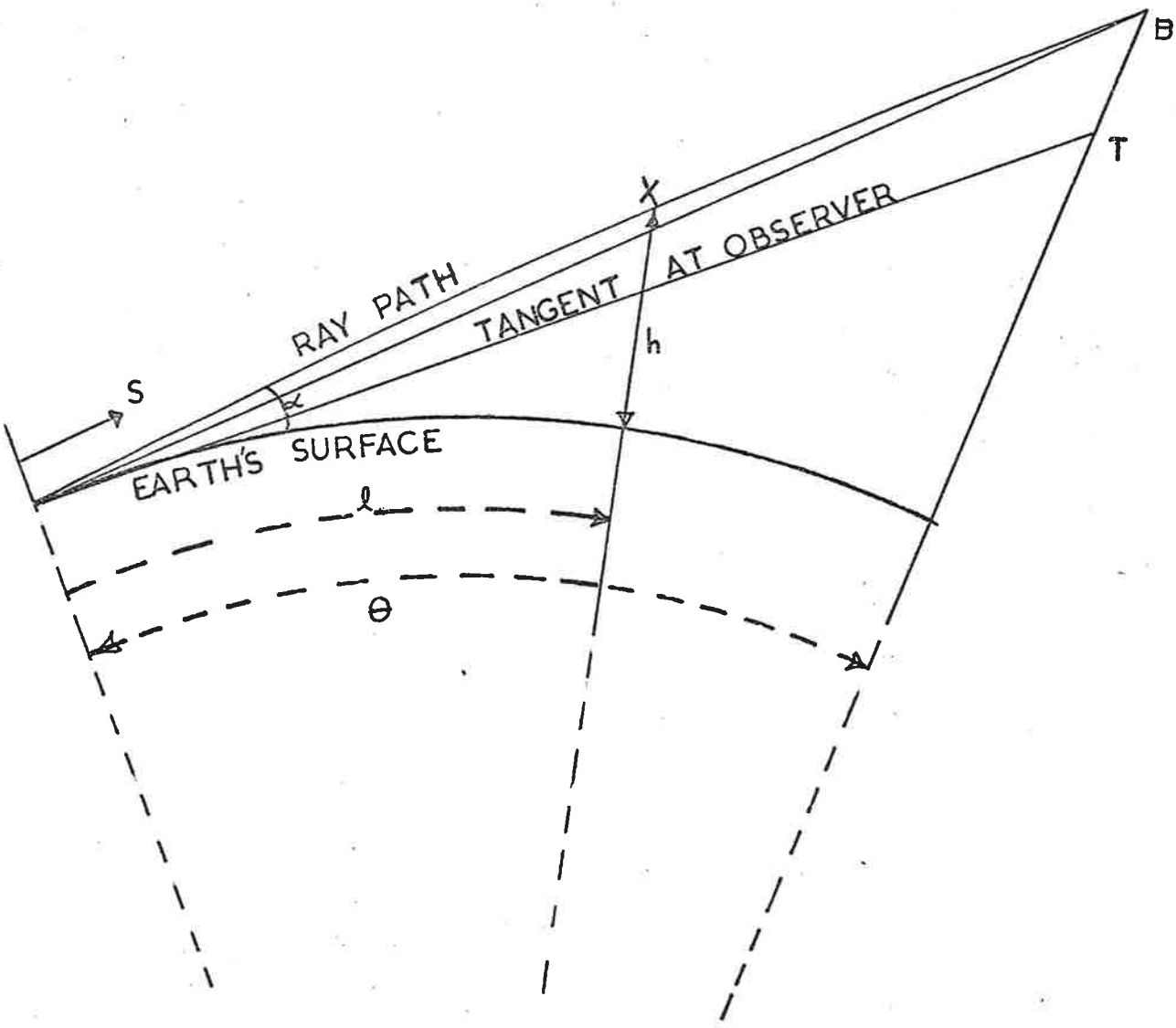

FIGURE 4.

$$\therefore \frac{1}{\sigma} = \frac{\cos\alpha}{R+h} - \frac{d\alpha}{dl}\cos\alpha$$

$$= \frac{\cos\alpha}{R+h} - \frac{d\alpha}{dh}\sin\alpha \qquad (3)$$

Now from equation 2 by taking logs and differentiating

$$d\alpha = \frac{dh\ \cot\alpha}{R+h} + \frac{dn\ \cot\alpha}{n}$$

substituting $d\alpha$ in equation 3 we have

$$\frac{1}{\sigma} = \frac{-1}{n}\frac{dn}{dh}\cos\alpha \qquad (4)$$

Here σ is the curvature radius. In terms of the angular deviation of the ray as it travels through the atmosphere, equation 4 becomes:

$$F = \frac{-2.06 \times 10^5}{n}\cos\alpha\ \frac{dn}{dh} \quad \text{seconds/foot}$$

dn/dh is the vertical change in refractive index per foot. Thus the curvature of the ray is proportional to the refractive index gradient of the atmosphere, and providing this is known the refraction angle on the sightline may be found.

The curvature of the sightline may be expressed in terms of measurable meteorological quantities such as the air temperature T and pressure P and in this form it becomes*:

$$\frac{1}{\sigma} = \frac{K\cos\alpha}{Cn}\ \frac{P}{T^2}\left(\frac{g}{c} + \frac{dT}{dh}\right)$$

where g is the acceleration due to gravity.

* See for example ref. 5.

On substituting an average value for the refractive index of air of 1.000292 and numerical values for the constants c, g and K, the curvature expression reduces to:

$$F = \frac{16.28\ P \cos\alpha}{T^2} \left(.0104 + \frac{dT}{dh}\right) \text{ seconds/foot} \quad (5)$$

where P is measured in millibars and T is the absolute air temperature.

In this form the curvature expression may be used to calculate the refraction angle, providing either the temperature gradient is approximately constant along the ray (i.e. a ray at zero elevation angle over level ground) or a satisfactory average value for the gradient is known. If the temperature gradient varies over the length of the sightline, a more accurate approach is to divide the atmosphere up into layers of approximately equal temperature gradient and perform the calculation for each layer in turn (6). This method has the disadvantage that the temperature/height graphs must be plotted before any computation can be performed, and it does not lend itself to being performed on a computer.

A more flexible method of computing the total curvature by integrating along the length of the sightline has been used by Angus-Leppan (7). He showed that the refraction angle is given by:

$$E = \frac{1}{X} \int_0^X (X - x)\, F(x)\, dx \qquad (6)$$

where X is the length of the sightline and x is the distance along the sightline where the curvature of the ray is:

$$F = A + B \frac{dT}{dZ}$$

The geometry of the sightline is given in figure 5.

The ground profile under the sightline is approximated as a straight line relation where the height of the sightline above ground Z is related to the distance from the observer x by:

$$Z = Z_1 + mx$$

$$\text{thus} \quad dZ = m\,dx$$

On performing the integration in equation 6 the refraction angle E becomes:

$$E = \frac{AX}{2} + \frac{B}{m}(T_2 - T_1) - \frac{BT_2}{m} + \frac{B}{mX}\int_0^X T\,dx \qquad (7)$$

where Z_1 and Z_2 are the heights of the sightline above ground at the observer and target ends of the sightline respectively, and T_1 and T_2 are the corresponsing temperatures.

Now at the target

$$Z_2 = Z_1 + mX$$

$$\text{or} \quad \frac{1}{m} = \frac{X}{(Z_2 - Z_1)} \qquad (8)$$

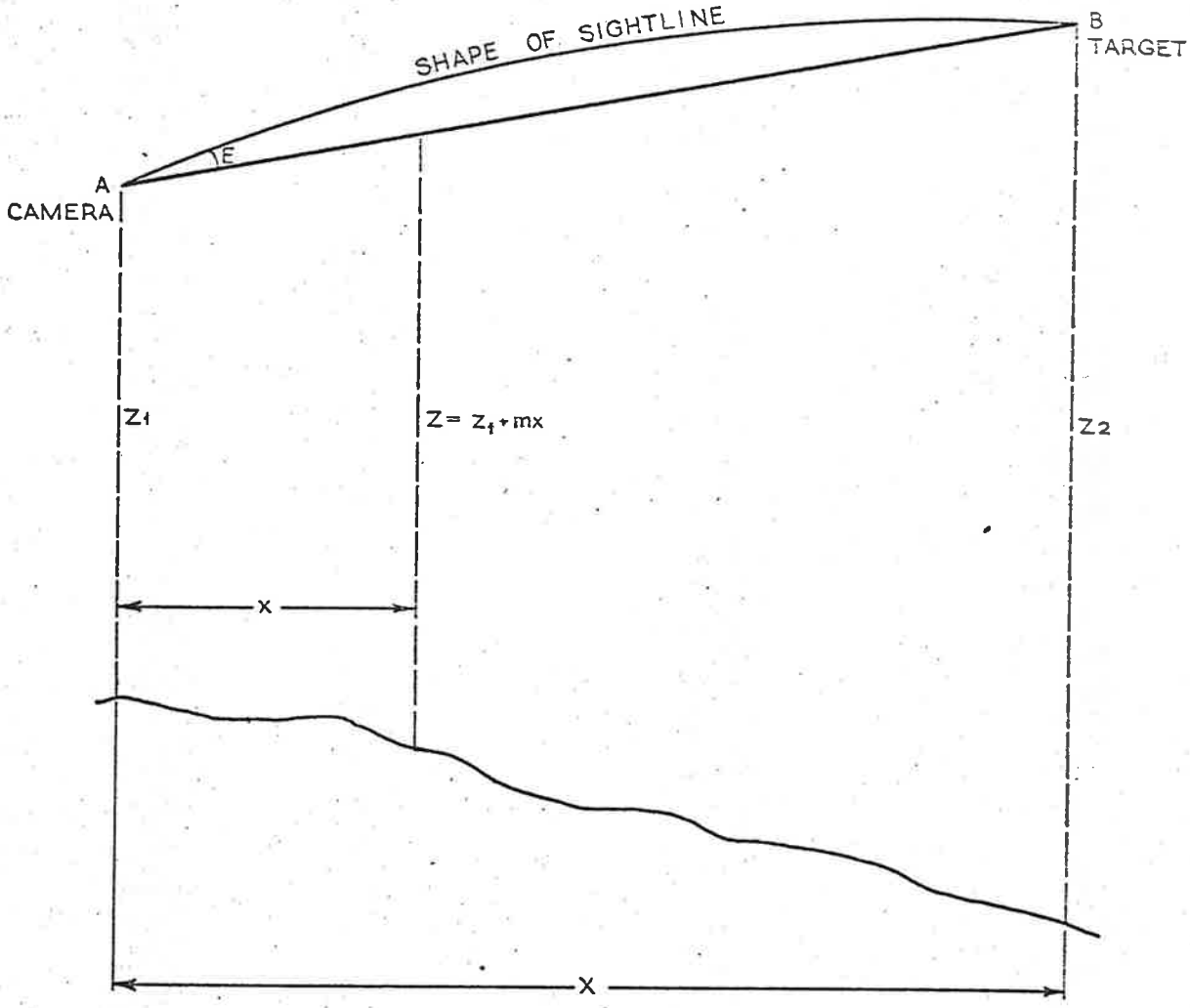

FIGURE 5. GEOMETRY OF THE SIGHTLINE

On substituting equations (5) and (8) in (7) we have

$$E = \frac{16.28PX}{T^2}\left(\frac{.0104}{2} + \frac{1}{(Z_2 - Z_1)^2}\int_{Z_1}^{Z_2} TdZ\right) \qquad (9)$$

The integration is performed with the zero of temperatures at Z_1. Thus during the day when the temperature decreases with height, the area is negative, and gives a negative refraction angle if it is numerically larger than $(.0052(Z_2 - Z_1)^2)$. At night, when the temperature generally increases with height, the area is positive and produces larger positive values of the refraction angle.

2.3 Calculation of Refraction by a Ray Trace

The deviation of a sightline due to atmospheric refraction may also be calculated by a ray trace technique (8). In this case the atmosphere is considered as a series of horizontal layers of air, and the path of the sightline through them is traced by applying Snell's law when the layer boundaries are crossed. Figure 6 shows the geometry of a typical sightline. A ray of light is traced from A, through the atmosphere and crosses the boundaries of refractive index layers at B and C.

At B the ray crosses from refractive index n_1 to refractive index n_2 and by Snell's law:

$$n_1 \sin i_1 = n_2 \sin i_2$$

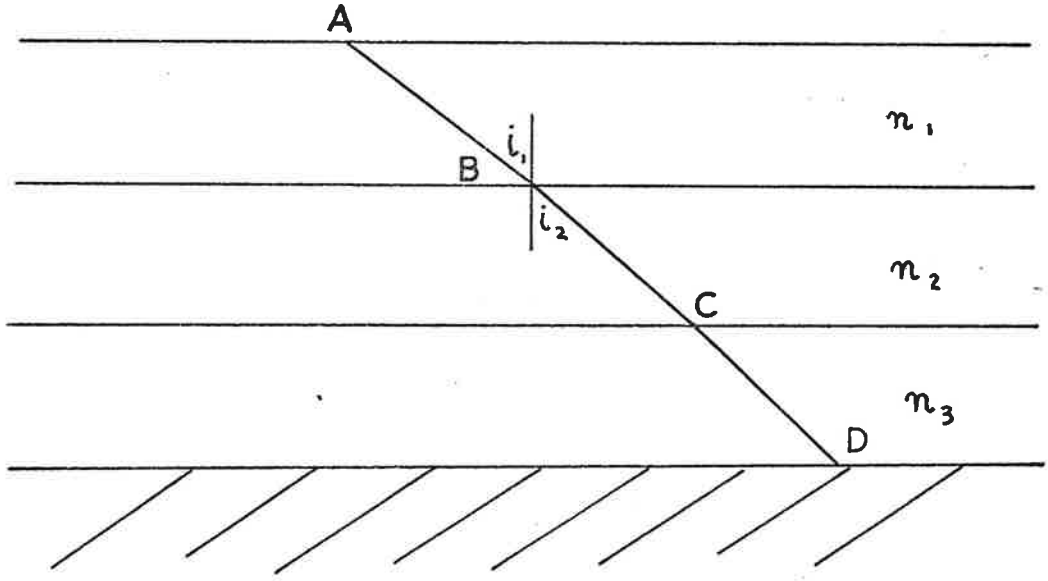

FIGURE 6. RAY TRACE GEOMETRY

If the change in refractive index is small we may put:

$$n_2 = (n_1 + dn) \quad \text{and} \quad i_2 = (i_1 + di)$$

Then:

$$n_1 \sin i = (n_1 + dn) \sin (i_1 + di)$$

Expanding:

$$\sin(i + di)$$

We have:

$$n \sin i = (n + dn)(\sin i + \cos i \, di)$$

which reduces to:

$$n \cos i \, di + dn \sin i + dn \cos i \, di = 0$$

If the atmospheric layers are thin and di and dn are small, any products of the two will be so small that they may be ignored without error.

Thus:

$$n \cos i \, di + dn \sin i = 0$$

$$\text{or } di = \frac{-dn}{n} \tan i \qquad (10)$$

In fact the refractive index of even a thin layer of the atmosphere will vary continuously so that the deviation of the sightline takes place throughout the layer. Integration of equation (10) between the height limits of the layer gives the total refraction which has taken place within the layer. Tan i is assumed to remain constant for each layer and is regarded as a constant in the integration.

Thus:

$$\Delta E = \tan i \, (\log_e n_1 - \log_e n_2)$$

ΔE is now the angle of refraction in radians and may be calculated in seconds of arc by multiplying the right hand side by a factor.

Thus the refraction angle due to the atmospheric layer is:

$$\Delta E = \tan i \, (\log_e n_1 - \log_e n_2) \times 206264.81$$

It is now a simple matter to trace the path of the ray through the atmosphere from the observed elevation angle at the observer, continuously modifying the angle (i) as each layer is crossed. The refraction angle is by definition half the total curvature of the ray.

The method may be extended to spherical layers by setting up a cartesian co-ordinate system and computing the position where each spherical layer boundary occurs. However, for the short ranges considered in this investigation, local topography masked the curvature of the earth and a "flat earth" treatment was considered of sufficient accuracy.

2.3.1 Limitations of the Ray Trace Treatment

A ray trace is based on Snell's law which is derived by considering the path of a monochromatic plane polarised wave as it crosses the boundary between two media of different dielectric constant. (See for example reference 9 p. 430).

In the atmosphere, or any media whose refractive index varies continuously, the treatment used is to divide the ray path up so that the ray is considered to cross a series of discontinuities in the media. Then by an integration process as described in section 2.3 the path of the ray between the discontinuities is considered.

At very low or zero elevation angles this assumption leads to error, as the ray path may lie along a surface of equal refractive index and the ray trace treatment therefore gives a zero answer (10). However, if the wave front is considered, a deviation takes place when the ray travels along a surface of equal refractive index. This is because there is a change in refractive index along the wave front. Thus different parts of the wave front propagate at different velocities and the wave front undergoes an angular rotation, i.e. the direction of propagation is altered.

To test the range of elevation angles over which the ray trace was valid, a series of ray traces at increasingly small elevation angles was performed through a model atmosphere. Only the lowest 10^{o} of elevation angle were considered and a constant range of 10,000 feet was used. A refractive index gradient

of $-6 \times 10^{-6}/_{1}000$ feet was chosen as being approximately an adiabatic gradient. Layer increments were 5×10^{-8} which amounted to a thickness of 8.3 feet.

The results were compared with the angular deviation of the wave front computed by considering the optical path lengths of two points a known distance apart on a plane wave front which advanced 10,000 feet through the same atmosphere as considered for the ray trace.

In figure 7 the portion of the wave front AB (separation Δx) advances 10,000 feet to A' B' in a medium with a refractive index gradient $\frac{dn}{dh}$.

Then the path length of BB' is (10,000 x n) and the path length of AA' is 10,000 $(n - \frac{hdn}{dh})$. The difference in path length is 10,000 h. $\frac{dn}{dh}$, where n is the refractive index half way along the ray path at PB, and h is the vertical distance of PA above PB ($h = \Delta x \cos\alpha$).

The angle of rotation of the wave front is then:

$$\tan^{-1} \frac{(10,000h. \frac{dn}{dh})}{\Delta x}$$

or substituting for h:

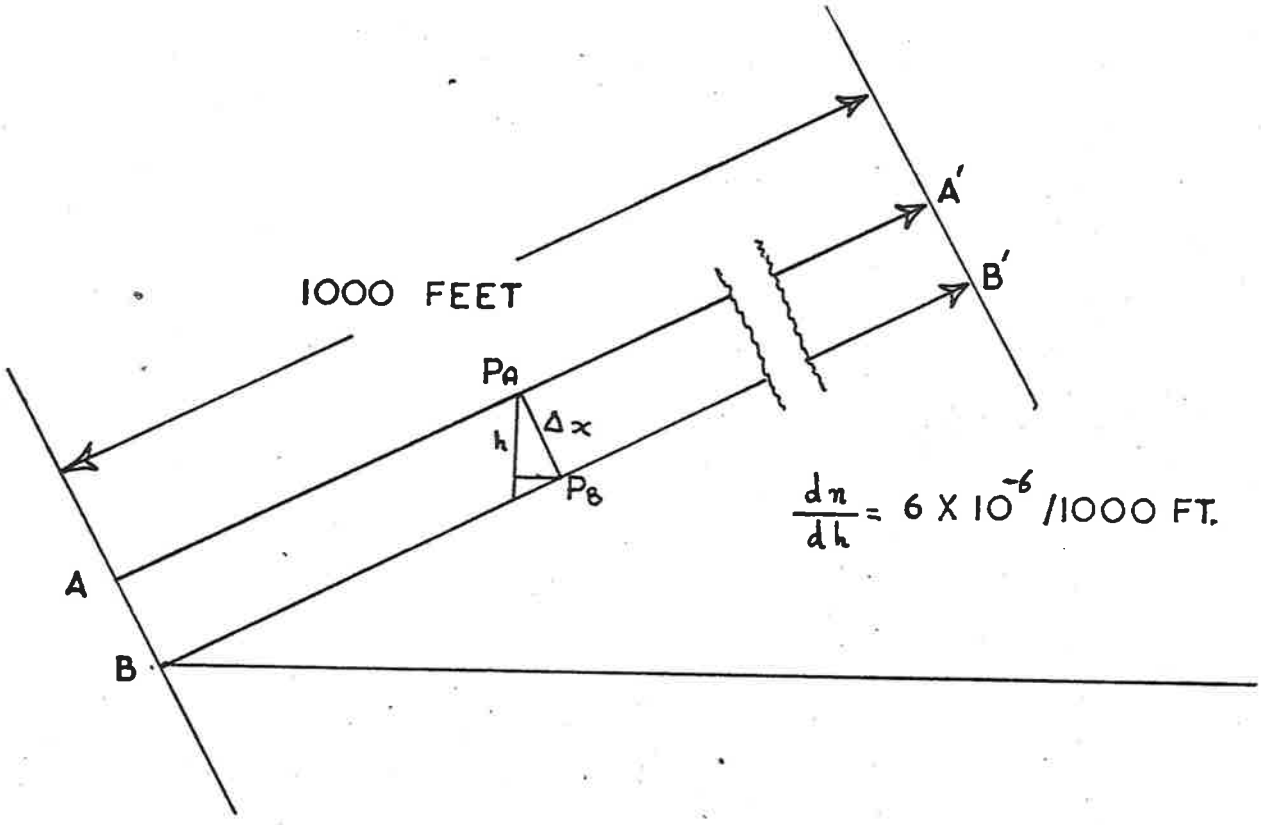

FIGURE 7. CALCULATION OF ANGULAR DEVIATION OF A WAVE FRONT

$$E = \tan^{-1}\left(10{,}000\frac{dn}{dh}\cos\alpha\right)$$

when $\frac{dn}{dh} = -6 \times 10^{-6}/1{,}000$ feet

and E is expressed in seconds of arc

$$E = 12.4\cos\alpha$$

Figure 8 shows the results obtained by the two methods. The ray trace gave good agreement down to the point at which the vertical increase in height of the sightline was the same as the layer thickness chosen for the computation. In the example shown, this occurred at an elevation angle of $.05^{\circ}$. Below this angle the ray trace is indeterminate unless smaller refractive index increments are used.

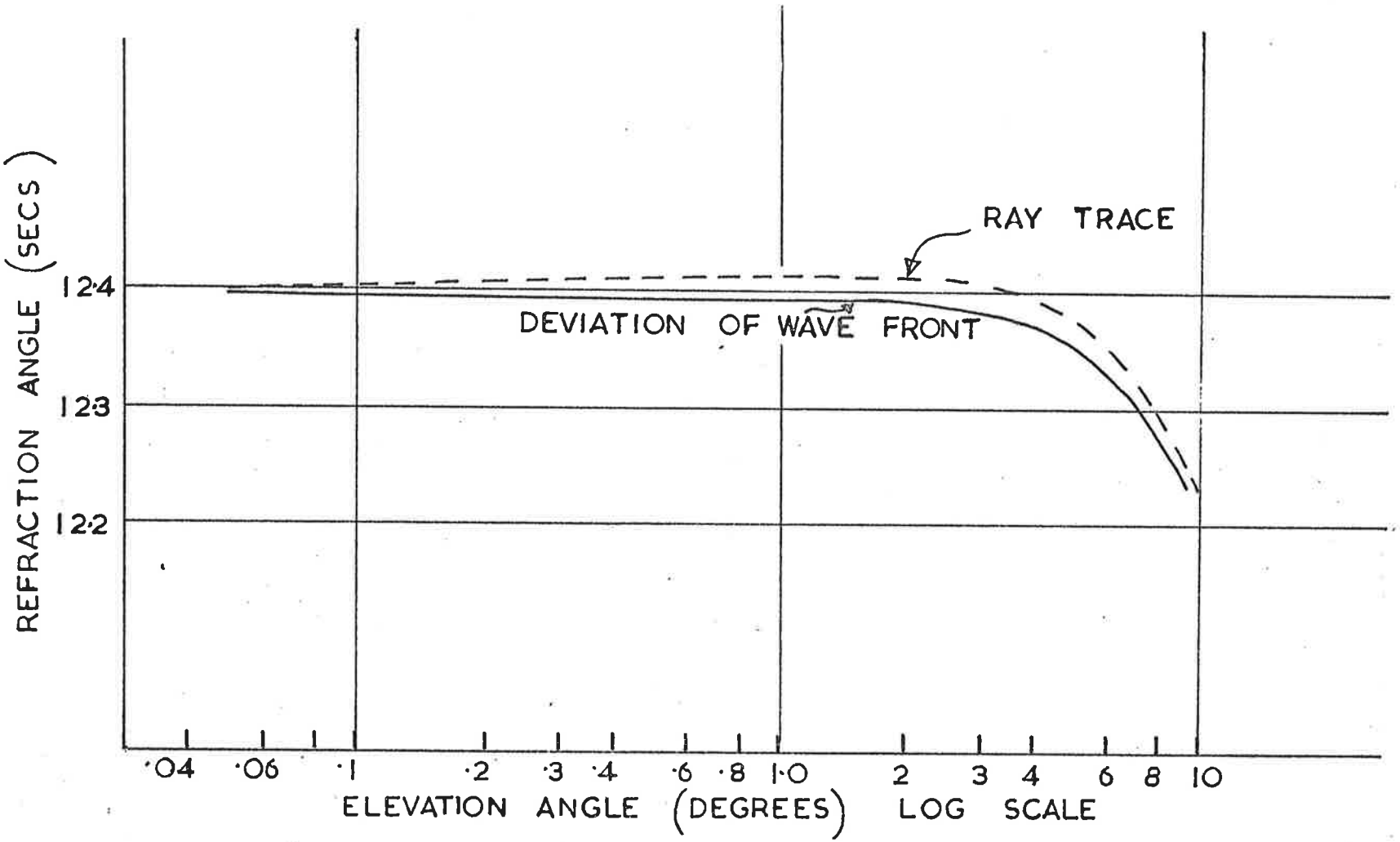

FIGURE 8. AGREEMENT BETWEEN RAY TRACE CALCULATION AND WAVE FRONT CALCULATION

3. MEASUREMENT OF REFRACTION

The diurnal variation of refraction has been measured on several occasions. Angus-Leppan (7) has reported on measurements made in South Africa, and Little (11) has made similar measurements in South Australia. Their results indicated that for observations made on sightlines near the ground refraction was at a minimum in the two hours after midday.

Unfortunately the question of seasonal variations in refraction was not considered as the methods they used to measure refraction, by taking reciprocal readings with survey theodolites, did not lend themselves to a long series of readings.

In order to measure seasonal trends in refraction, measurements taken over a minimum of 12 months would be necessary. A long series of measurements such as this are best made with automatic equipment as it is impracticable to plan a day and night experiment involving visual observations lasting more than a few days.

The experimental arrangement chosen was first used by Johnson and Roberts (12). They measured refraction angles over a fixed horizontal sightline by using a telescope of 20 inches focal length to view two targets at distances of 1019 feet and 2380 feet. The targets were marked with regular graduations and by estimating the apparent position of the cross wires of the telescope on the target graduations they were able to calculate the difference in the refraction angle for the two sightline lengths.

The advantage of this method of measurement was that only one instrument was needed and the elevation angles measured were not effected by random movements of the telescope.

In order to perform a continuous series of refraction readings, a similar experimental arrangement to that used by Johnston and Roberts was set up. The targets were mounted 100 feet and 8,600 feet from an automatic camera fitted with a long focal length lens and pictures were taken every 5 minutes day and night.

3.1 The Experimental Apparatus

3.1.1 The Targets

The two targets employed were low voltage tungsten filament lamps.

The distant target was mounted 12 feet above the ground on a hill which rose about 40 feet above the surrounding country. The near target consisted of two lamps which were mounted on a 10 foot high 4" x 4" hard wood post. The bottom of the post was buried 2 feet in the ground and guy wires were used to hold it steady.

The general arrangement of the experiment and the terrain beneath the sightline is shown in figure 9.

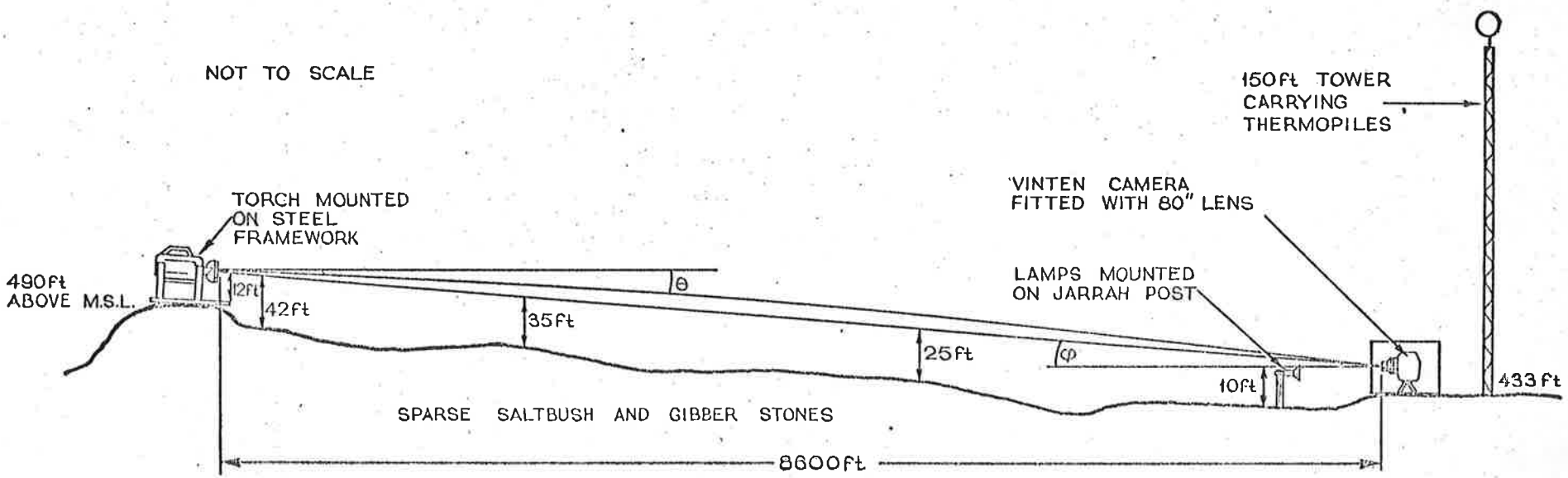

FIGURE 9. GENERAL ARRANGEMENT OF REFRACTION MONITOR AND TEMPERATURE RECORDING EQUIPMENT

3.1.2 The Lens

The lens used was an f/14 cassegrain reflector of 80 inches focal length. The field of view (figure 10) was divided horizontally. The top half gave an image of the distant target. The lower half was fitted with a compensating mirror system so that the image of the near target was brought to the same focus as the image of the distant target. The elevation angle of the sight-line was approximately 16 minutes of arc.

3.1.3 The Camera

The camera and timing equipment (13 and 14) were constructed in 1962 and used to study the effects of atmospheric seeing on the visibility of distant objects. On the completion of this work the equipment was used for measurements of atmospheric refraction.

The camera was a 35 mm "vinten instrumentation" cine camera converted to single frame operation. It was triggered electrically from a timing circuit and took one frame approximately every 5 minutes. An electric clock was built into the camera and its face was imaged onto one corner of each frame to show when the frame was taken.

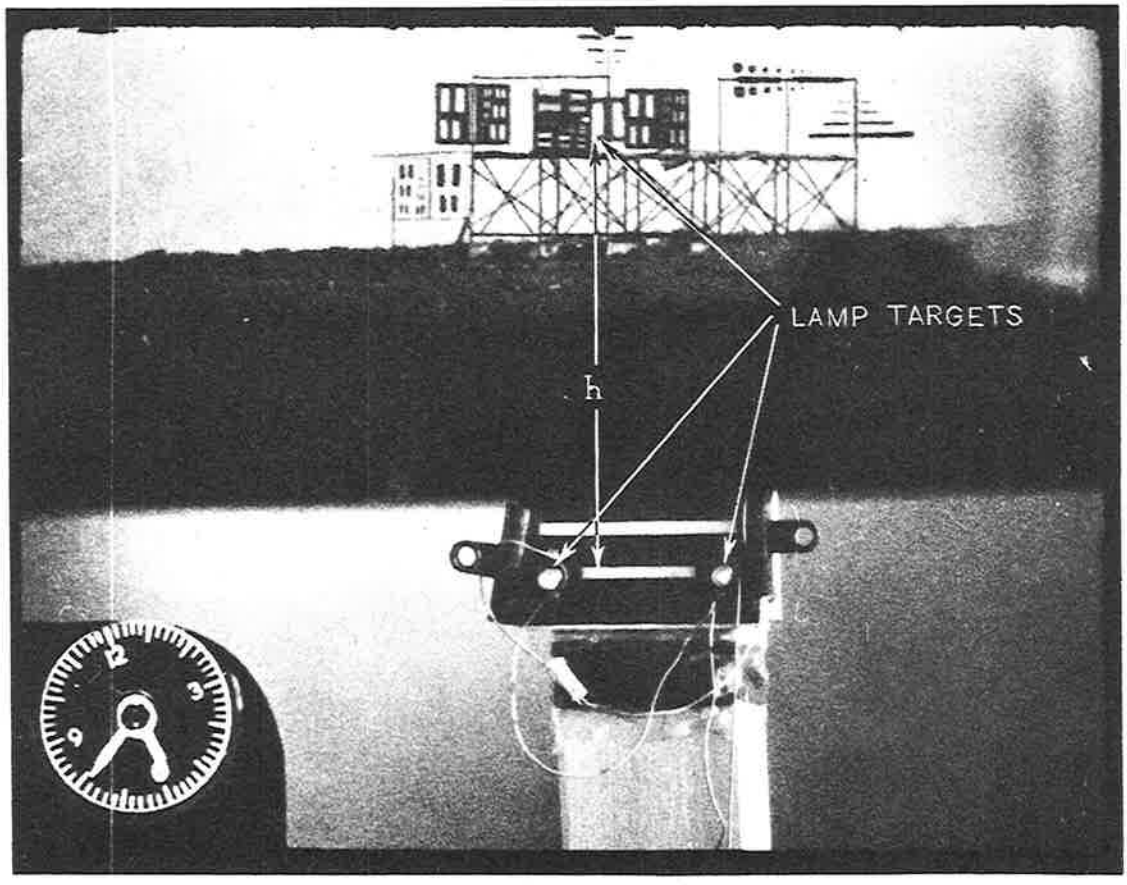

FIGURE 10. FIELD OF VIEW OF THE CAMERA

The camera, lens and timing circuit were housed in an air conditioned hut in which the temperature was maintained at about 21°C.

3.2 Film Reading and Calibration

Using a lens of 80 inches focal length an image movement of 0.001 inches at the focal plane represents a change of 2.6 seconds in the apparent elevation angle of the object. If the movement is measured on a Boscar film reader one Boscar unit represents 0.43 seconds of arc.

Early films were read using a travelling microscope but for the majority of the films a Boscar film reader was used.

The distance between the images of the two targets and the time shown by the clock were read on each frame (figure 10).

The refraction angle in seconds of arc was given by

$$R = 0.43 (h - d)$$

where d was the distance between the two targets for zero refraction error. h and d are in Boscar units.

The numerical constant varied slightly depending on the Boscar machine which was used.

The monitor system was calibrated by taking reciprocal readings visually with a Kern theodolite and a Ziess automatic level along the same sightline as the recording camera. Because of its superior stability and ease of reading, the automatic level was used on the open hillside, while the theodolite was operated from inside the building. The readings were taken in the morning and evening while the automatic camera was working.

The refraction angle was found by subtracting the elevation angle read from one end of the sightline from the mean elevation angle computed from both instruments. An allowance was made for the difference in the apparent vertical at the two measuring sites caused by curvature of the earth.

Thus in figure 8 the refraction angle in seconds of arc is given by:

$$R = \frac{(\phi + \theta + \not\phi)}{2}$$

where ϕ is the elevation angle of the automatic level measured by the theodolite, θ is the elevation angle of the theodolite measured with the automatic level and $\not\phi$ is the correction for earth curvature given by

$$\not\phi = \frac{L \times 60}{6080} \text{ seconds}$$

where L is the length of the sightline in feet.

3.3 Errors

An assessment of the reading error involved in measuring the films was made for one sample day. Each frame was read by five operators, and the standard deviation in their readings was calculated (figure 11). The readings were least accurate about midday when atmospheric turbulence caused considerable image blurring on the films.

Before installation, stability checks were carried out on the compensating mirror system, which showed that no significant errors would be introduced providing the temperature remained approximately constant.

The most likely source of error in the system is vertical movement of the near target. The smallest angle which could be measured on the film was 2.6 seconds (.001 inches on the film), and at a range of 100 feet, this represented a movement of about .014 inches at the near target.

3.4 Seasonal Trends in the Diurnal Refraction Cycle

For these measurements the equipment was run continuously day and night. Due to the large amount of film reading which was entailed in this work, the analysis was restricted to the first seven days of each month. During this time a group of 3 readings was taken every half hour day and night.

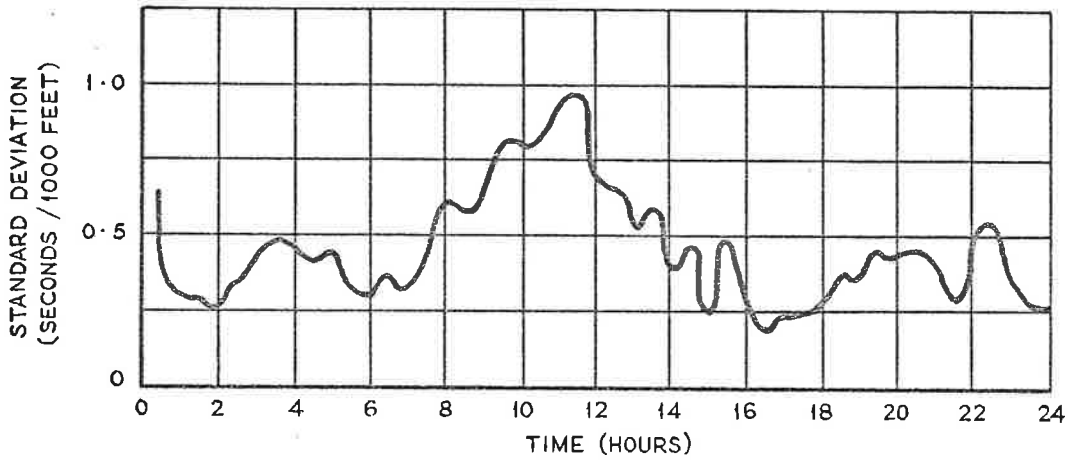

FIGURE 11. STANDARD DEVIATION OF FILM READING ERROR FOR THE FILM TAKEN ON 3.5.67

Figures (12-16) show the average reading for each month together with the maximum and minimum refraction recorded in the first week. The arrows beneath the graphs indicate times of sunrise and sunset. The results have been expressed in terms of the diurnal range of refraction by measuring the mean maximum and minimum refraction angles from the monthly graphs. Figure 17 shows the diurnal range of refraction together with the diurnal range of air temperature, number of hours of sunlight, and amounts of rainfall for the first week of each month. The weather information shown in figure 17 was obtained retrospectively from a weather station some thirty miles from the working area but in similar terrain.

3.4.1 Discussion of Results

During the day the refraction angle was usually near zero with a minimum recorded in the two hours after midday. There was always a slow increase in refraction from about 3 hours before sunset until several hours after. Night time refraction angles were between 5 and 10 seconds/1,000 feet in clear weather, and there was often a marked peak in the curve for the readings taken at dawn. The refraction angle dropped from its night time value after the sun had been up for about an hour.

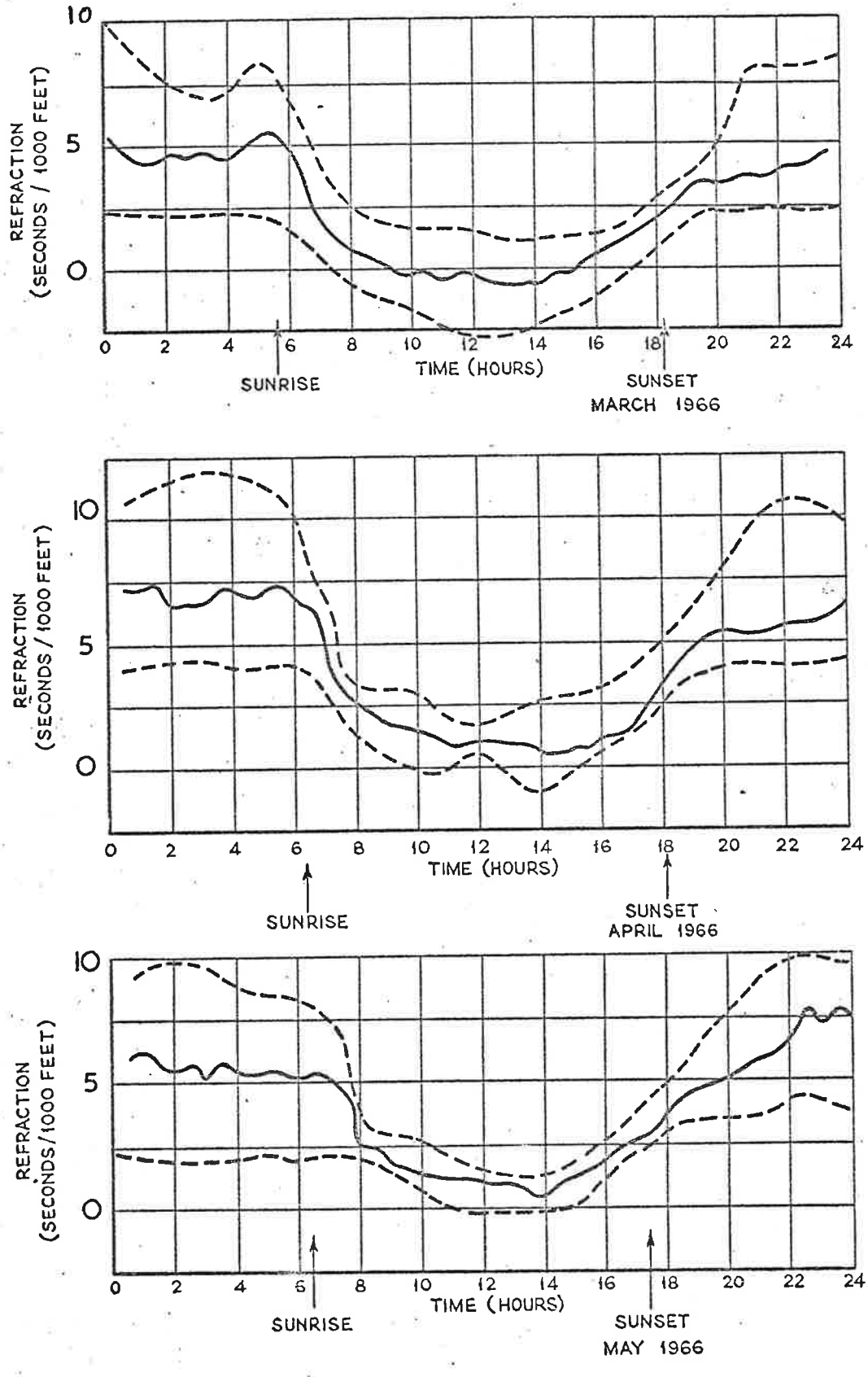

FIGURE 12 DIURNAL VARIATION OF REFRACTION DURING MARCH, APRIL AND MAY 1966

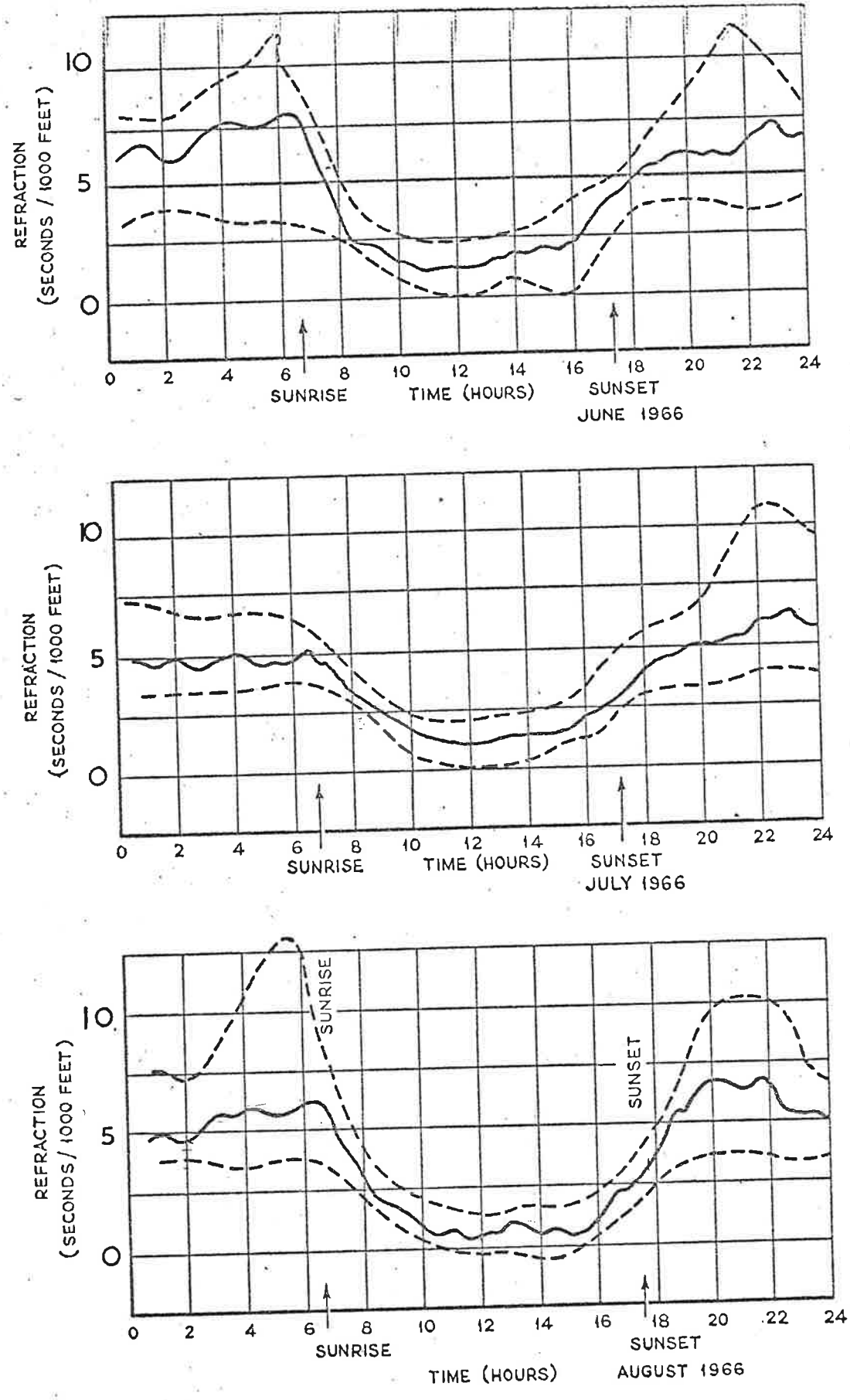

FIGURE 13 DIURNAL VARIATION OF REFRACTION DURING JUNE, JULY AND AUGUST 1966

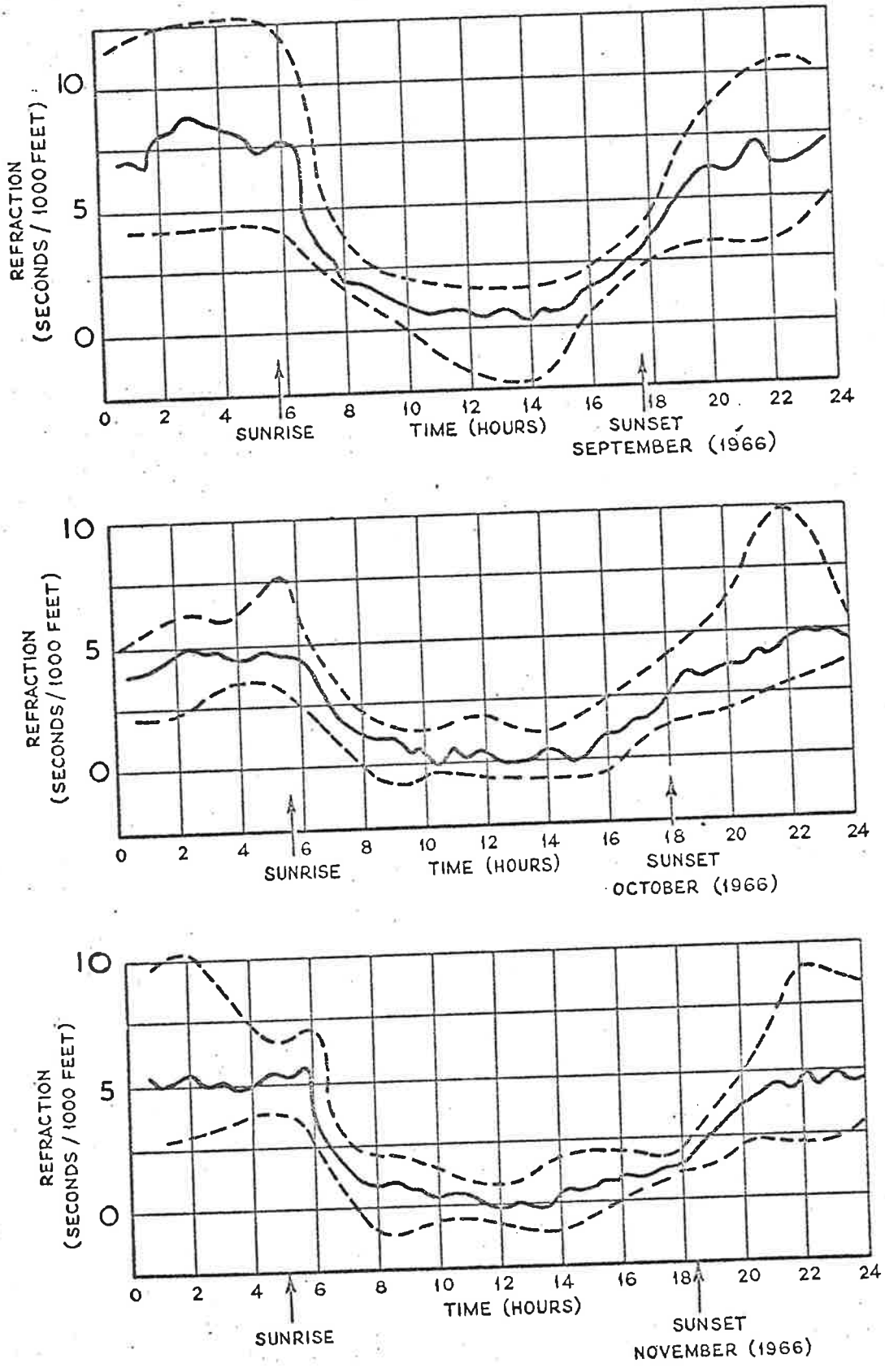

FIGURE 14 DIURNAL VARIATION OF REFRACTION DURING SEPTEMBER, OCTOBER AND NOVEMBER 1966

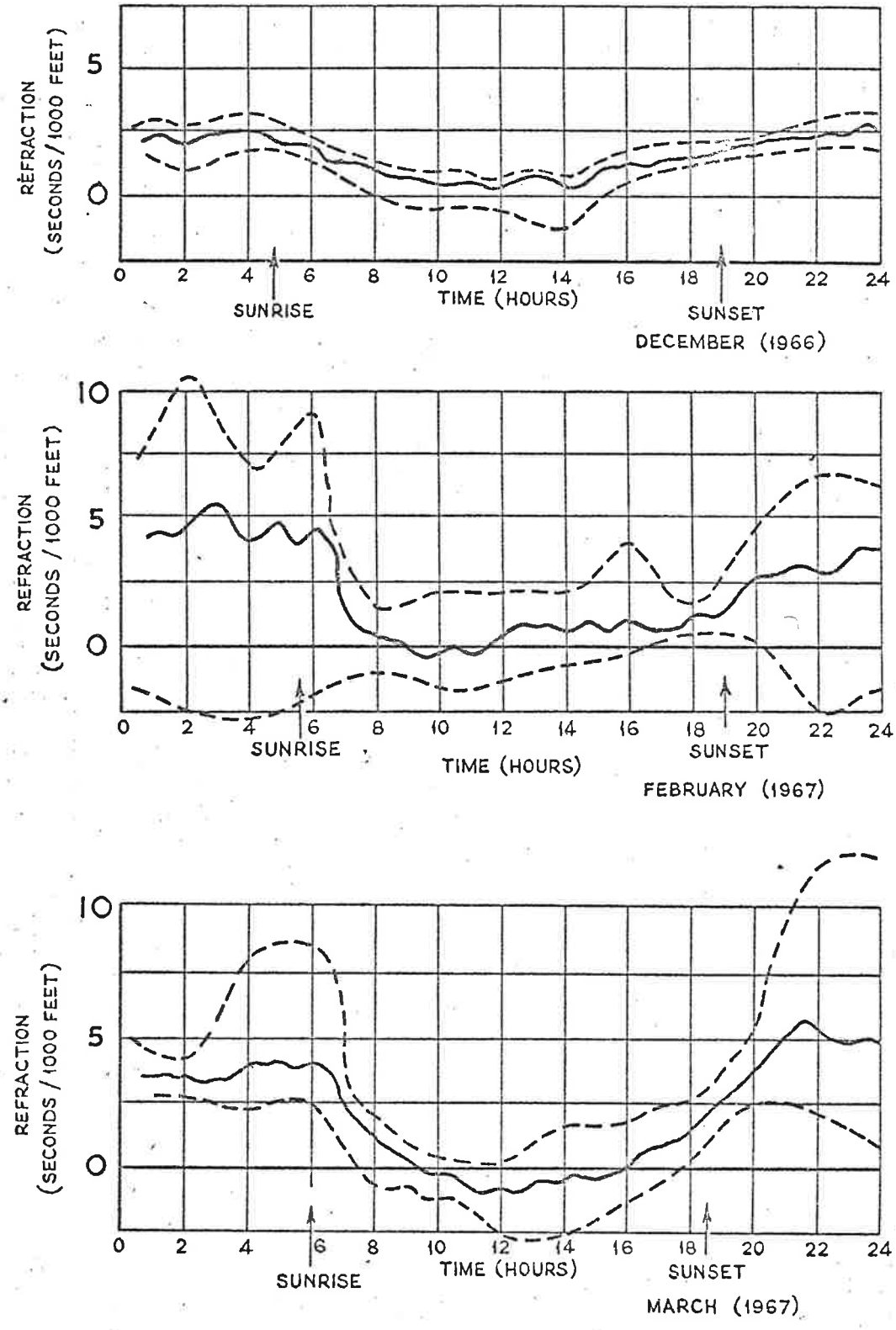

FIGURE 15 DIURNAL VARIATION OF REFRACTION DURING DECEMBER 1966, FEBRUARY 1967 AND MARCH 1967

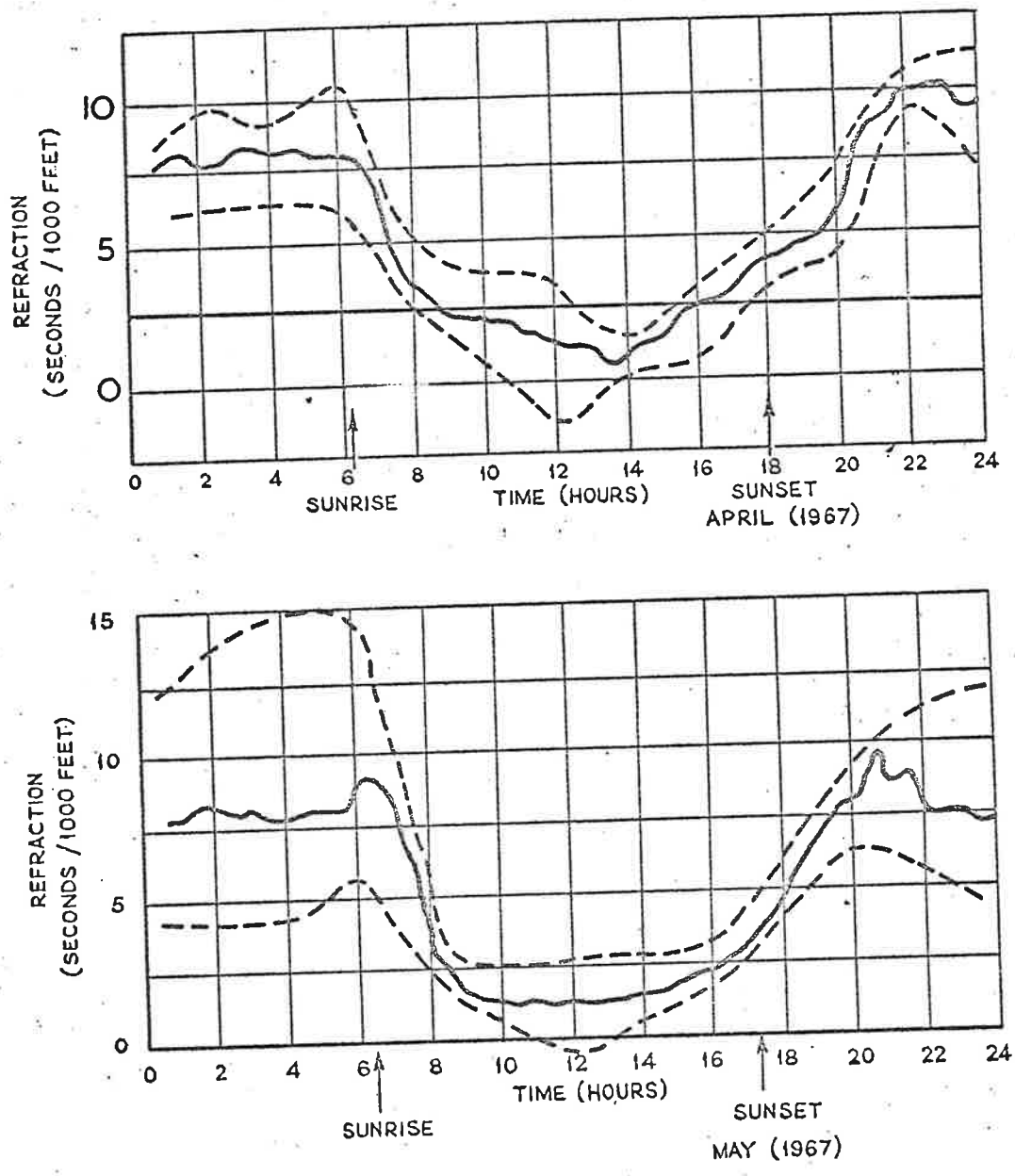

FIGURE 16 DIURNAL VARIATION OF REFRACTION DURING APRIL AND MAY 1967

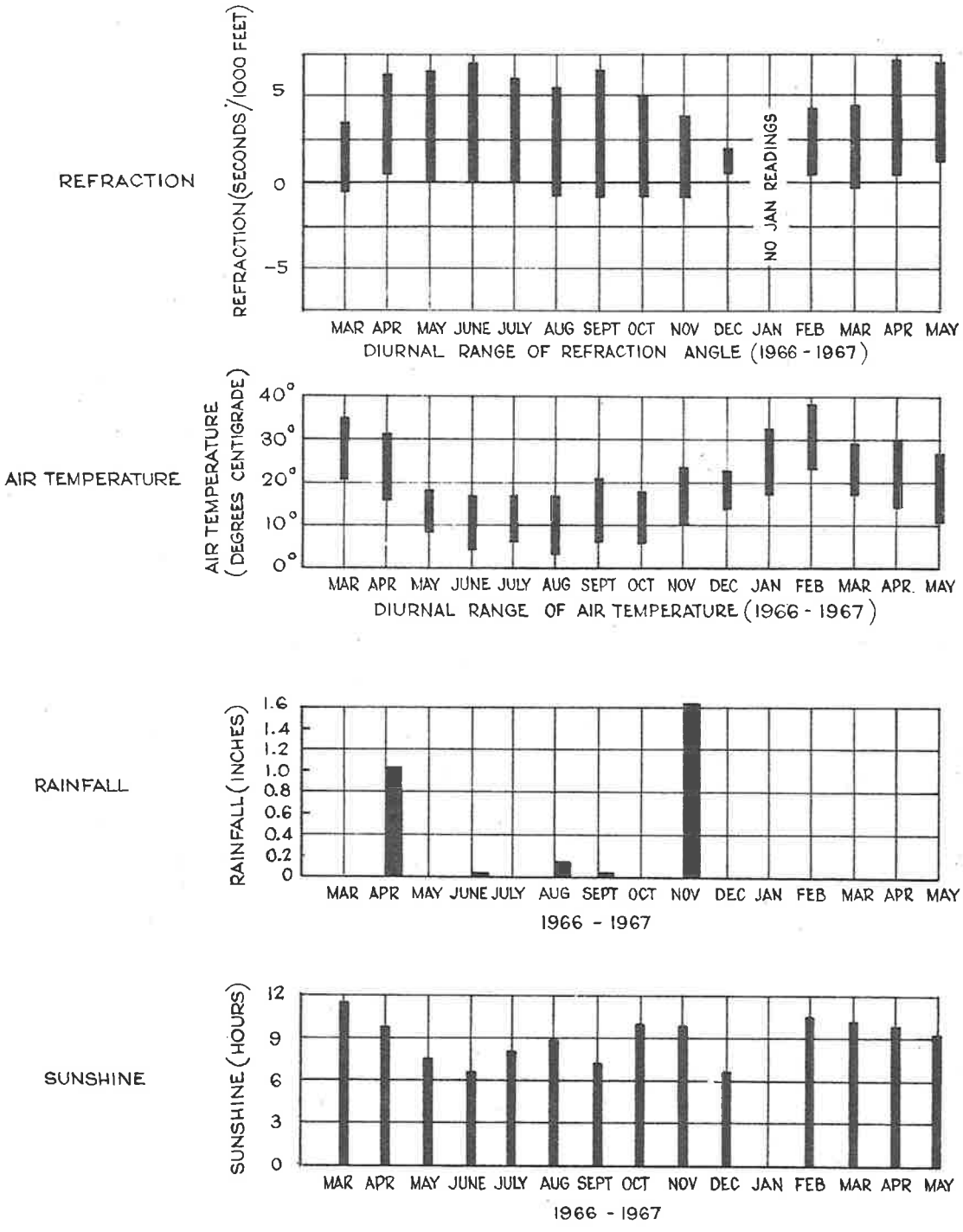

FIGURE 17. WEATHER INFORMATION DURING REFRACTION MEASUREMENTS

No appreciable seasonal trends were evident in the 15 month recording period. Day time refraction was always near zero. At night there was some indication that larger refraction angles were measured in cooler weather, but the trend was small enough to be caused by secondary effects such as movement of the near target.

A rainfall recording coincided with a reduction in refraction angle measured at night, and produced a fall in the diurnal range of refraction. This result was expected, as it is well known that the presence of cloud cover reduces the diurnal range of temperature, and the magnitude of the temperature gradient.

An important conclusion from this survey was that refraction effects on horizontal sightlines near the ground were always small about midday both summer and winter. At night large refraction angles could be expected throughout the year.

4. TEMPERATURE MEASURING EQUIPMENT

Section (2) has shown that in order to calculate the refraction angle on a sightline, it is necessary to know the refractive index gradient, or the temperature and pressure gradients across the sightline. As the refraction measurements were made over a fixed sightline, a 150 foot mast at the camera end of the sightline was used as a mount for temperature recording equipment. (See figure 9)

Temperature gradient measurements have been made on masts and towers in various parts of the world. Some of the earliest measurements were made by Johnson & Heywood (15), who used platinum resistance thermometers to measure the air temperature at discrete heights on a 310 foot tower at Leafield in Southern England. Similar measurements were made in Egypt by Flower (16). More recently copper resistance thermometers were used by the Brookhaven National Laboratory to perform measurements on a 420 foot tower on Long Island in the U.S.A. (17). Thermistors have also been used for making temperature measurements. A short series of measurements made in South Africa was reported by Angus-Leppan (7). They are regularly used in balloon borne Radio Sonde temperature measuring equipment. The most recently reported temperature measurements were made by the U.S. Army in New Mexico. In this case thermocouple equipment was used on a 200 foot tower (18).

A thermocouple system was chosen for our measurements as suitable thermocouple wire was readily available and the electrical output could

be recorded easily. Other advantages of a thermoelectric system were ease of calibration, superior stability, and low cost.

4.1 The Thermoelectric Equipment

28 swg copper and constantan wires were used for the thermocouples. In order to produce an E.M.F. sufficiently large to be recorded by a pen recorder, a multiple junction arrangement was used.

Twelve thermocouples were operated together to form a thermopile as shown in figure 18. A series of these thermopiles was arranged up the mast to measure the temperature differences between heights of 5, 10, 30, 49, 68, 92, 116, 146 feet above ground. The junctions were positioned closer together near the ground where higher temperature gradients were encountered. In addition to the temperature difference measurement, the air temperatures at the top and bottom of the tower were measured by single copper constantan thermocouples referenced to a 45°C automatic hot junction.

4.1.1 Heat Shields and Heat Sinks

The top and bottom junctions of adjacent thermopiles were enclosed in the same aluminium heat shield which consisted of twin inverted aluminium cups mounted one inside the other, with

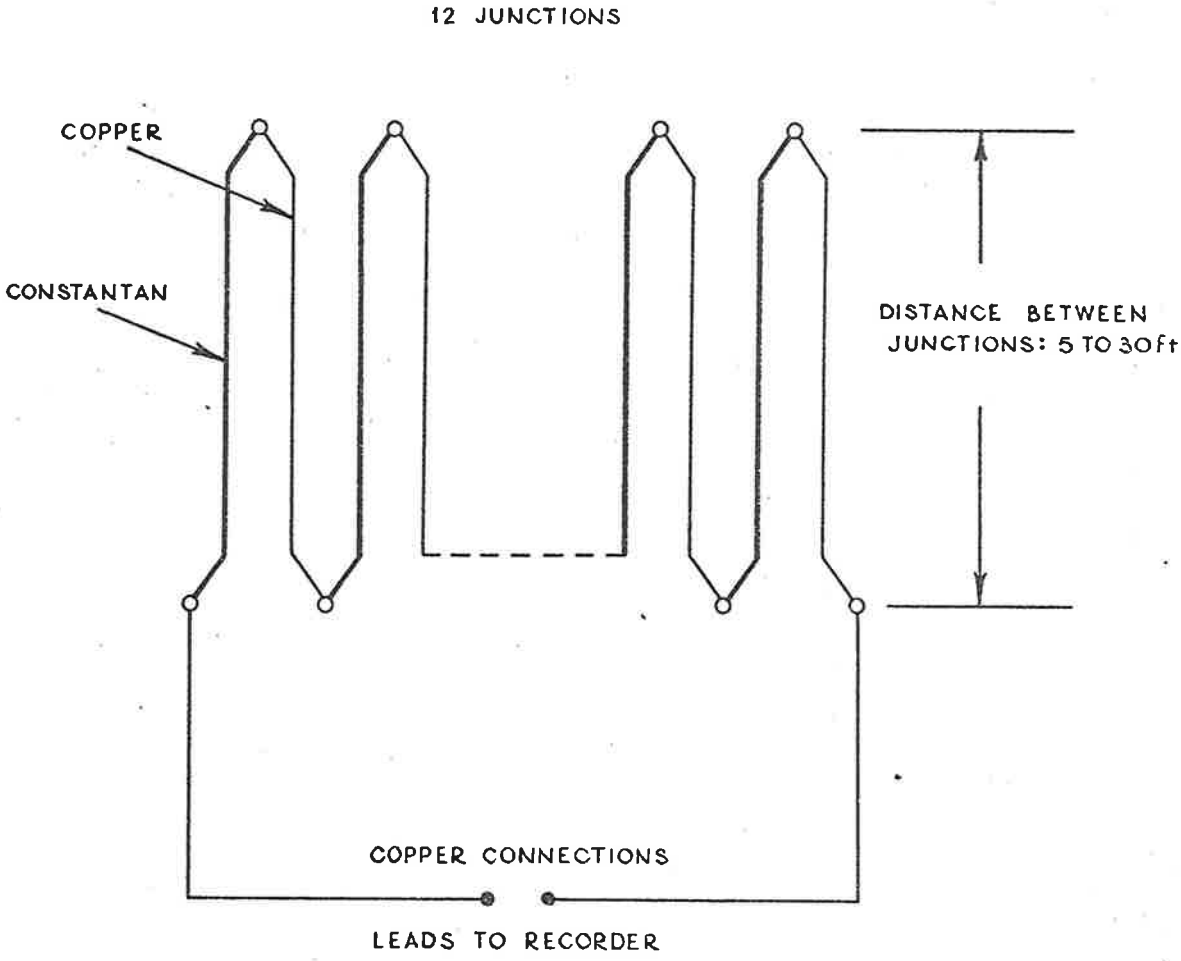

FIGURE 18. THERMOPILE ARRANGEMENT

a quarter inch air gap between them as shown in figure (19). The thermocouple junctions were mounted on vertical matrix boards attached to a removeable base plate. Beneath the base plate was mounted an electrical blower unit which created an air flow of about 6 ft/sec over the thermocouples. The air was exhausted through holes drilled in the sides of the radiation shields. Calculations on the heat dissipation of the motors showed that negligible errors were introduced by proximity of the blower units to the thermocouples. The shield units were mounted 2 feet away from the tower on angle iron brackets.

Initial tests of the system indicated that the records would be confused by short time temperature variations during the day. To prevent this, damping was introduced into the system by adding a 2.5 gm brass heat sink to each thermocouple junction. The response time of the system was thus increased to about six minutes to record a temperature change of $1^{\circ}C$.

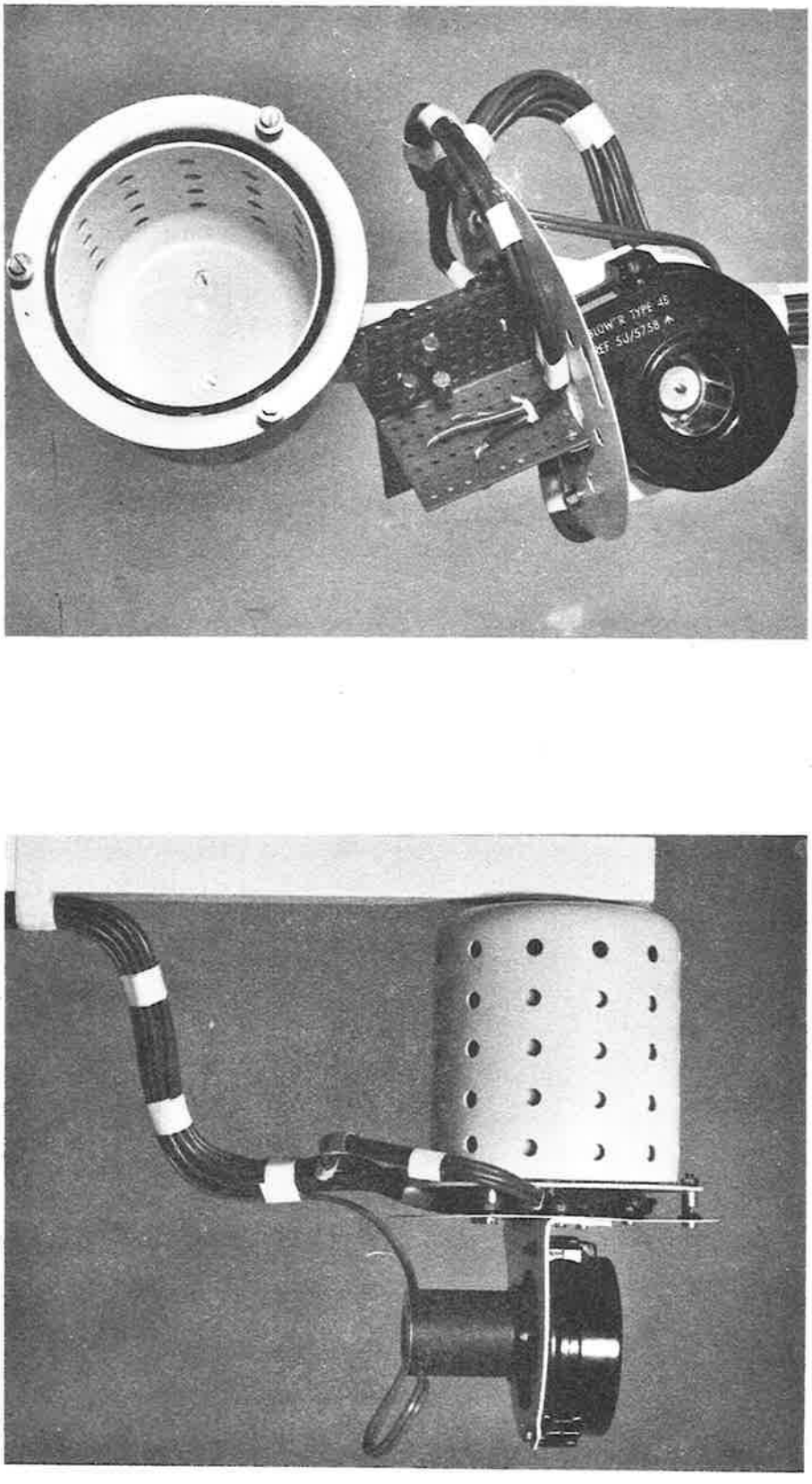

FIGURE 19. THERMOCOUPLE MOUNTING ARRANGEMENT

4.1.2 Recorder System

The recorder used was a 12 channel potentiometric strip chart recorder with a sensitivity of 2mv for full scale deflection on a 10 inch wide chart. Accuracy was ±5% of full scale deflection.

The electrical zero was adjusted to 40% of the chart width and the outputs of the thermopiles were such that a temperature difference of 1°C between ends produced a deflection of 22.8% of the chart width.

In order to record the outputs from the air temperature thermocouples on the same recorder, the zero for the relevant channels was shifted electrically by the arrangement shown in figure 20. The shift voltage, was recorded negatively as E11. Hence the air temperature was given by

$$T^{\circ}C = 45 - \frac{(E8 - E11)}{38}$$

where E8 was the displaced output voltage from the thermocouple,

45 the temperature of the automatic oven in °C,

38 the characteristic of the thermocouple in $\mu v/^{\circ}C$.

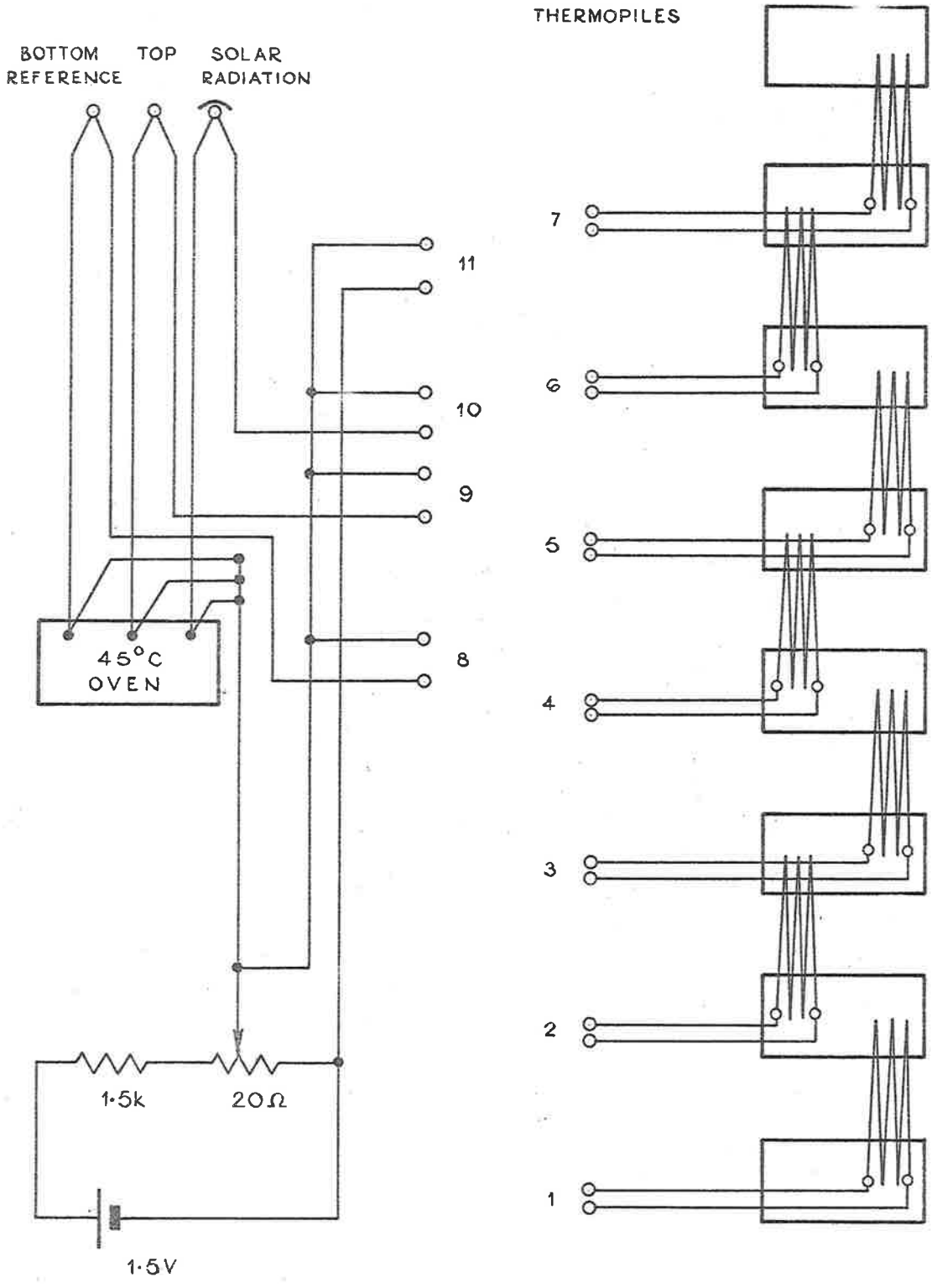

FIGURE 20. ELECTRICAL CONNECTIONS TO RECORDER

4.1.3 Data Reduction

The records were read for a 10 minute period (12 recordings of temperature on each channel) every two hours, and all the readings for one channel were put on an IBM data card.

In order to simplify the computations, a linear relationship between temperature difference and thermal emf was assumed. This introduced an error in the results as in the range 0 - 45°C there is a nonlinearity in the temperature EMF relationship which represents a departure from a straight line of 0.3°C. The main effect of this was to cause a maximum error of 0.3°C in the value of the air temperature. A negligible error was introduced into the temperature gradient readings as the thermocouples were operated about half way between 0 and 45°C where the assumed line was tangential to the actual temperature EMF curve.

The computer programme (Appendix 1) calculated the temperatures at the base of the tower and hence the temperature at all other junction positions by a summation process on the thermopile outputs.

The temperature and temperature gradient information was printed out and a punch card was produced showing the temperature height relation for each time of day.

These cards were used later to calculate the monthly mean and standard deviation.

4.2 Correlation of Measured and Calculated Refraction

In this section refraction is calculated by computing the curvature of the ray be equation 9. The work is dealt with in two parts. In the first part a series of readings with the refraction monitor over 9 days in August 1967 are compared with the refraction calculated from temperature gradient measurements made on the mast at the same time. The second section deals with refraction measurements made over a variety of sightlines several miles from the temperature mast.

4.2.1 Measurements on Fixed Sightline

Temperature information useful in the calculation of refraction on the chosen sightline was available from the tower at discrete heights of 5, 10, 30, 49 and 68 feet above ground. In order to deduce a more detailed temperature/height curve for the graphical integration, a Lagrange interpolation formula was used. This produced the temperature at 2 feet intervals between 10 and 42 feet above ground as shown in figure 21.

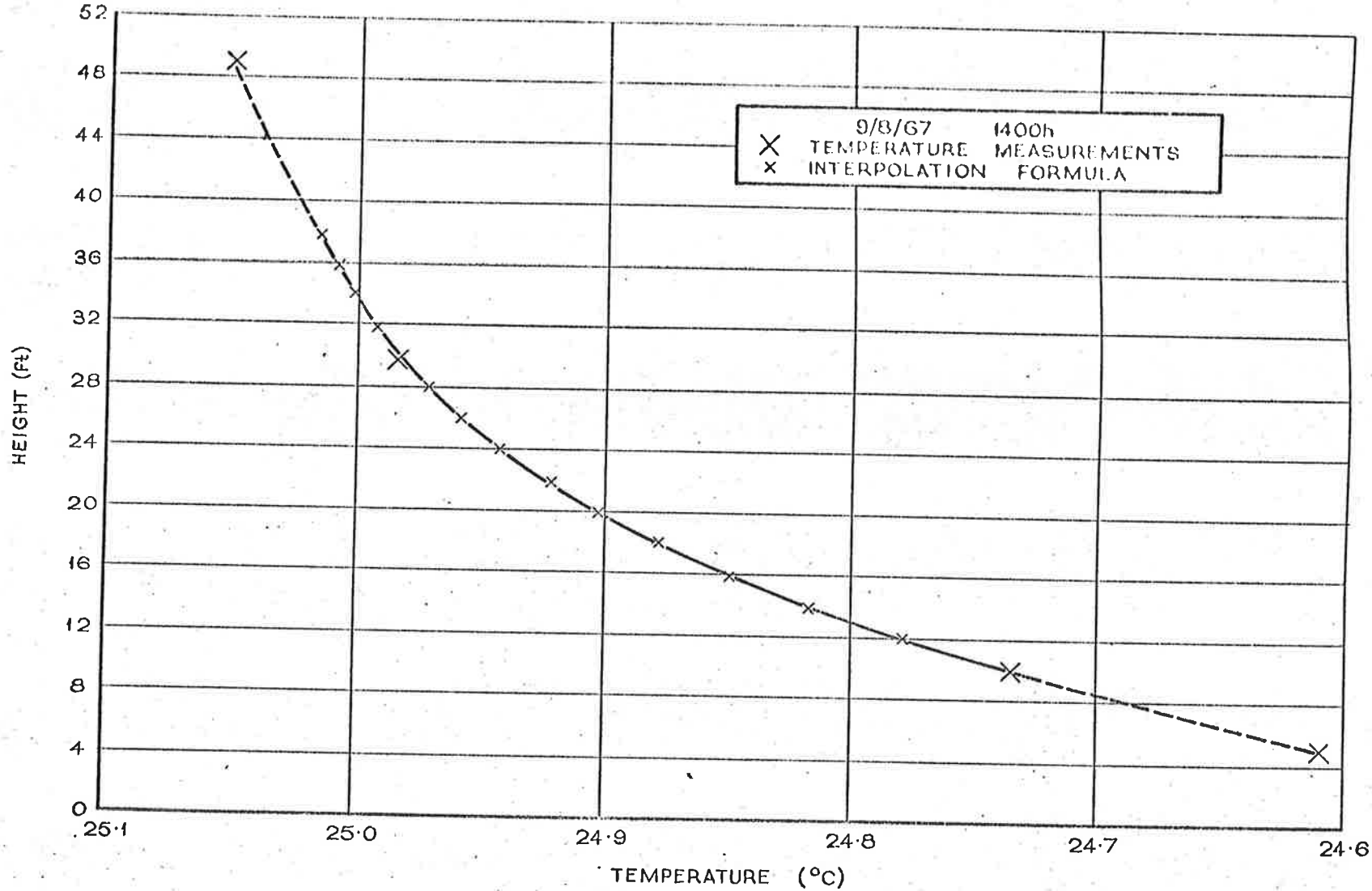

FIGURE 21 FIT OF LAGRANGE INTERPOLATION FORMULA TO THE TEMPERATURE/HEIGHT CURVE

Simpson's rule was used to perform the integration. The fortran program used for the computation is shown in Appendix II. Figures 22 , 23 and 24 show the diurnal variation of calculated and measured refraction for nine days in August 1967. Weather conditions for the measuring periods were sunny and warm. Figure 25 shows the relationship between measured and calculated refraction angles, and Figure 26 the standard deviation of the points.

4.2.2 Night Time Refraction Measurements

In order to extend the correlation measurements to other sightlines away from the vicinity of the temperature measurement mast, a night time experiment was set up. The elevation angles of lights at ranges of up to 10 miles were measured with a theodolite located four miles from the site where the temperature measurements were made. Figure 27 shows the geometry of the experiment. The results are expressed in terms of the change in the elevation angle which was measured during the night. The measured refraction angles which appear in the results are calculated from

$$R_m = (\alpha t - \alpha 1) + Rc_1$$

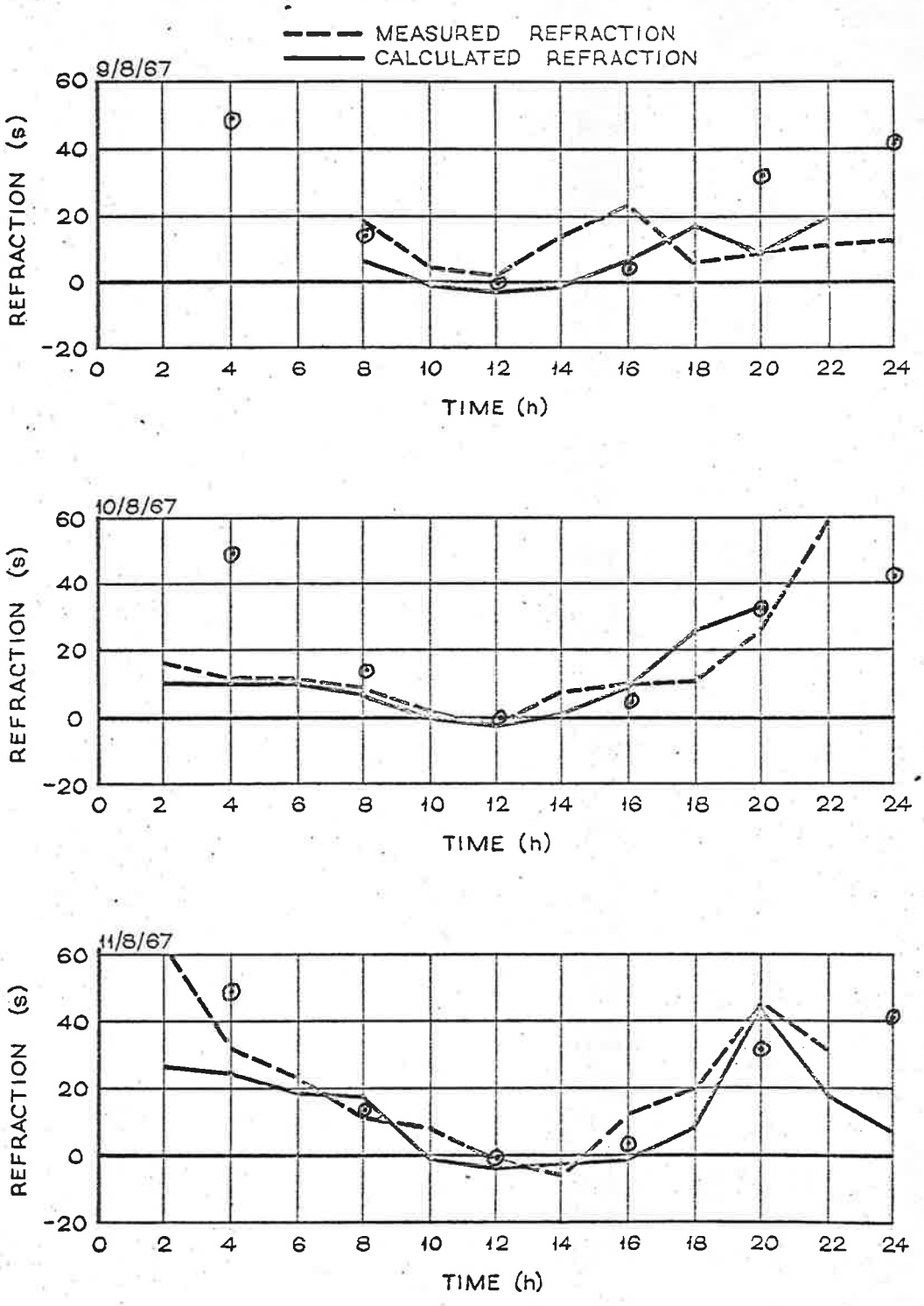

FIGURE 22 DIURNAL VARIATION OF CALCULATED AND MEASURED REFRACTION

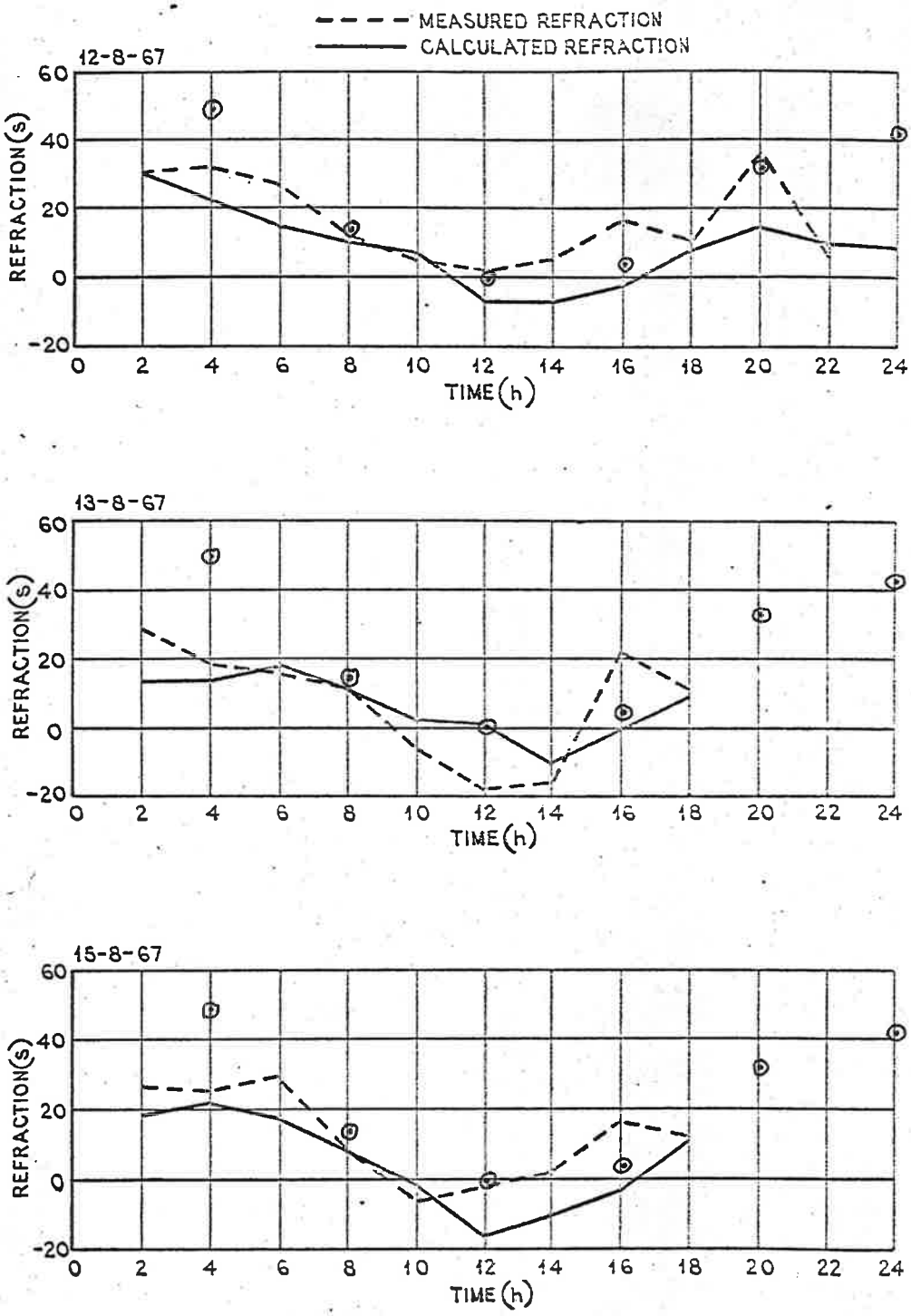

FIGURE 23 DIURNAL VARIATION OF CALCULATED AND MEASURED REFRACTION

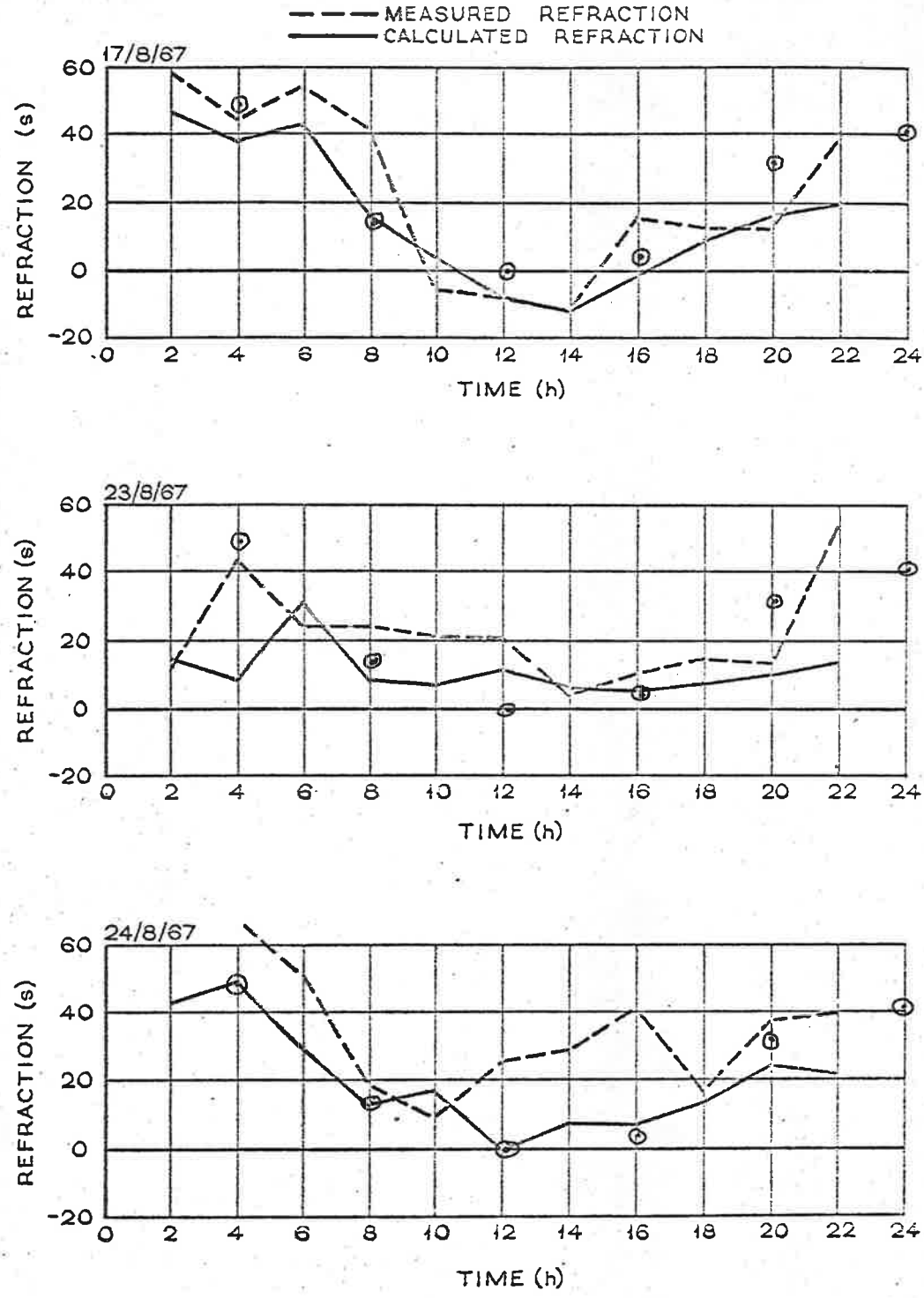

FIGURE 24 DIURNAL VARIATION OF CALCULATED AND MEASURED REFRACTION

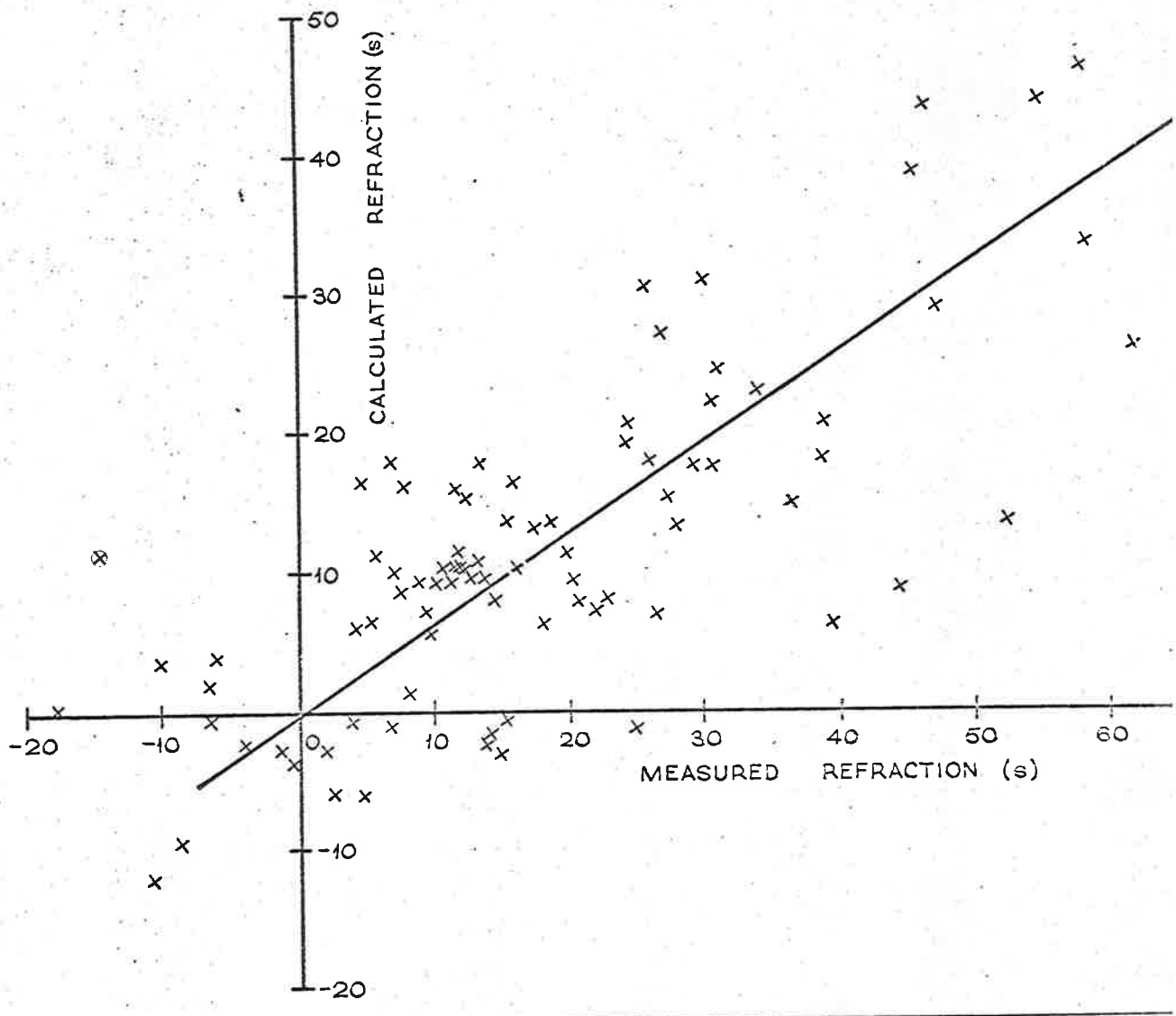

FIGURE 25 CALCULATED AND MEASURED REFRACTION ANGLES (MONITOR RESULTS)

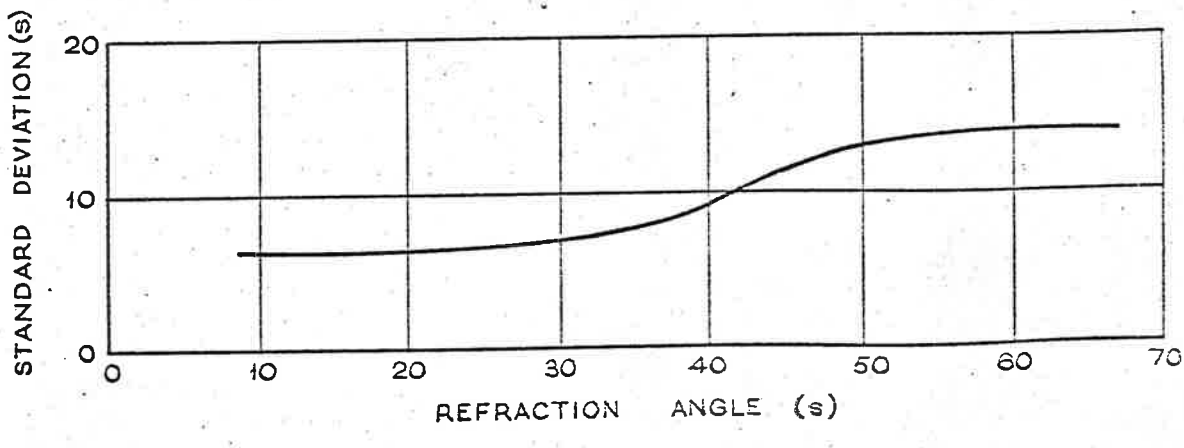

FIGURE 26. STANDARD DEVIATION OF CALCULATED REFRACTION (MONITOR RESULTS)

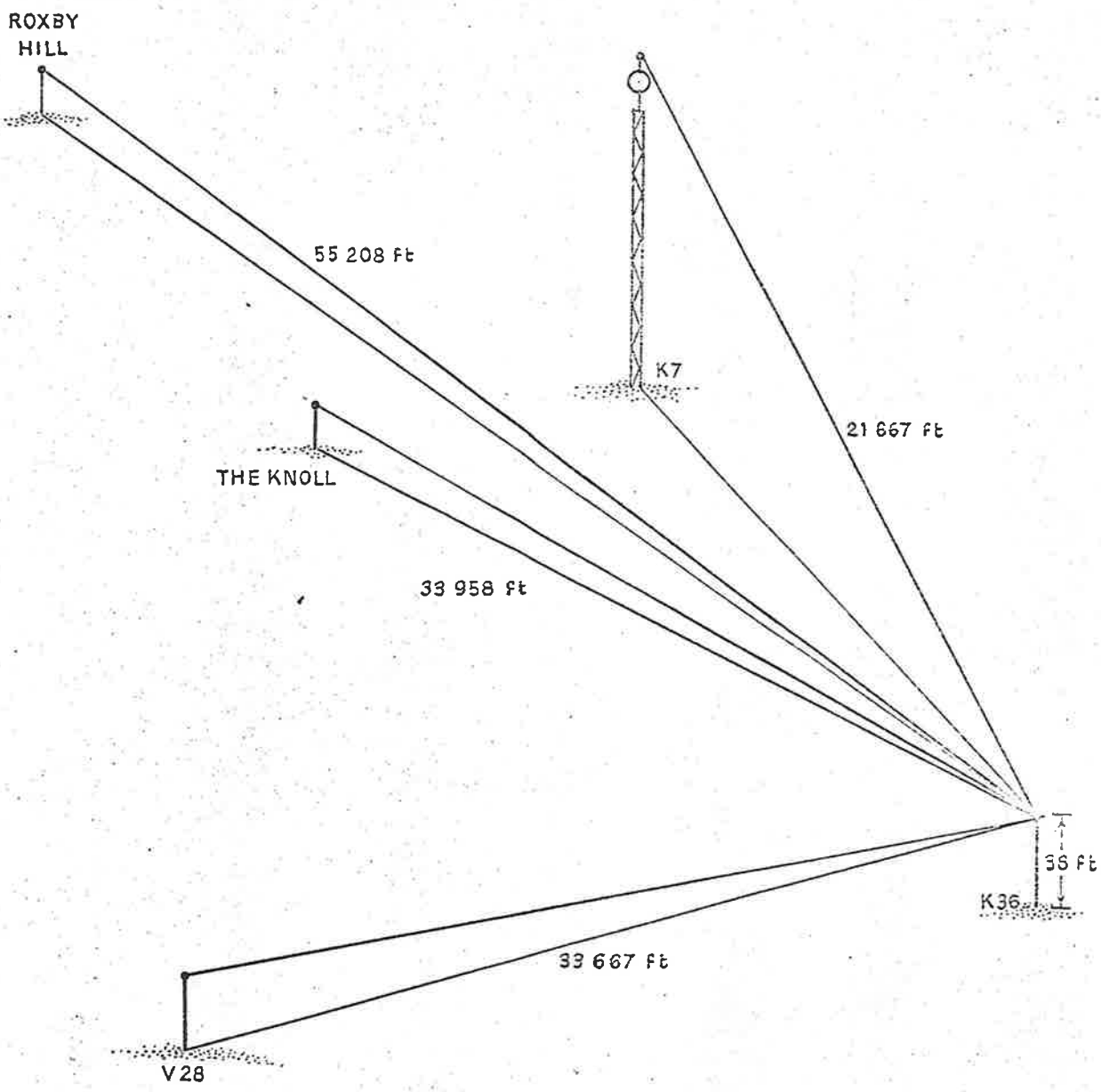

FIGURE 27 NIGHT TIME REFRACTION EXPERIMENT

α t is the elevation angle measured at time t

α 1 is the first elevation angle measured during the night

Rc_1 is the refraction angle calculated for the atmospheric conditions prevailing when the first reading of the night was made.

This treatment of the results was necessary as the exact positions of the lights which were viewed during the experiment were not known. Thus the elevation angle (at zero refraction) of each light when viewed by the theodolite could not be calculated.

The temperature measurements for the night time experiment were obtained by reading the temperature record over the period of time it took to take the refraction readings. This was between 5 and 10 minutes for each set.

4.2.3 Calculation of the Refraction Angle

Linear interpolation of the temperature gradients between junction positions was used to calculate the air temperature at 4 foot intervals from the height of the observer (38 feet) to the height of the optical target on top of the temperature tower (162 feet). Simpsons rule was again used to perform the integration. The sightlines to the other lights were approximately

horizontal at a constant height above ground. For these results the temperature gradient at 38 feet was used to calculate the refraction angle from equation 5. (Refraction angle = half total curvature of the ray).

Figure 28 shows the measured and calculated refraction angles plotted against time. Figure 29 shows the relationship between measured and calculated refraction and Figure 30 the standard deviation. All temperature measurements taken during the night are shown in Table I.

4.2.4 Discussion of Results

The results from the refraction monitor tests and those for the night time experiment have been dealt with separately in the analysis. This has been done because, due to either some peculiarity associated with the measuring system or the terrain under the sightline, the relationship between calculated and monitor measured refraction was not unity; as was the case for all other measurements. However the measurements are included as they provide useful information on the irregularities of the diurnal refraction cycle. They also show the correlation and the anomalies which are found between calculated

TABLE I.

TEMPERATURE MEASUREMENTS TAKEN DURING NIGHT REFRACTION EXPERIMENT

	5	10	30	49	68	92	116	146 ft
1435 hours	11·24°C	11·11	10·58	10·73	10·29	10·20	9·94	9·72
1813	8·08	8·21	8·32	8·39	8·46	8·53	8·53	8·44
1840	7·56	7·58	7·69	7·78	7·85	7·89	7·89	7·80
1900	7·29	7·38	7·49	7·53	7·60	7·64	7·60	7·49
1925	7·03	7·12	7·23	7·30	7·37	7·39	7·35	7·20
1940	6·76	6·85	6·98	7·07	7·16	7·20	7·20	7·05
2000	6·76	6·85	7·00	7·07	7·11	7·13	7·06	6·88
2030	6·24	6·53	6·82	7·00	7·11	7·18	7·16	6·98
2050	5·45	5·91	6·33	6·66	6·90	7·05	7·05	6·87
2110	5·13	5·44	5·88	6·23	6·56	6·89	6·96	6·83
2130	4·92	5·18	5·53	5·82	6·11	6·46	6·70	6·64
2150	4·13	4·33	4·68	4·97	5·32	5·67	6·00	6·18
2230	3·87	4·07	4·40	4·71	4·95	5·13	5·27	5·38
0320	3·61	3·61	3·74	3·78	3·82	3·91	3·95	3·86
0343	4·13	4·13	4·28	4·35	4·42	4·49	4·49	4·31
0411	4·92	4·92	5·01	4·01	4·97	4·97	4·90	4·70
0430	4·66	4·66	4·71	4·73	4·69	4·69	4·65	4·47
0500	4·66	4·66	4·75	4·79	4·75	4·75	4·68	4·50
0528	4·92	4·88	4·95	4·95	4·91	4·84	4·75	4·55
0603	5·45	5·41	5·45	5·45	5·38	5·34	5·23	5·03
0620	5·71	5·69	5·73	5·71	5·64	5·60	5·47	5·29
0635	5·71	5·71	5·80	5·80	5·71	5·69	5·58	5·40
0645	5·71	5·69	5·73	5·71	5·64	5·60	5·49	5·29
0650	5·71	5·69	5·73	5·73	5·66	5·64	5·55	5·35

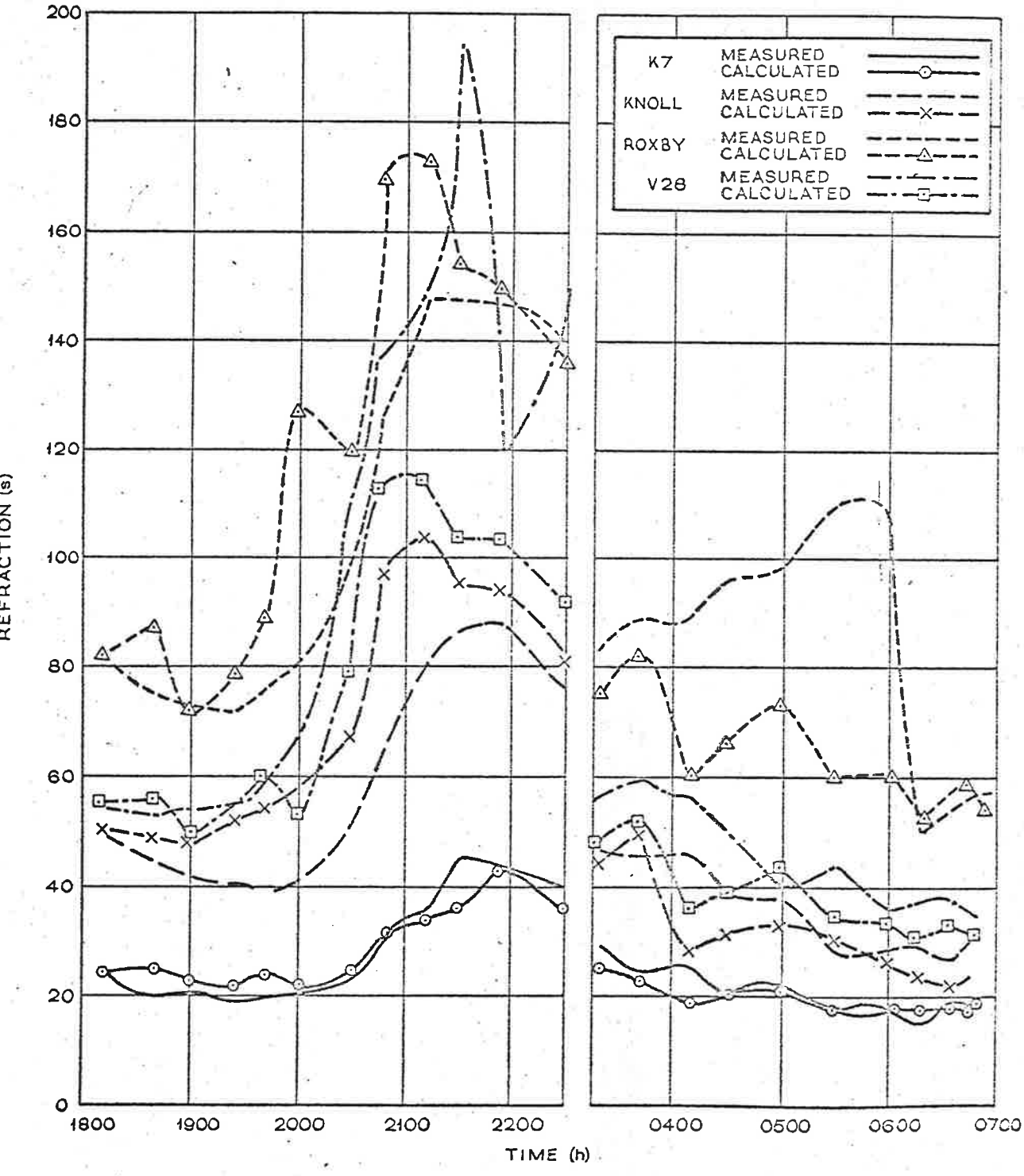

FIGURE 28 CALCULATED AND MEASURED REFRACTION ANGLES (NIGHT EXPERIMENT)

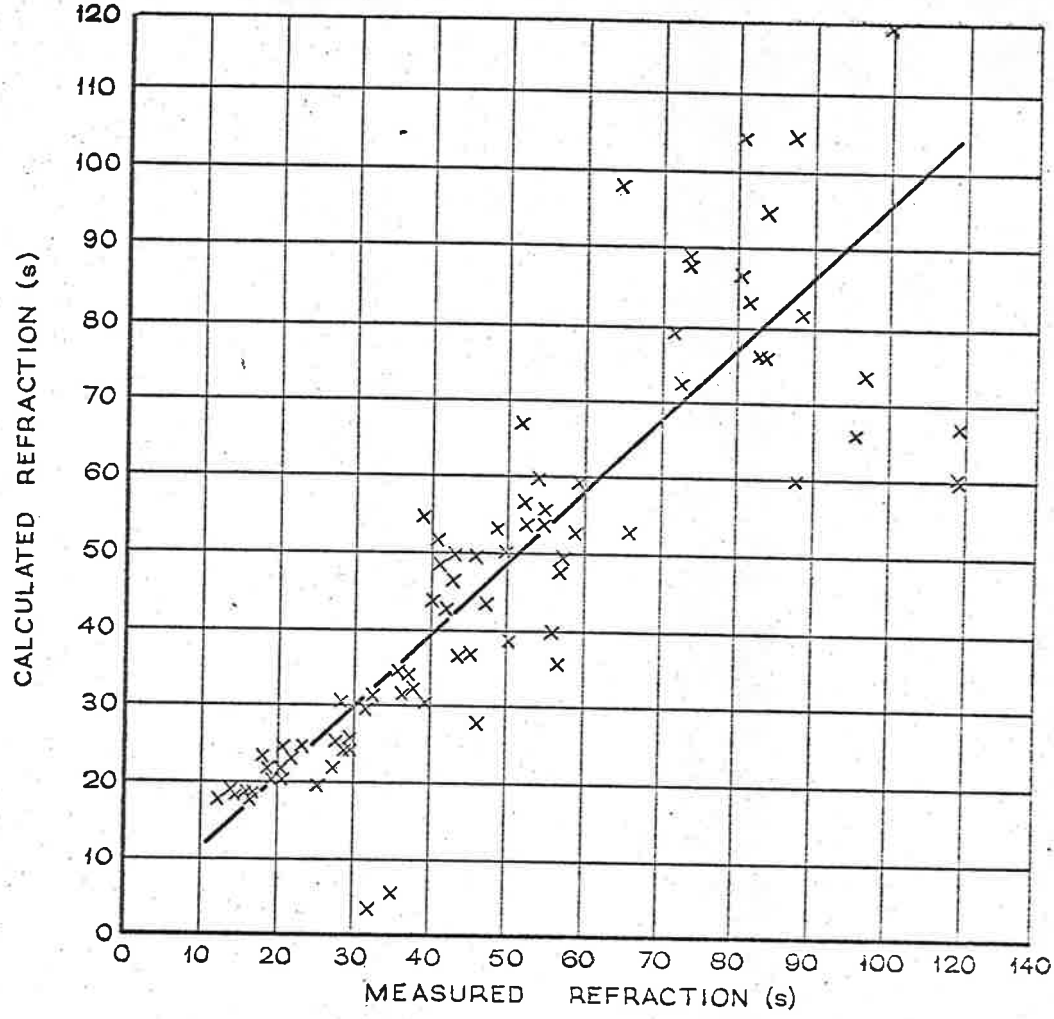

FIGURE 29. CALCULATED AND MEASURED REFRACTION ANGLES (NIGHT EXPERIMENT)

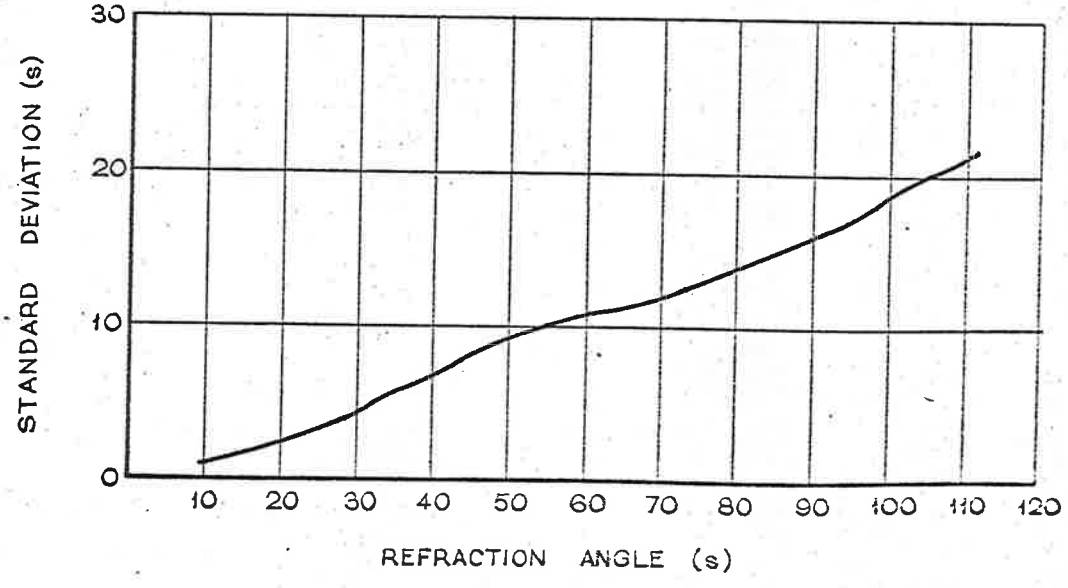

FIGURE 30 STANDARD DEVIATION OF CALCULATED REFRACTION (NIGHT EXPERIMENT)

and measured values of refraction very near the ground. The large scatter on the results gives some indication of the disagreement which is likely between measured refraction angles and the angle calculated from temperature measurements taken at the same time and in the same locality. The standard deviation was larger at low refraction angles than was found from visual observations. Generally the smaller refraction angles were measured during the heat of the day when bad seeing conditions gave rise to high frequency image movements. Some of this movement was recorded by the camera because each measured refraction angle was obtained from only three frames taken at 5 minute intervals and an exposure of 1/100 second. A longer observation period as was used on the night time experiment tended to average out the higher frequency movements and produced a more representative figure for the refraction angle.

The results from the night experiment were remarkably good, as the sightline lengths were very long and at low elevation angles. The temperature measurements were made on a treeless, sparcely vegetated plain but two of the sightlines

were over sparce woodland for much of their length.

For these measurements the standard deviation was greater at the higher refraction angles. At night large changes in refraction occur at much lower frequencies than during the day. The general trends are indicated by the temperature gradient equipment, but there appears to be a time lag before these changes are felt at other places near by. However the disagreement between measured and calculated refraction angles was not more than 20% at any time.

The very large refraction angles measured during the night time experiment are worthy of note. On the longest sightline of 55,000 feet the refraction angle reached a maximum value of over 160 seconds of arc during a half hour period. In terms of the computed position of an object this would give an error of more than 40 feet in the calculated height.

The fact that temperature gradient measurements made in one location could be used to provide accurate refraction corrections on long sightlines several miles away makes the system much more flexible. Once a temperature measuring system has

been set up the results obtained from it could be used to provide refraction corrections over quite a wide area.

4.3 Temperature Gradient Averages

In the course of the work done on correlating calculated and measured refraction, a large number of temperature gradient measurements were made during the month of August, 1967. Average values for the temperature and temperature gradient were calculated for six times of day during the month. Figures 31-36 show all the temperature measurements made at these times. In each case the mean temperature is shown by a broken line. The graphs are of interest as they exhibit a large spread of air temperatures, but a much smaller spread of temperature gradients, at each time. Figure 37 shows the six mean temperature profiles for the month and figure 38 shows the mean temperature gradients and standard deviation for the month. The mean temperature, mean temperature gradient and standard deviation were computed by the fortran programme shown in Appendix III.

The mean temperature gradients were used to calculate the expected refraction angle over the 8,600 foot fixed sightline for August, 1967. This predicted refraction is shown on the daily refraction graphs (figures 22-24) and it is shown also in figure 39 together with the

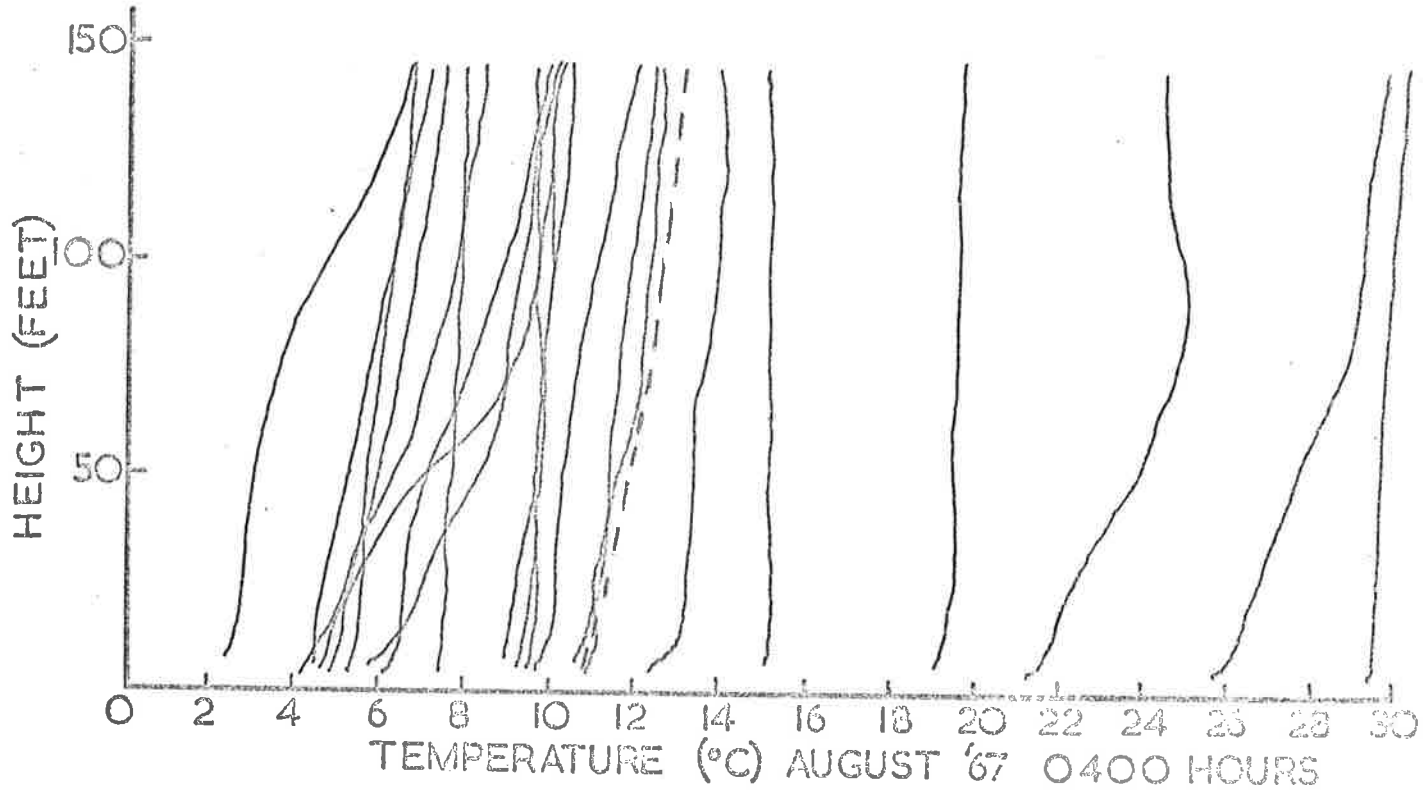

FIGURE 31. TEMPERATURE MEASUREMENTS MADE AT WOOMERA

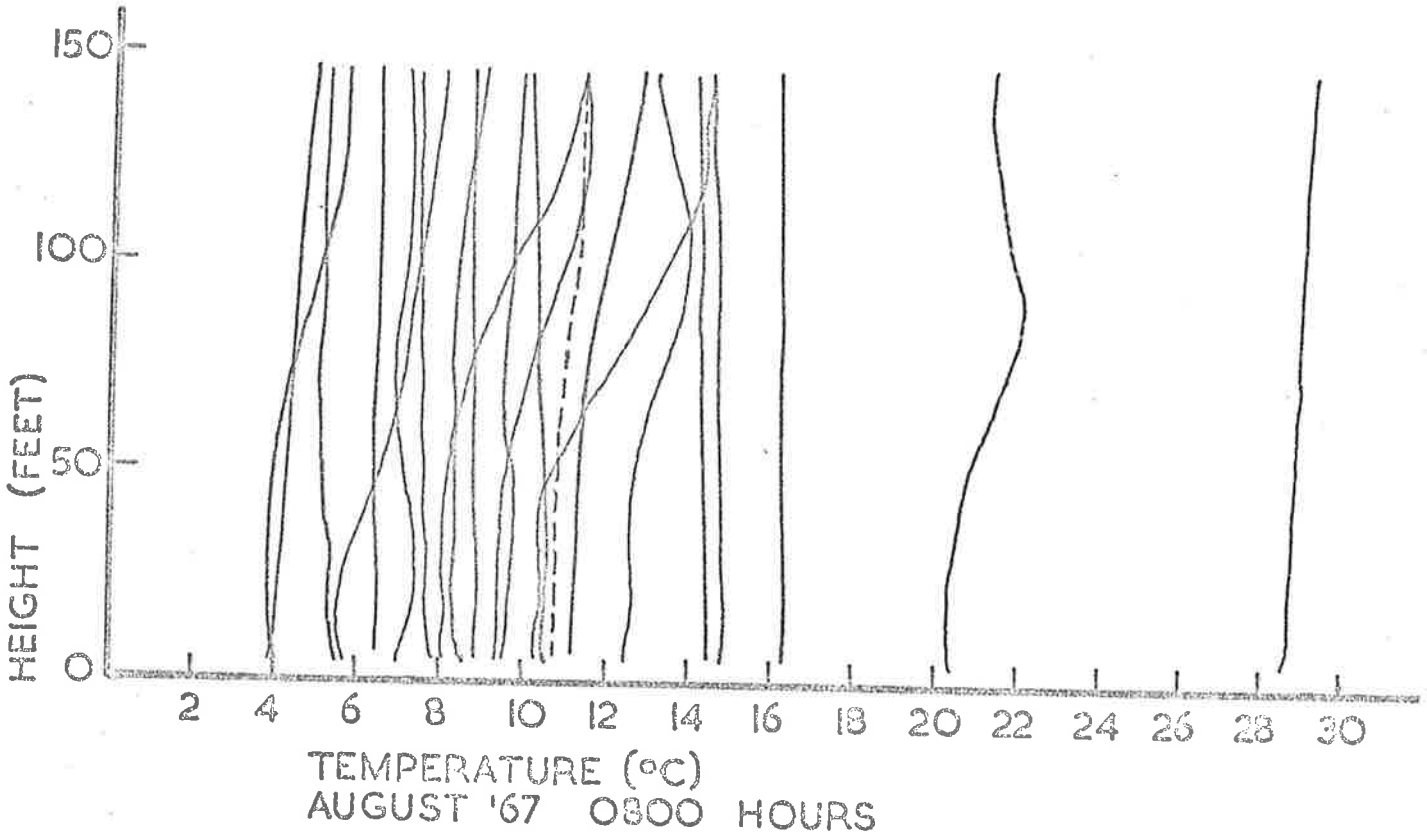

FIGURE 32. TEMPERATURE MEASUREMENTS MADE AT WOOMERA

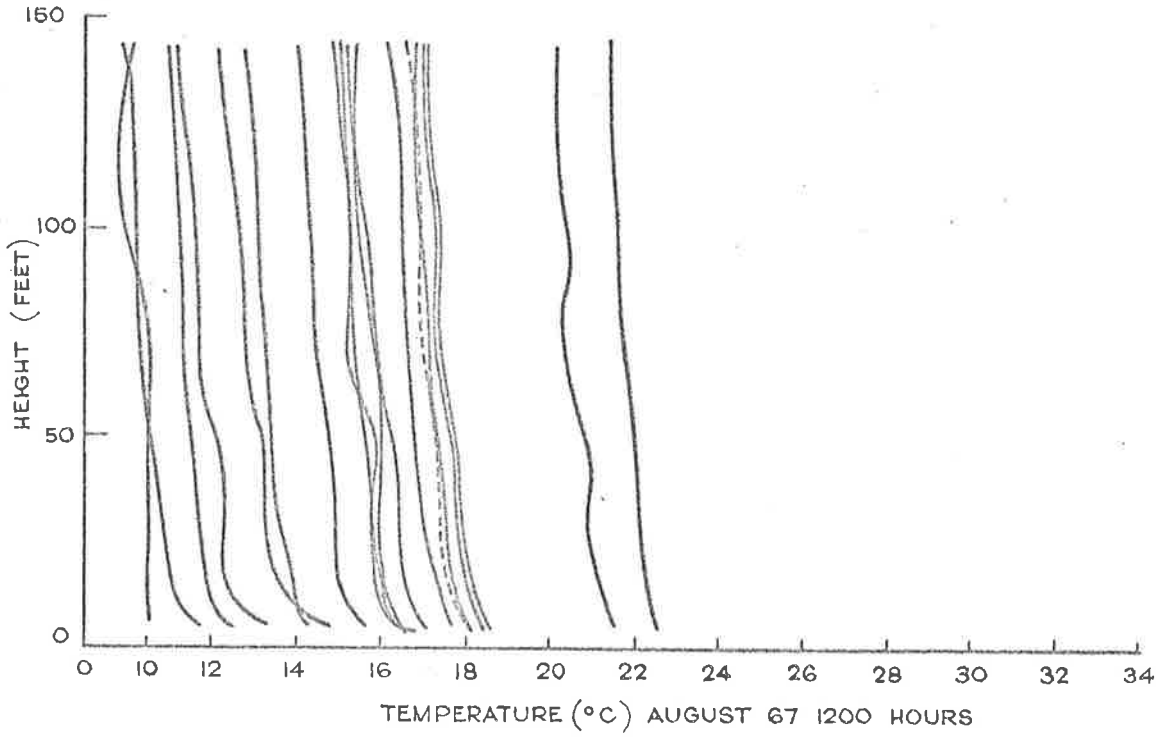

FIGURE 33 TEMPERATURE MEASUREMENTS MADE AT WOOMERA

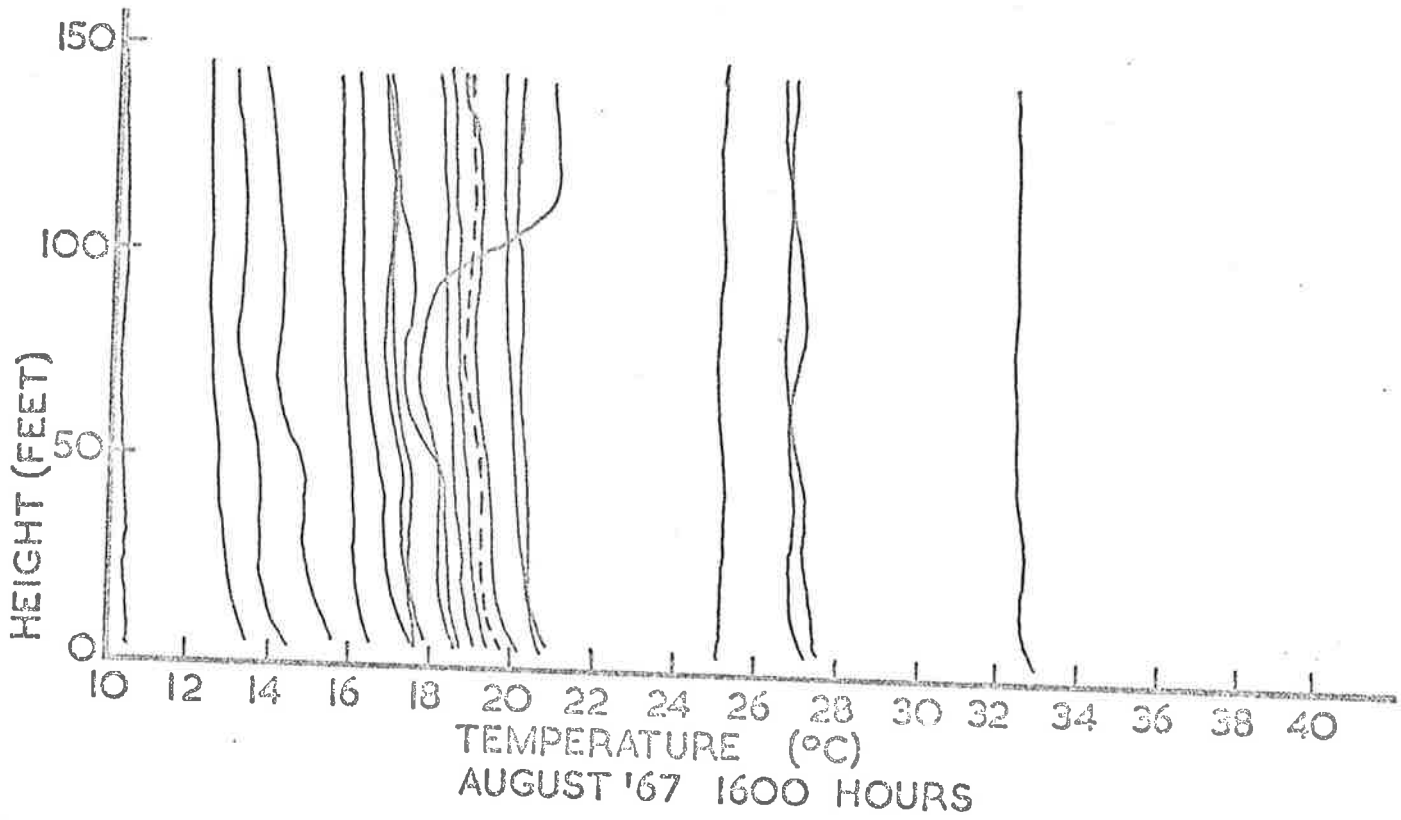

FIGURE 34. TEMPERATURE MEASUREMENTS MADE AT WOOMERA

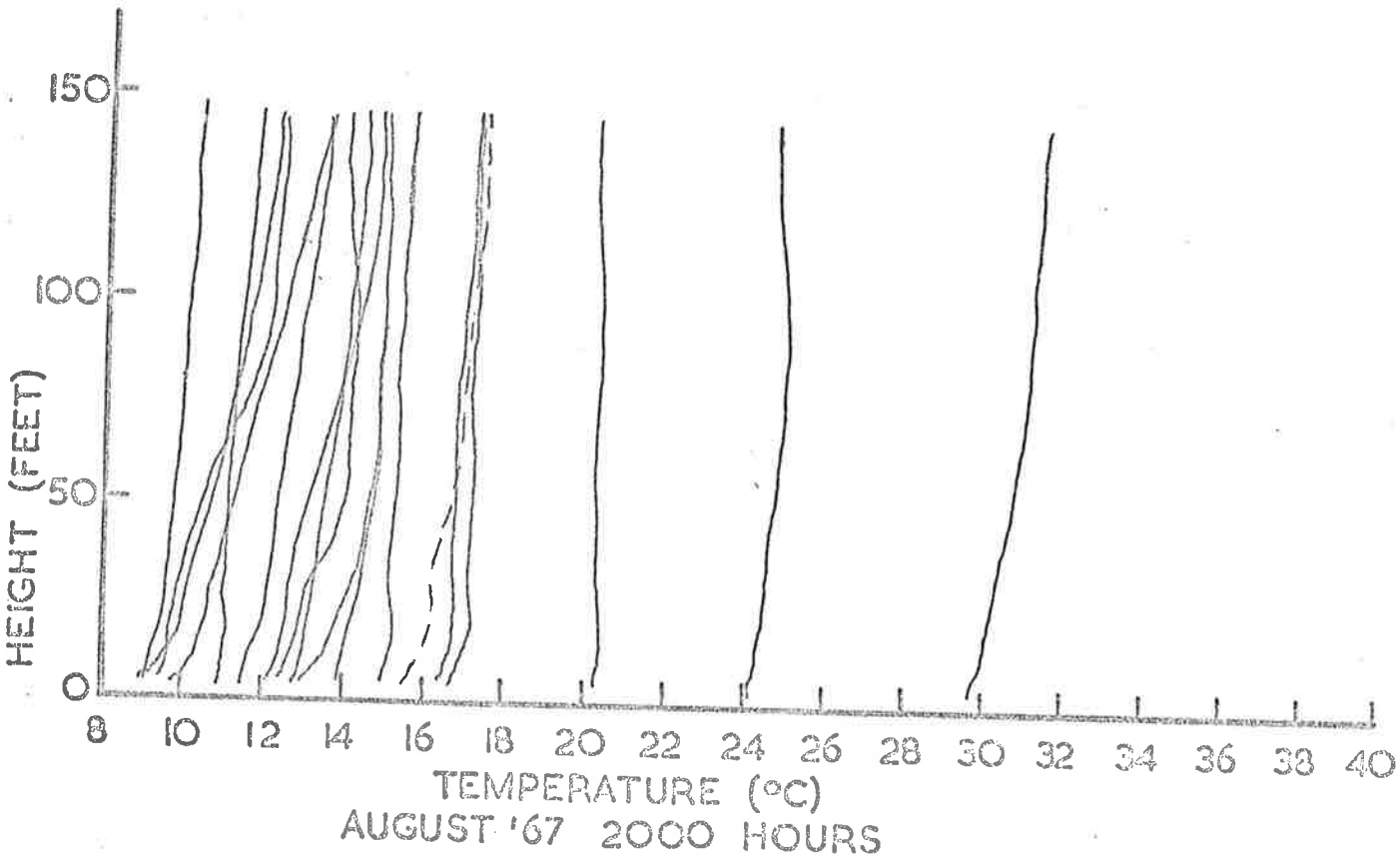

FIGURE 35. TEMPERATURE MEASUREMENTS MADE AT WOOMERA

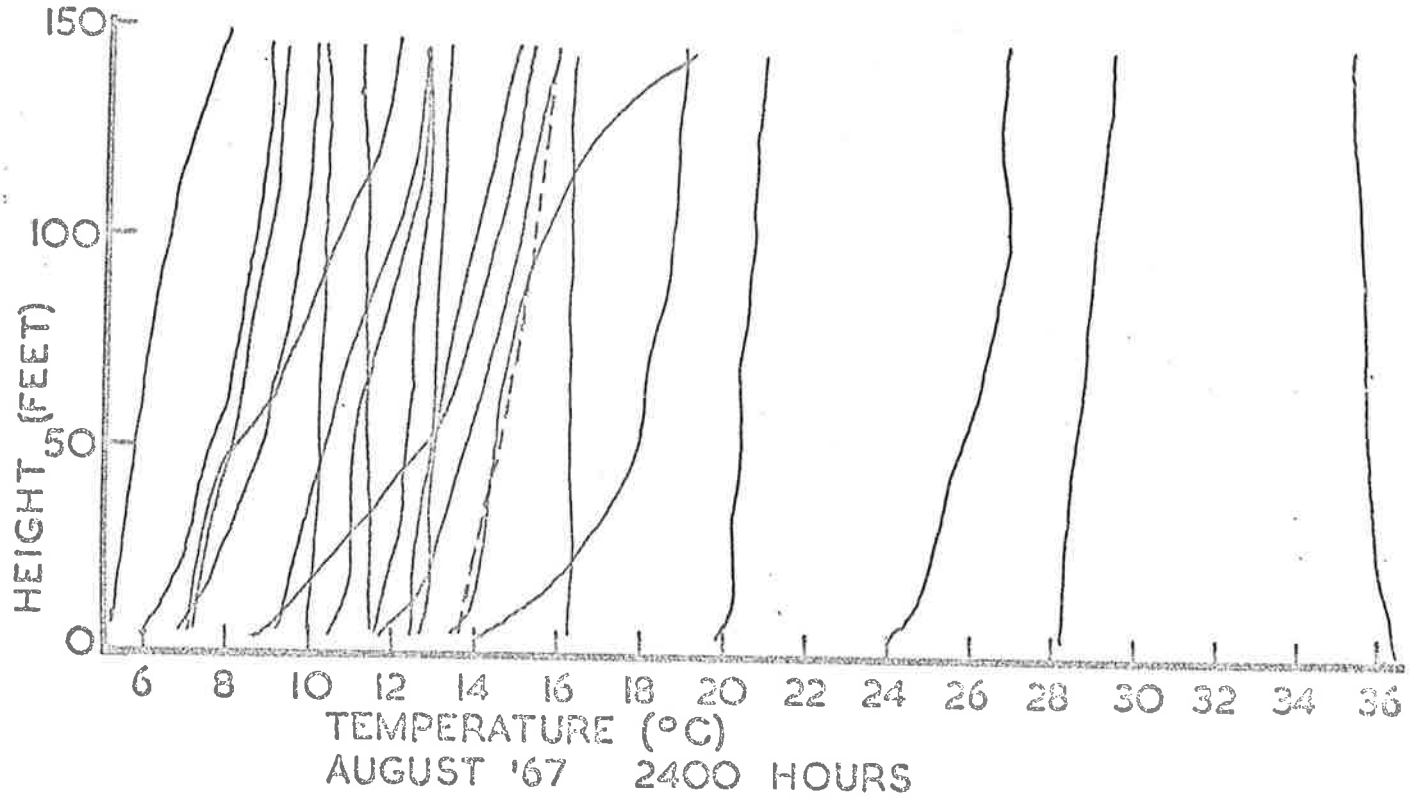

FIGURE 36. TEMPERATURE MEASUREMENTS MADE AT WOOMERA

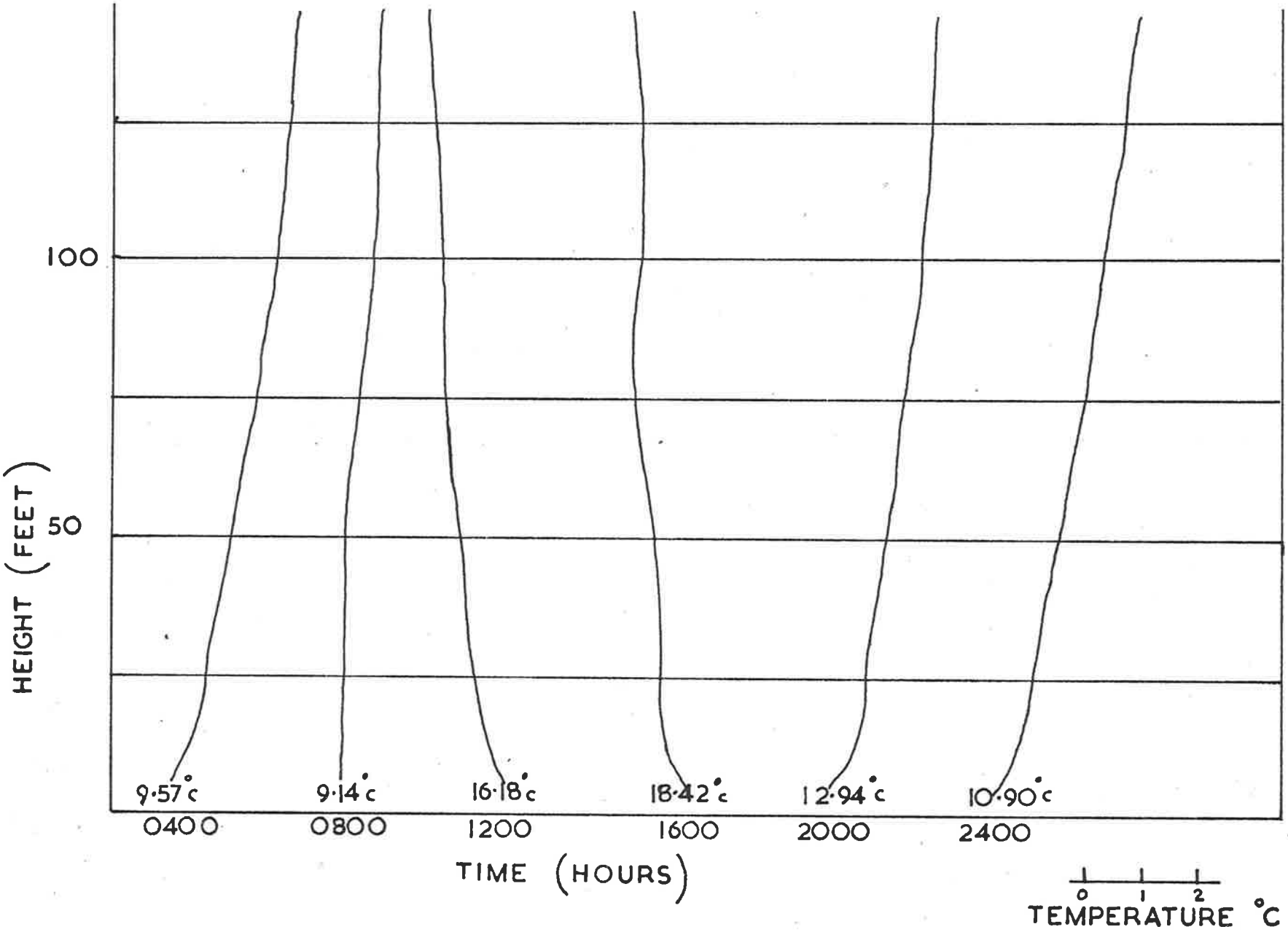

FIGURE 37. MEAN TEMPERATURE GRADIENTS AUGUST 1967.

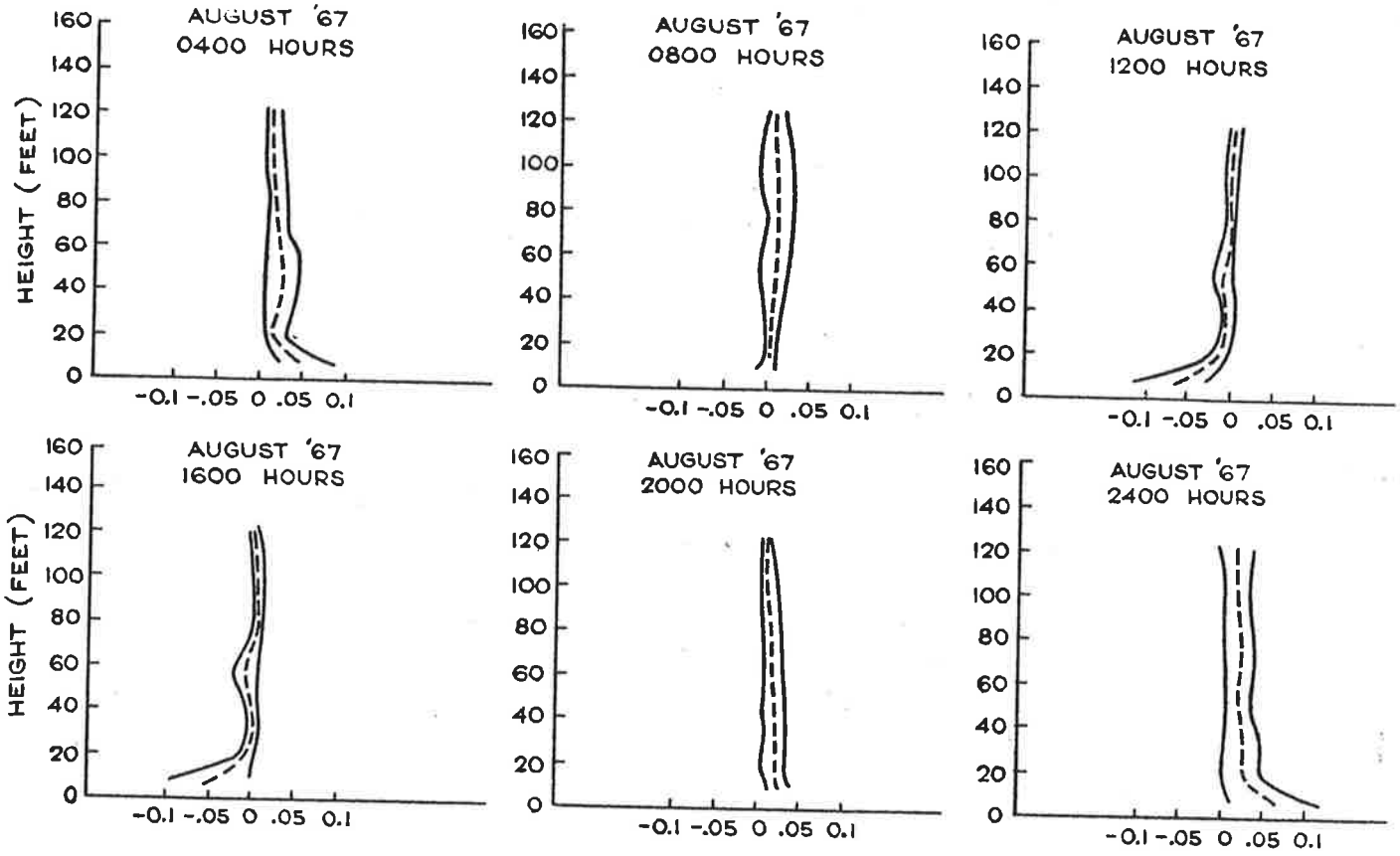

FIGURE 38 MEAN TEMPERATURE GRADIENT AND STANDARD DEVIATION

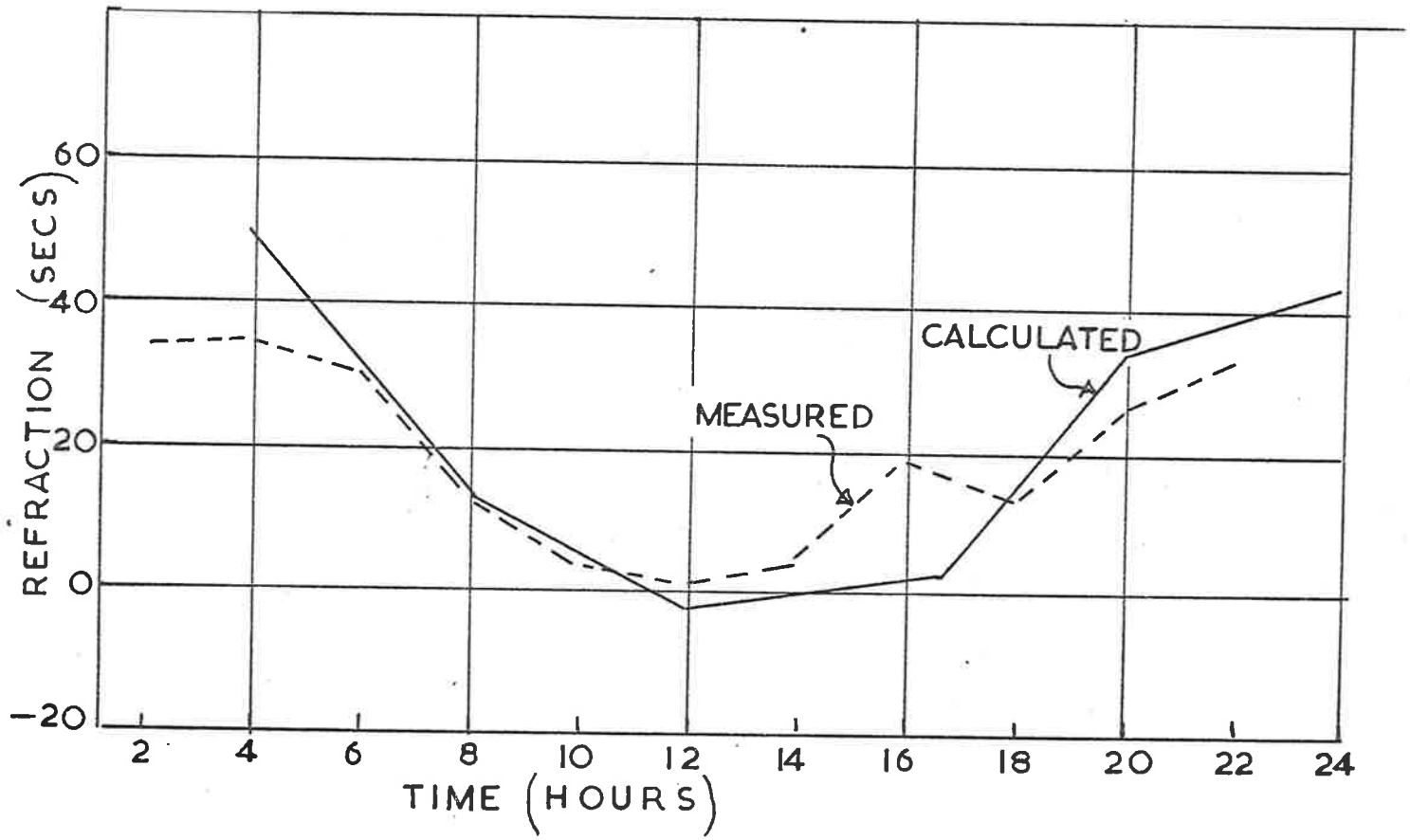

FIGURE 39. AVERAGE VALUES OF MEASURED AND CALCULATED REFRACTION IN AUGUST 1967.

mean diurnal refraction angle calculated from the nine days measurements.

Figure 40 shows the mean square error between the refraction measured during the nine days in August and the refraction calculated from temperature measurements made at the same time. Also shown is the M.S.E. between the measured refraction and that calculated from the mean temperature gradient.

The effect of this temperature profile on sightlines of varying range and elevation angle is shown in figure 41. The curves were calculated by equation 9 assuming the observer was 10 feet above the ground. Where the vertical height of the sightline was above the top of the temperature measuring mast an adiabatic temperature gradient was assumed.

4.3.1 Discussion

The refraction angles calculated from the mean temperature gradient showed good agreement with the measured values during the middle of the day, but poor agreement at night. Figure 40 shows that the M.S.E. between calculated and measured refraction was no worse in this period when a mean temperature gradient was used. At night the

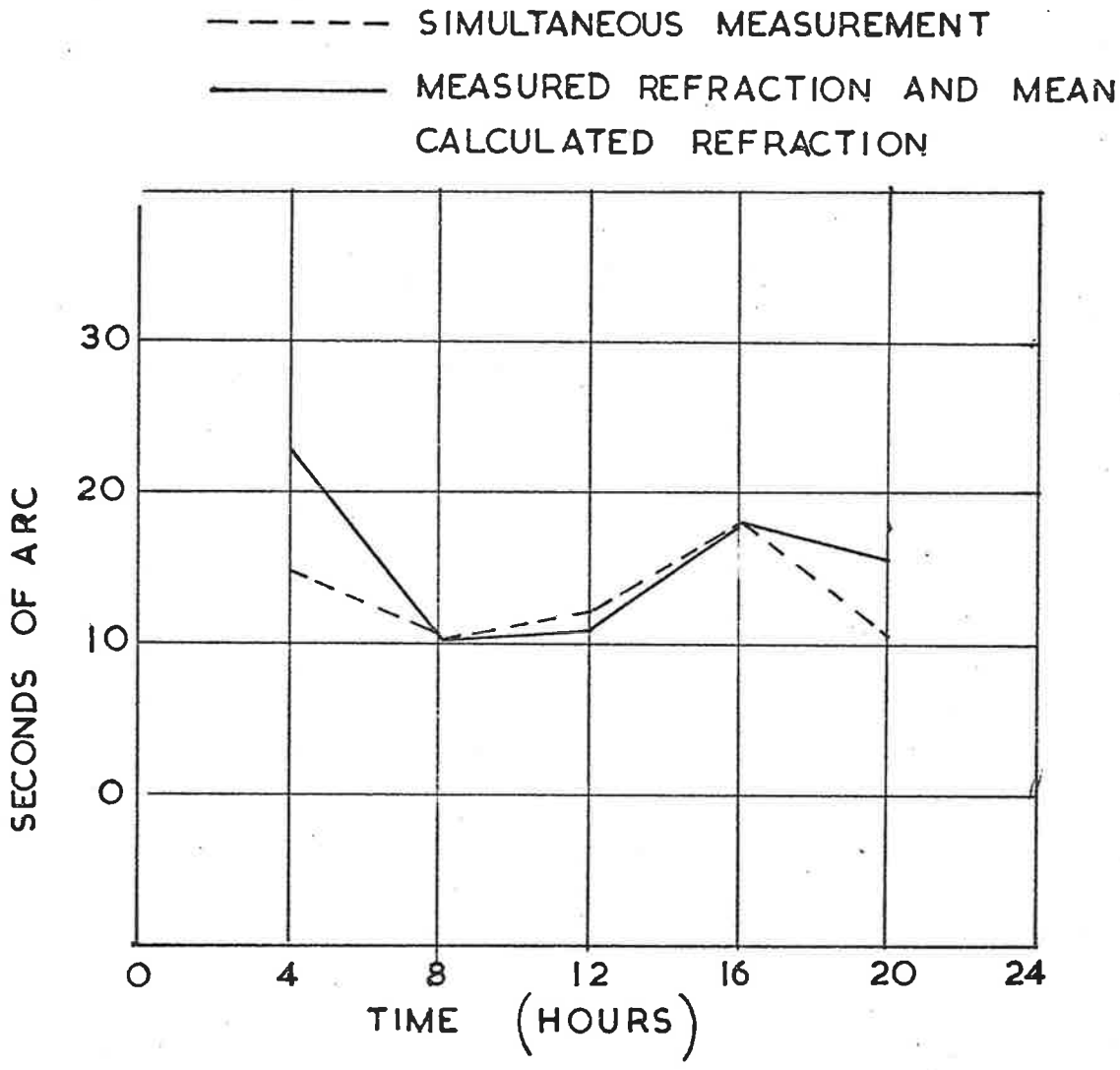

FIGURE 40. MEAN SQUARE ERROR OF MEAN CALCULATED REFRACTION FROM MEASURED REFRACTIOI

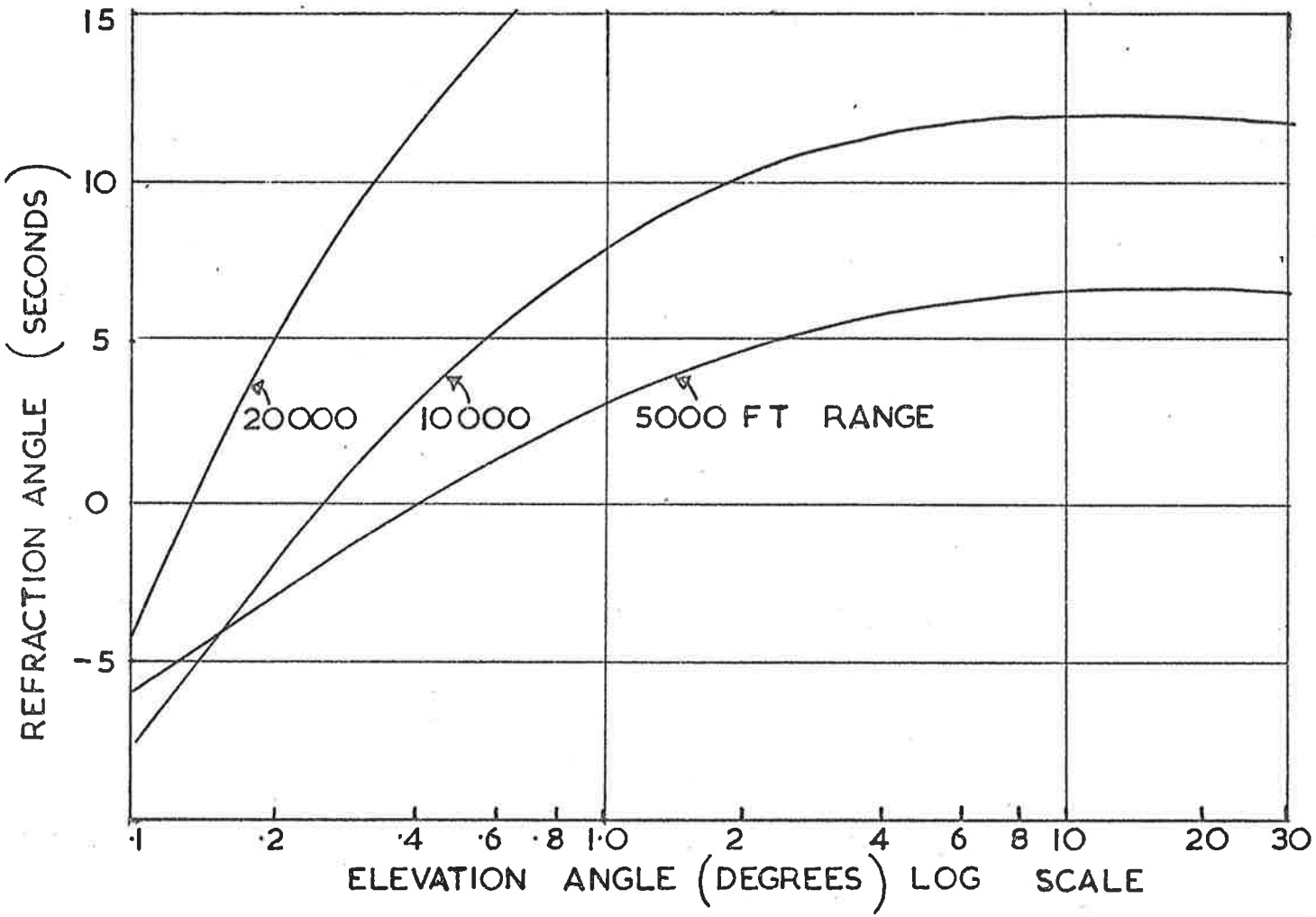

FIGURE 41. VARIATION OF REFRACTION WITH ELEVATION ANGLE

temperature measurements made when the refraction readings were taken gave a better agreement than the refraction angles calculated from the mean temperature profile.

Use of a monthly average could only be made in good weather conditions as no allowance could be made for the effect of cloud cover without a considerable amount of analysis of temperature gradients under varying conditions. A more flexible approach is to derive a mathematical model for the atmospheric temperature gradient as a function of height and time of day as described by Angus-Leppan (19). In this model the effect of cloud cover may be allowed for by altering the constants in the model.

It is proposed to continue the temperature measurements for a full year so that average values are available for each month. The large amount of record analysis involved in this work and the derivation of a temperature function is however outside the scope of this thesis.

A point of interest in figure 41 is the effect of the refractive index inversion in the lowest layers of the atmosphere. At an elevation angle of 0.2° a sightline 5,000 feet long has a refraction

angle of -5 seconds. The 10,000 foot sightline at the same elevation has a refraction angle of -4 seconds, and the 20,000 foot sightline has a refraction angle of +3 seconds at the same elevation. The reason for this apparent anomaly is that the shorter sightline lies predominantly in a region where the refractive index increases with height while the longest sightline has a considerable portion of its length in a region of negative refractive index gradient which masks the effect of the lower layers of air.

Over the three ranges which were considered in the calculations, refraction was proportional to range above about 0.6° elevation angle, and at zero elevation angle. In the region between zero and 0.6°, refraction did not always increase with range. This result illustrates the need to compute the refraction angle over the whole length of a sightline at a low elevation angle. If an average value for the refractive index or air temperature gradient is taken in conditions where a density inversion is present, the height at which the average is taken becomes very critical.

5. REFRACTOMETER

In order to check the validity of the calculated refractive index figures, and provide some portable measuring equipment, an optical refractometer was made, which measured directly changes in refractive index at a wavelength of 5461 Å. The instrument recorded refractive index changes continuously, and was sufficiently sturdy to be used while suspended under a tethered meteorological balloon.

5.1 Refractive Index Gradients in the Lower Atmosphere

Some idea of the sensitivity required from the instrument can be gained if reference is made to the relationship between refractive index (n) pressure (P) and temperature (T), at optical wavelengths in air.

To a good approximation:

$$(n - 1) = \frac{P}{T} \times 79.72 \times 10^{-6} \qquad (11)$$

where P is in millibars and T in degrees Kelvin.

In the atmosphere the stable condition is an adiabatic temperature gradient which amounts to a decrease of temperature at a rate of $3^{\circ}C/1{,}000$ ft. increase of height. Pressure decreases by 1 mb/30 ft., and combined with the temperature drop produces a refractive index drop of about $6 \times 10^{-6}/1{,}000$ ft.

Superimposed on this basic refractive index gradient is a daily cycle, caused by temperature changes due to the heating and cooling of the ground, as discussed in section 2.1

During the night the refractive index gradient is larger than the adiabatic gradient and easily measured. During the heat of the day the refractive index gradiant is reduced near the ground and a refractive index inversion often occurs. Inspection of refractive index gradients calculated from measured temperature gradients showed that the inversion near the ground was quite small and in order to see sufficient detail the instrument would need to be capable of resolving a change in refractive index 5×10^{-8}.

5.2 Description of the Instrument

5.2.1 Measuring Principle

The interferometer arrangement used in the instrument was first described by Kosters (20 & 21) and has been used more recently by Terrein (22) and Svensson (23).

The measuring system consisted of a two beam interferometer in which fringes at a suitable monochromatic wavelength were produced and photographed by a 16 mm camera. One beam passed through

a vacuum chamber effectively Lcm long while the other passed through a similar chamber, filled with air, the refractive index of which was to be measured.

The path length through the vacuum chamber was Lcm and the equivalent vacuum path of the air filled chamber was nL, where n was the refractive index of the air. Thus the difference in path length between the two beams was:

$$L(n - 1)$$

and the fringe shift caused by the introduction of the vacuum path $\frac{L}{\lambda}(n - 1)$ fringes. If the refractive index of the air changed by Δn then the interference fringes moved a distance $\Delta n.\frac{L}{\lambda}$ fringes.

The sensitivity of the refractometer is defined as the change in refractive index required to produce a movement of one fringe in the interference system. It is given by λ/L. The instrument used light of wavelength 5461Å and the sensitivity was 1.078×10^{-6} change in n per fringe.

5.2.2 Interferometer Components

The beam splitter (24 & 25) consisted of two 30°, 60°, 90° glass prisms cemented together as shown

in figure 42. The surfaces in contact were coated with a semi-reflecting aluminium film.

Collimated light from a mercury arc lamp entered one of the hypotenuse faces at normal incidence and was split into two beams by the aluminium film. The beams underwent total internal reflections at the hypotenuse faces and passed through the cell. A mirror reflected the beams back through the cell to the beam splitter, where they re-combined and passed to the camera via a lens, aperture stop, and Wratten No. 58 filter. Both the collimator and camera optical system were folded by front aluminised mirrors to reduce the physical dimensions of the instrument.

The cell is shown diagrammatically in figure 42. It had two chambers, the larger of which was evacuated to a pressure of 10^{-3}mm mercury and the other was open to the atmosphere. The optical images of A and D (figure 42) coincide and the interference fringes produced are displaced by changes in the refractive index of the air. The images of B and C also coincide and the fringes formed are used as reference fringes.

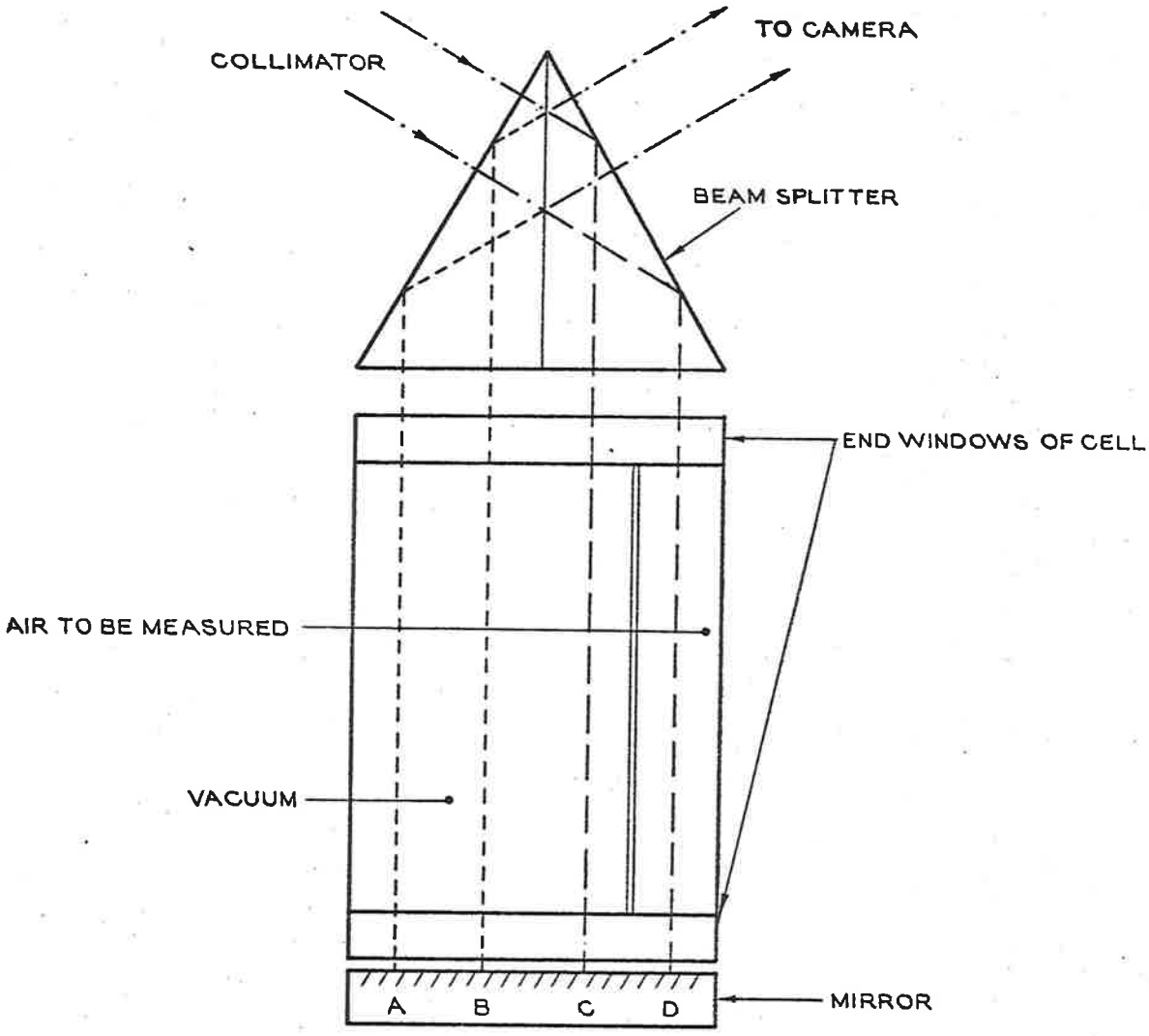

FIGURE 42. INTERFEROMETER ARRANGEMENT SHOWING THE INTERFEROMETER CELL

Tilt fringes were introduced into the system by means of a wedge incorporated in one side of the beam splitter. The construction of the instrument is shown in figures 43 and 44.

The interferometer components were all mounted on the stainless steel cell assembly which consisted of two coaxial tubes joined by end plates. The beam splitter was cemented into a stainless steel holder which was screwed to the top end plate of the cell. The mirror was cemented to a mounting plate which was spring loaded against three adjusting screws at the bottom end of the cell.

The lamp, collimator, and camera lens systems were all mounted in a light tight aluminium alloy box screwed to the beam splitter holder at the upper end of the cell assembly. The camera was mounted on top of the box, and a radiation shield to protect the cell from solar radiation was mounted from the bottom. The shield consisted of a white painted resin bonded paper tube. In the bottom of the tube was a fan driven by a 9 volt d.c. motor to draw air through the refractometer from a row of holes located near the top of the shield. The air was drawn through the tube at approximately 2 ft/s.

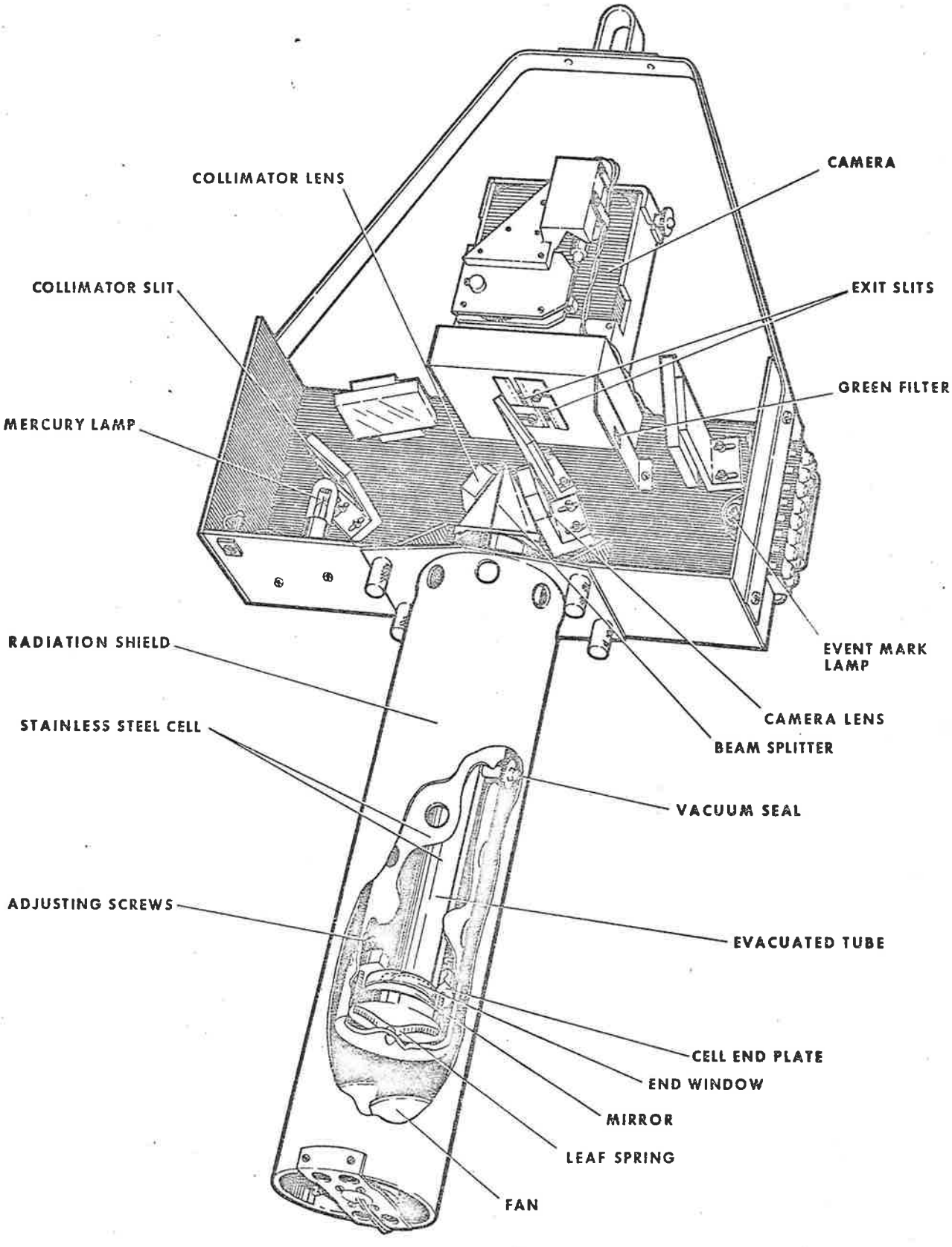

Neg. No. D67/319

FIGURE 43. GENERAL ARRANGEMENT OF REFRACTOMETER

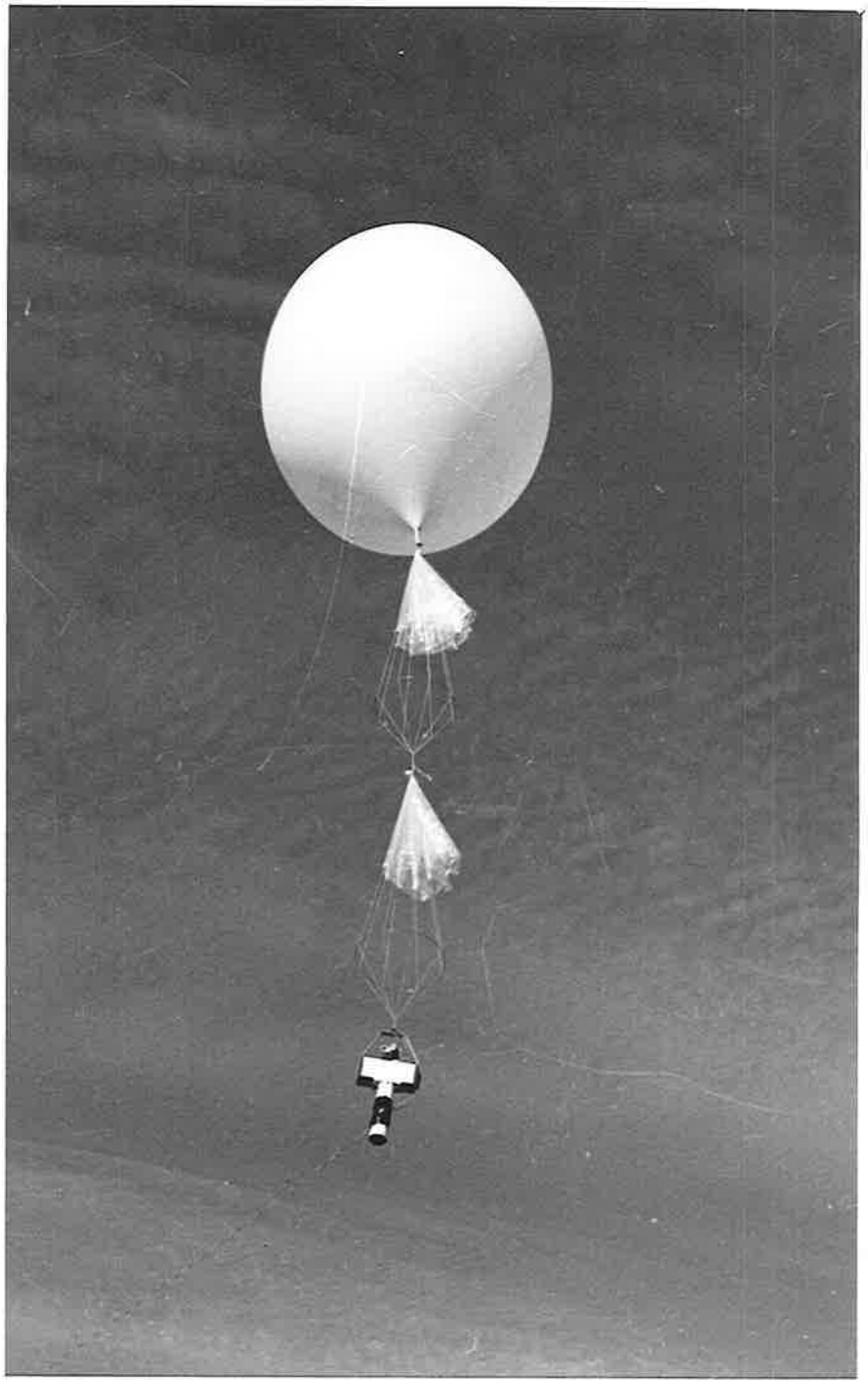

FIGURE 44 REFRACTOMETER LIFTED BY A TETHERED WEATHER BALLOON

When in use, the instrument was hung from a single suspension point and was pendulus with a natural frequency of 3/4 hertz. In this position (figure 43) the cell assembly was supported from its top end and was not in contact with any other part of the refractometer. This method of mounting reduced distortions of the interferometer components when the temperature of the structure changed. The cell was sufficiently stiff that only small deviations of the fringe system occurred when the instrument was allowed to oscillate about its suspension point.

This method of assembly and suspension proved very satisfactory and the interference fringes were stable even when the equipment was being used in 25 miles/hour winds. The refractometer was subjected to several hard knocks, intentional and otherwise, but no damage resulted and only slight adjustment of the interference fringes was necessary. The total equipment weight was 8.2 lb.

5.2.3 Camera System

The camera was a 16 mm cine magazine modified so that the film was driven at a constant speed by a 9 volt d.c. motor working through reduction gearing.

The film speed was controlled to about 8 inches per minute by adjustment of the motor current. Plus X negative film was used.

The complete field of view at the film plane is shown in figure 45(a). To record fringe movements continuously two 0.043 inch slits were placed in front of the slowly moving film as shown in figure 45(b). Half the film width was occupied by the reference fringes and the other half by the measuring fringes. Figure 45(c), shows the effect on the film when the refractive index increased at a rate of 5×10^{-6} per second. In practice, much smaller changes occurred.

When required, an event mark was recorded, by illuminating the exit slits with white light from a tungsten filament lamp.

5.2.4 Auxillary Equipment

The lamps and motors were run from a 24 volt battery supply on the ground. Three wires were necessary to run the equipment. These were wound on a geared winch and power was supplied to them through slip rings. The electrical circuits are shown in figure 46.

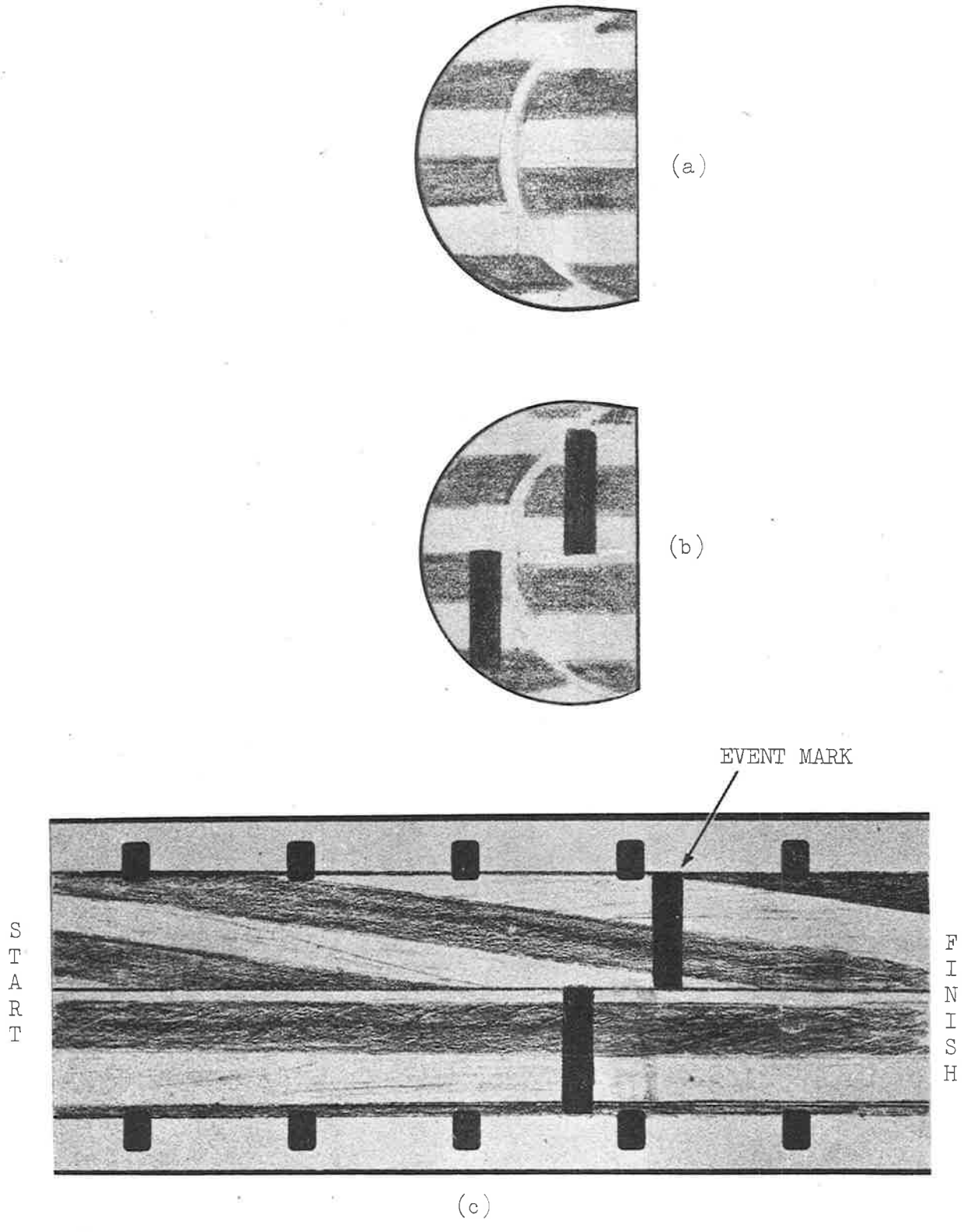

FIGURE 45. FRINGE MOVEMENT RECORDING SYSTEM

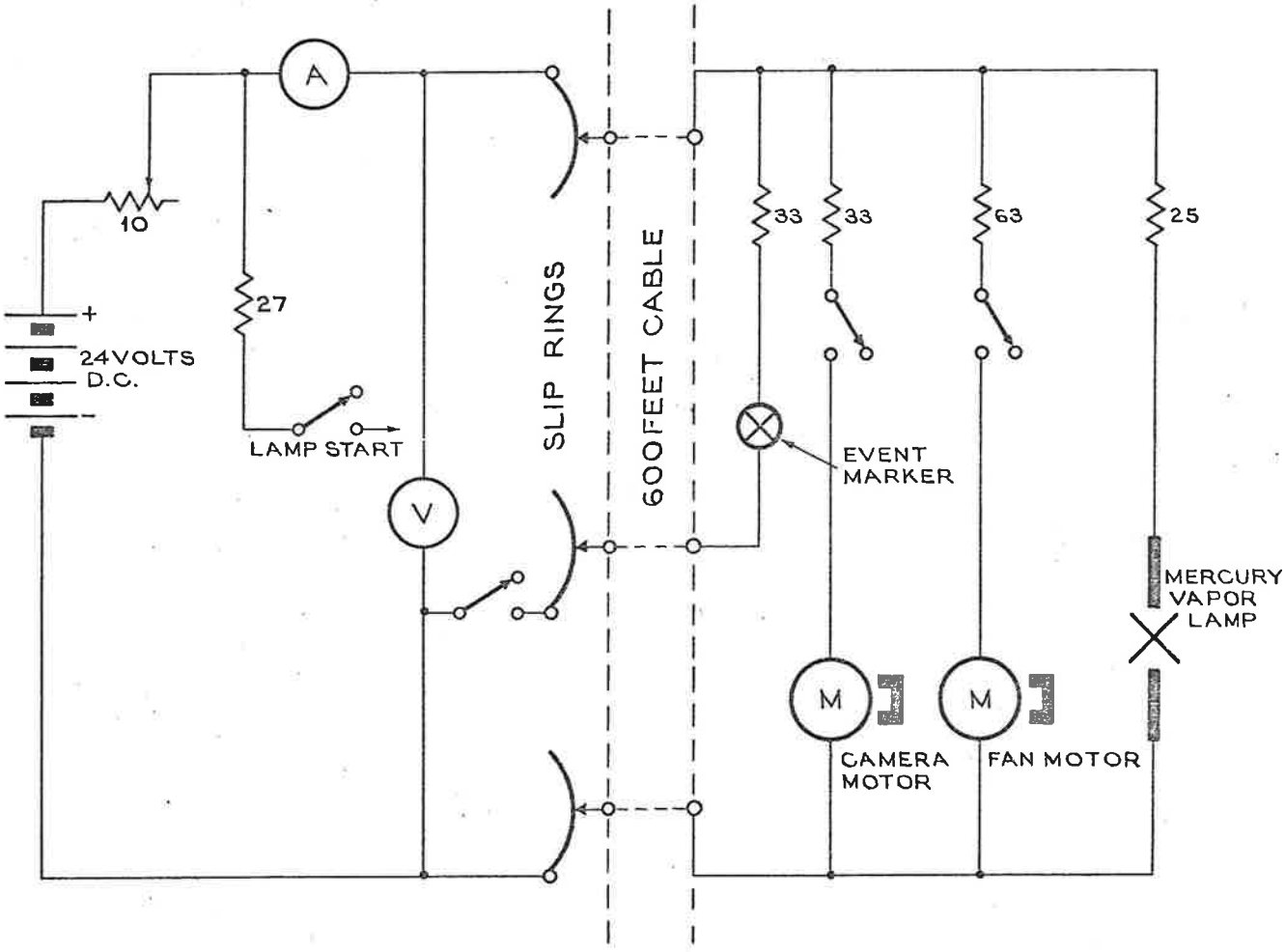

FIGURE 46. REFRACTOMETER ELECTRICAL SUPPLIES

5.3 Measuring Procedure

5.3.1 Method of Use

The instrument was lifted in steps above the ground while supported from a tall mast, crane, or tethered balloon. The step lengths were varied from 10 to 20 ft near the ground, where the refractive index changed rapidly, to about 30 or 40 ft at heights of 100 ft or more, where the refractive index change was more regular. The camera was run both ascending and descending, and after each change in height the instrument was held stationary for 10 seconds so that a sample of air could be drawn through the cell. The instrument measured the change in refractive index and the absolute value was calculated from temperature and pressure measurements. Several runs were needed to give a representative profile as local variations in the refractive index occurred.

5.3.2 Measurement of films

When the instrument was suspended in the air, motor vibrations caused some blurring of the interference fringe records. Under these conditions the fringe movements on the film could be determined

to 1/20 of a fringe, which is equivalent to a refractive index change of 5.4×10^{-8}.

Movements of the interference fringes which monitor refractive index were measured in relation to the reference fringes rather than the edge of the film. This eliminated errors due to instabilities in the mirror systems or distortions of the refractometer body, which could cause the image forming rays of both fringe systems to be deviated.

The films were read with a "Peak" 7 X magnifier which consisted of a Ramsden type eyepiece with a calibrated graticule. The measuring procedure was as follows:-

(a) The fringe spacing was determined by measuring from one fringe to the same position on the next fringe.

(b) The distance from a reference fringe to a suitable refractive index monitoring fringe was measured on the film taken at ground level.

(c) At each subsequent height, the same measurement was made until ground level was reached again.

(d) Multiplication of the number of fringes of movement by 1.078×10^{-6} gave the change in refractive index.

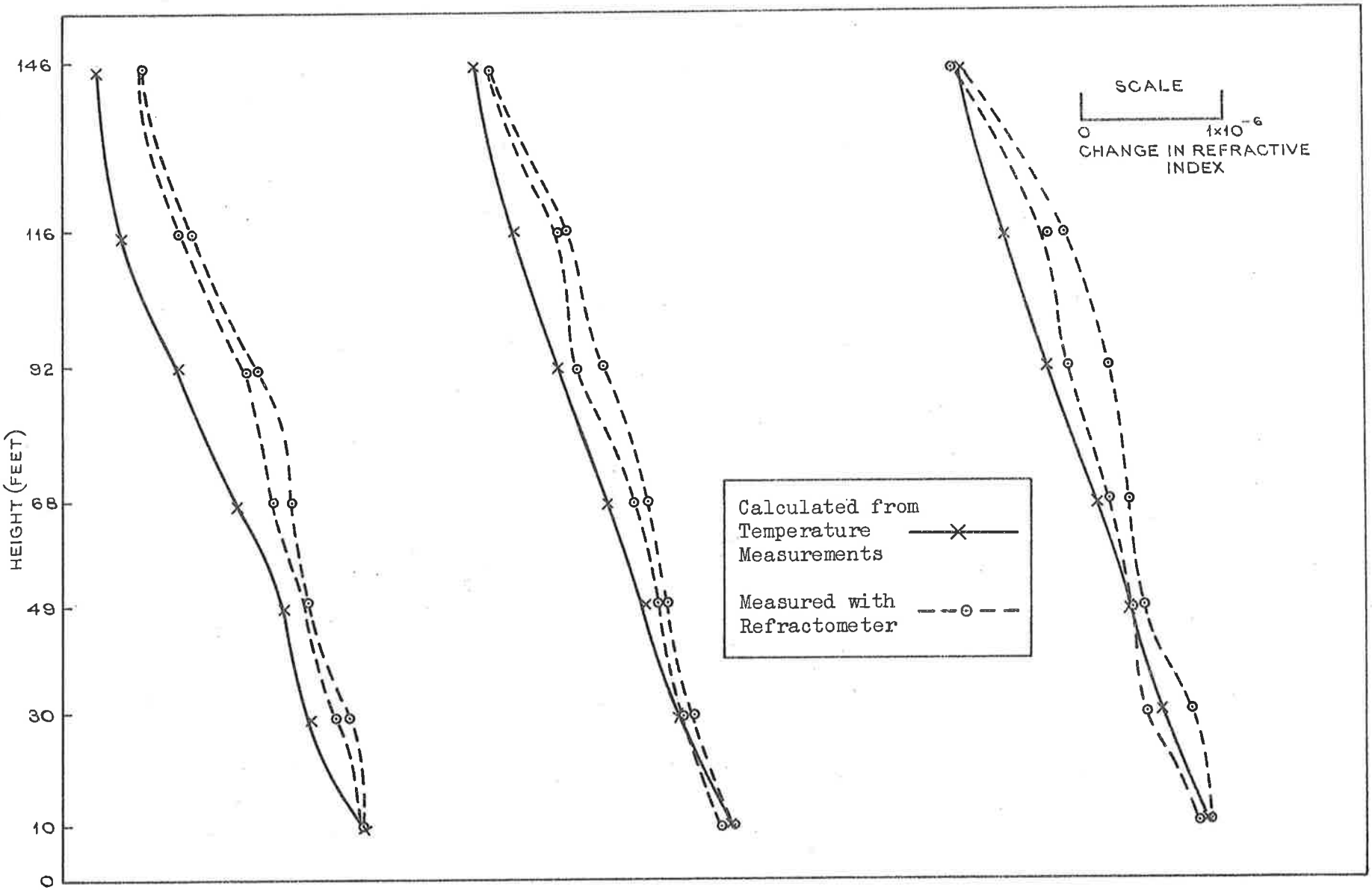

FIGURE 47. REFRACTIVE INDEX MEASUREMENTS TAKEN AT 1530 HOURS ON 8/8/67 AT WOOMERA

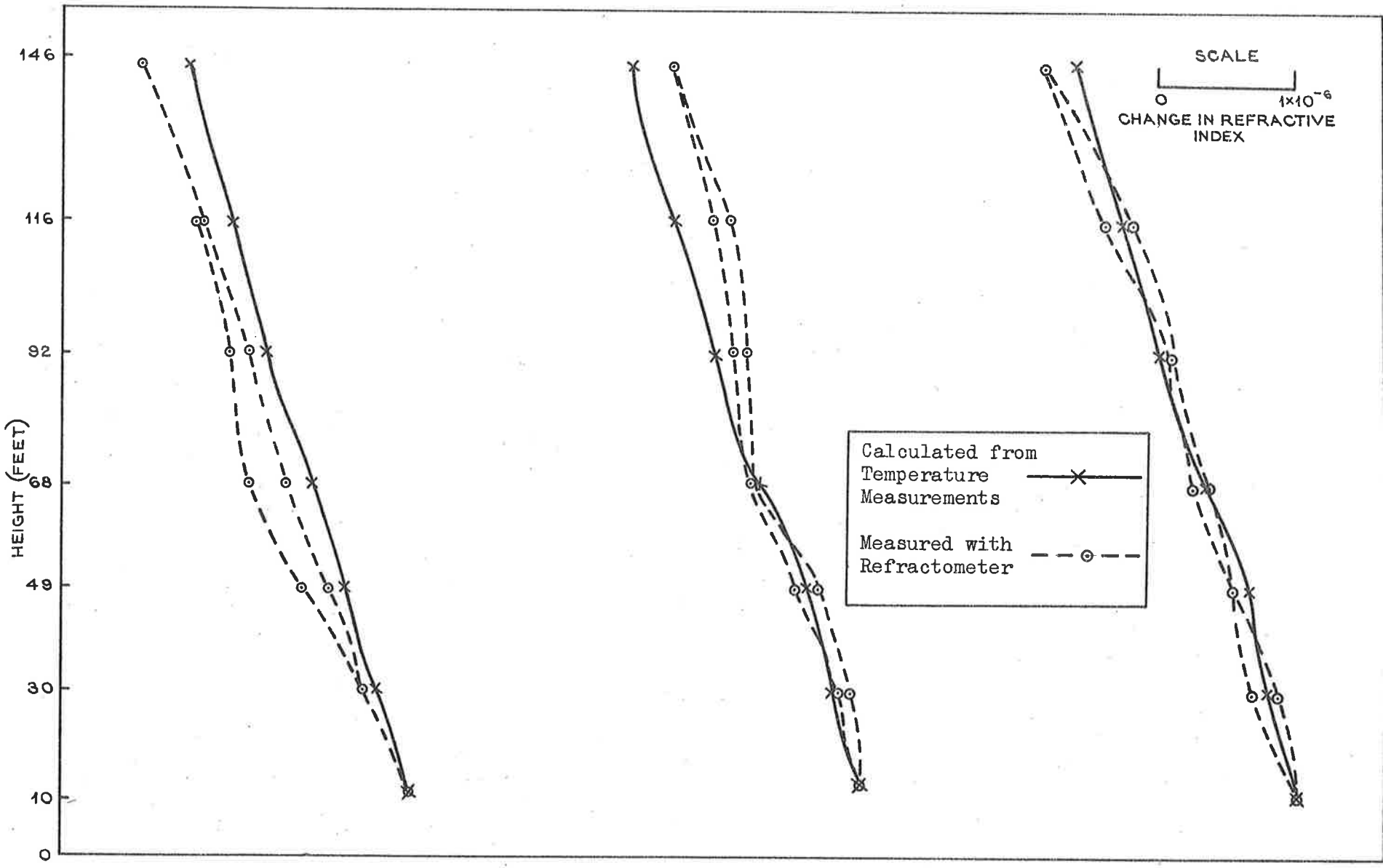

FIGURE 48 REFRACTIVE INDEX MEASUREMENTS TAKEN AT 0920 HOURS ON 9/8/67 AT WOOMERA

5.3.3 Refractive Index Measurements

Figures 47 and 48 show some refractive index measurements made at Woomera, compared with calculated values of refractive index derived from temperature measurements.

For the tests the instrument was operated from the 150 ft mast described in section (1). The refractive index was calculated by equation 11, and the pressure gradient was assumed to be 1mb/30 ft.

The refractometer was winched up and down the mast and an event mark was put on the film at each thermocouple junction position. Each round trip took approximately five minutes. The films were read to give the refractive index change over the height interval separating the junction positions. Figures 47 and 48 show two sets of three runs, taken at different times of day in cool sunny weather. Each set was measured in a fifteen minute period.

Owing to the slow time response of the thermocouples (about 1 deg/min) the calculated refractive index graphs remain substantially the same during the 15 minutes when the refractometer was in use. The refractometer results display small variations, as the instrument had a respons time of about one second, and was effected by the small temperature changes which the thermocouple equipment was designed to ignore.

5.4 Calculation of Refraction from Refractometer Measurements

In order to assess the usefullness of the refractomete in the field, it was used in conjunction with the refrac-

tion monitor described in section 3 to measure the refractive index gradient while measurements of refraction were being made.

Two methods of calculating refraction were used. The first was the ray trace method described in section 2.3, and secondly the refraction was calculated in terms of the ray path by equation 4.

5.4.1 Measurements

During one day in August 1967 the refractometer was used to measure the refractive index gradient at the temperature measuring mast every two hours throughout the day. The measuring procedure was as described in section 5.3.1. Figure 49 shows the refractive index gradients measured during the day.

5.4.2 Ray Trace Calculation

The smallest change in refractive index which could be resolved by the refractometer, 5×10^{-8}, was chosen as the layer thickness for the ray trace calculation. The height at which the layer boundaries were crossed was estimated from figure 49. Cards were punched with refractive index and height information and the computer programme shown in Appendix IV used to perform the ray trace calculation. Output from the computer was the total deviation of the ray. The refraction angle was by definition

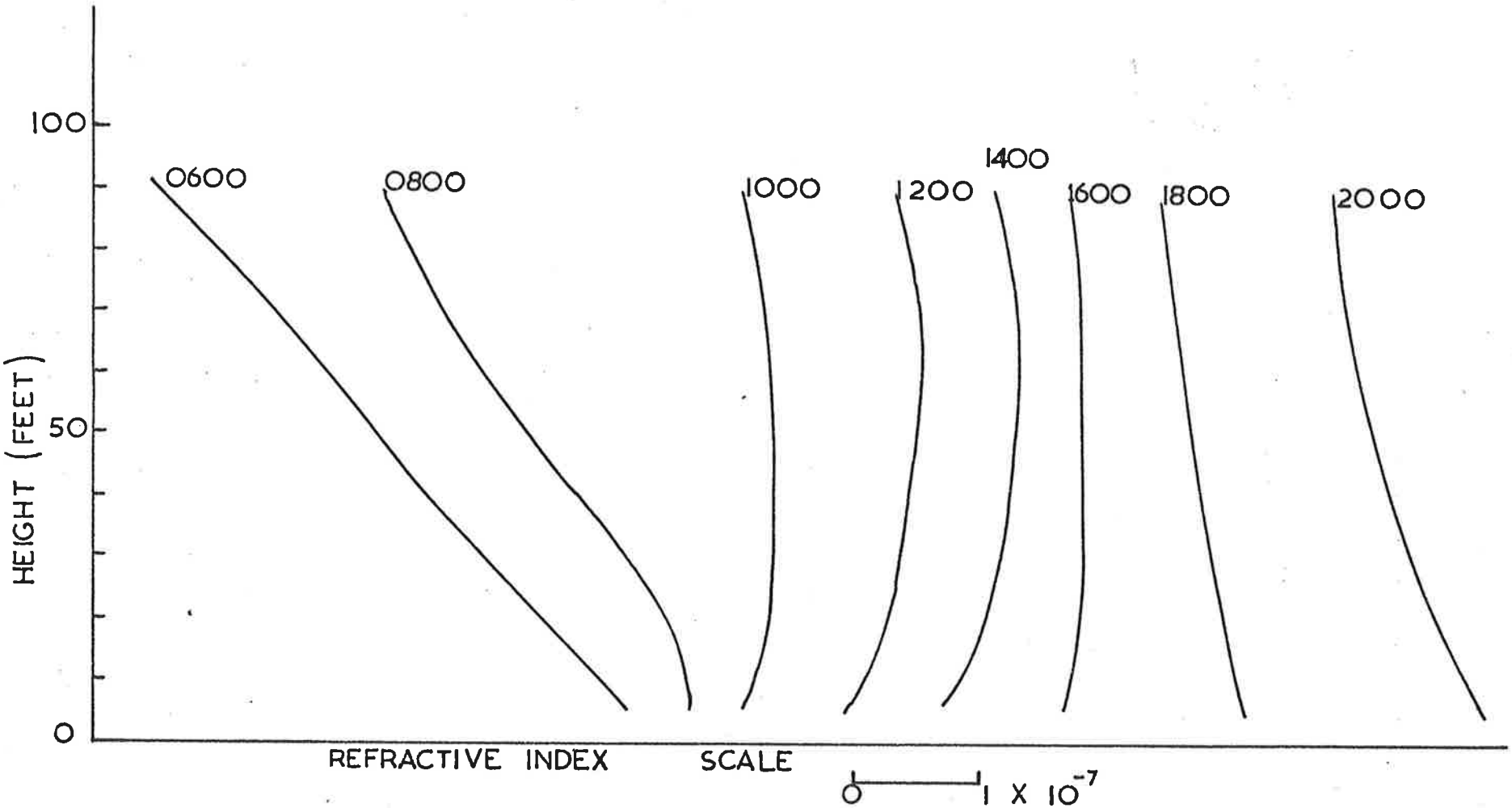

FIGURE 49. REFRACTIVE INDEX PROFILES MEASURED ON 17/8/67

half this angle. The measured and calculated refraction angles are shown in figure 50.

5.4.3 Curvature of Ray Path

In calculating the curvature of the ray path a similar treatment to that used for the temperature measurements was used. A simple straight line representation for the ground under the sightline was used as in the case of equation 5.

The refraction angle was given by equation 6.

$$E = \frac{1}{X}\int_{o}^{x} (X - x)\, F(x)\, dx$$

where $F = B.\frac{dn}{dz}$ from equation 4.

Then

$$E = \frac{Bx}{(z_2 - z_1)^2}\int_{z_1}^{z_2} ndz \text{ seconds}$$

in this case $B = \frac{-2.0618 \times 10^5}{T}$

The refraction angle was evaluated with a computer programme similar to that shown in Appendix II. Refractive index figures were read in for heights up to 100 feet above ground and an interpolation formula was used to calculate the refractive index at 2 foot intervals between 10 and 42 feet above ground. Simpson's rule was used to

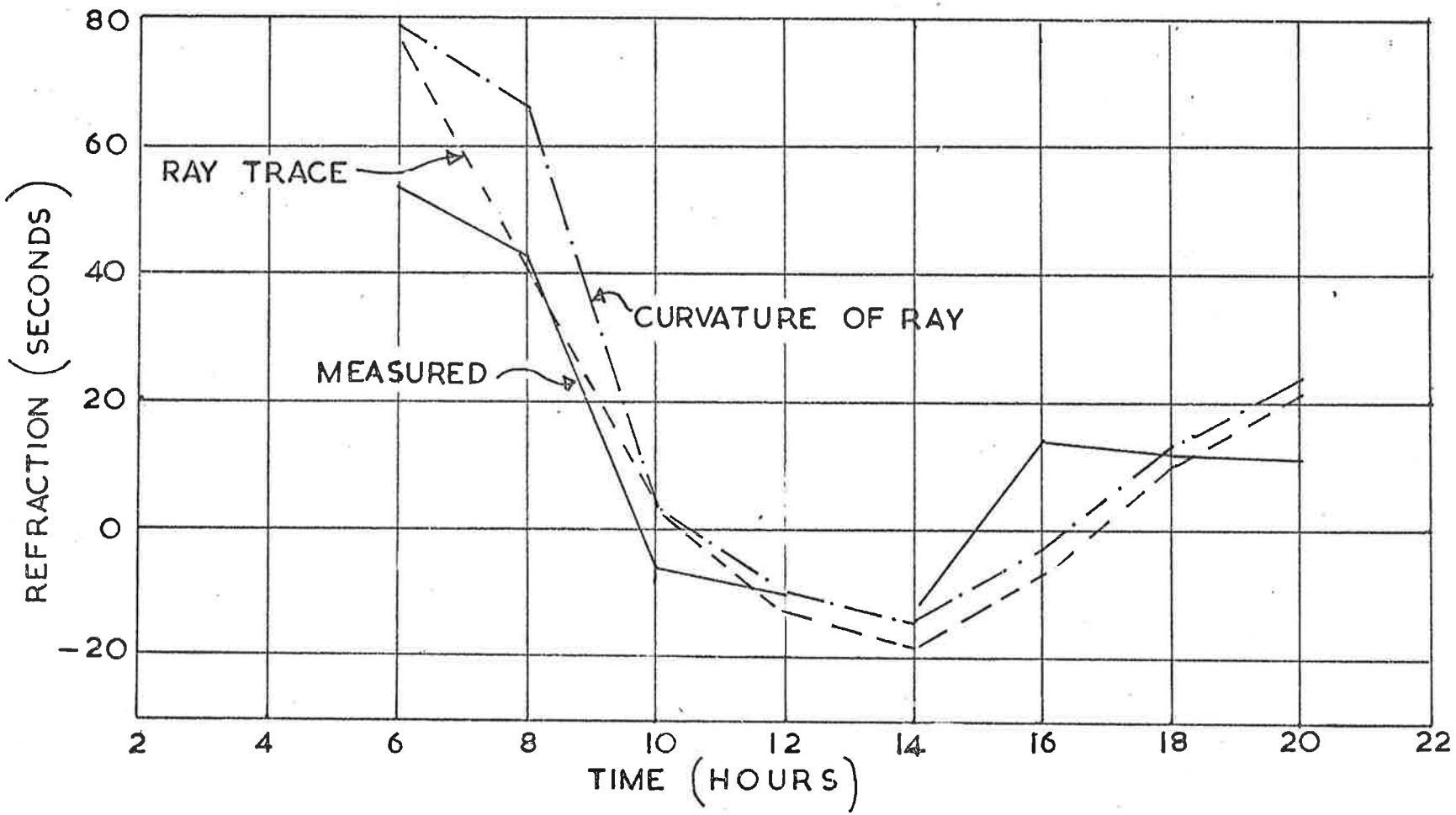

FIGURE 50. MEASURED REFRACTION AND REFRACTION CALCULATED FROM REFRACTOMETER MEASUREMENTS

evaluate the integral.

Figure 50 shows the refraction angles computed by this method together with the value measured by the refraction monitor.

5.5 Errors

Sources of error in the instrument were changes in the cell length caused by thermal expansion and changes in the atmospheric pressure, which caused small movements in the measuring fringes but did not effect the reference fringes. Also, the cell distorted due to uneven heating, and the fan produced a small pressure reduction in the measuring space.

5.5.1 Changes in the Temperature of the Refractometer Cell

The difference in optical path length between the vacuum and air paths through the cell was given by:

$$\frac{L}{\lambda}(n - 1) \text{ fringes}$$

When the temperature of the cell rose, the effective length increased by a factor of 10^{-5} per degree centigrade. Thus the path length difference altered by:

$$\frac{L}{\lambda}(n - 1) \times 10^{-5} \text{ fringes}$$

When $L = 50.72$ cm $\lambda = 5461 \times 10^{-8}$ cm and $n = 1{,}00292$ the path length difference changes by 2.7×10^{-3} fringes per degree centigrade.

Since the resolution of the instrument corresponded to 1/20th of a fringe, this error was negligible.

5.5.2 The Effect of Air Pressure Changes on the Length of the Cell

A height rise of say 500 ft produced a pressure reduction of about 16 mb, which caused a reduction in stress along the cell of 16×10^{-3} dynes/cm^2.

Assuming that the Young's modulus of the steel cell walls is 20×10^{11} dynes/cm^2 the change in strain along the cell is 8.3×10^{-9}. For a cell length of 25.4 cm this amounts to a change in length (ΔL) of 21×10^{-8} cm.

Thus the fringe shift produced by the pressure reduction is $(n - 1)\frac{\Delta L}{\lambda} = 1.22 \times 10^{-7}$ fringes, which may safely be ignored.

5.5.3 Distortion of the Cell

When the cell bent, the fringe system rotated, and the fringe spacing altered. This was recorded on the film as a movement of both the reference and the measuring fringes. Thus it was possible to reject those records where it occurred. In fact providing the refractometer was allowed half an hour to warm up to the ambient air temperature, no serious cell bending occurred.

If the refractometer was allowed to swing violently about its suspension point, the cell distorted and a slight wavering of the film record was produced. Normally the drag of the power supply cables was sufficient to damp out any such oscillations.

5.5.4 Pressure Reduction Due to Fan

The action of the fan which drew air through the cell caused a slight depression of the air pressure in the refractometer. The air flow was kept as slow as possible but there remained an error of 1/6 fringe between "fan on" and "fan off". All readings were therefore taken with fan on.

5.6 Discussion

The refractometer proved to be a workable method of measuring the refractive index gradient in the atmosphere. Expected problems due to solar radiation were overcome by shielding the interferometer components and making the cell assembly a stiff single unit supported only at its top end. When this had been done the interference fringes remained quite stable after an initial period in which the components warmed up to the air temperature. The Kosters beam splitter arrangement also helped the temperature stability as the light paths of both beams were symmetrical, and they travelled

almost the same distance through glass.

The camera system was a cheap and easy method of recording all movements of the interference fringes but careful film reading was necessary to obtain the refractive index gradient to the desired accuracy.

Of the errors which were considered, none were large enough to affect the results significantly.

Providing the average of several measuring runs with the refractometer were used, the calculation of the refraction angle gave very similar results to those obtained from the temperature measuring equipment. The ray trace results were comparable with the results from the curvature equation and showed similar trends. The main problem with the refractometer was the labour involved in using it and the considerable care needed in measuring the films and plotting the results.

In calm conditions the instrument was used successfully supported by a tethered meteorological balloon, but for all the measurements discussed in section 5.4 it was operated from the temperature measuring mast as the height could be controlled more easily.

6. CONCLUSIONS

A survey of atmospheric refraction angles on a fixed sightline in typical Australian inland conditions has been conducted. The diurnal variation of refraction was remarkably constant throughout the year. In daylight hours refraction was usually small both in clear and cloudy weather. In the afternoon and evening in clear weather it slowly increased and at night large refraction angles were measured. At dawn the refraction angle dropped quickly to its day time value. In the presence of cloud cover much smaller night time refraction angles were measured.

Two methods of determining the vertical gradient of refractive index in the atmosphere were used. The easiest and most reliable method was to measure the air temperature gradient, assume a pressure gradient and hence calculate the refractive index gradient. The refractive index gradient was also measured directly with a refractometer which was constructed so that it could be used in the open atmosphere in the heat of the day. The refractometer was more complicated than the thermoelectric equipment. It needed more careful handling and more detailed analysis of the records was necessary to calculate the refractive index gradient. However the refractometer had the advantage that it could be used to measure the refractive index gradient in any location, providing the wind speed was low enough to allow it to be lifted by a gas filled balloon.

It has been shown that measurements of the air temperature gradient could be used to compute the refraction angle on a sightline. The measurements of temperature gradient were still useful even when the sightline was several miles from the temperature measuring site. If

simultaneous optical and temperature measurements were not available, the average temperature gradient taken over a period of a month in similar weather conditions could be used to calculate the refraction angle during the day with good accuracy. At night poor agreement was obtained when the mean temperature gradient was used as large variations of temperature gradient occur from place to place after dark. The effect of the day time mean temperature gradient on sightlines other than those used in the correlation experiments was calculated. The results from this analysis indicated that in hot daytime conditions the refraction angle on a sightline at an elevation angle of less than about 1^{o} did not necessarily increase with range. Above 1^{o} elevation the refraction angle increased in proportion to an increase in range.

The ray trace method of calculating refraction gave similar results to the curvature method but was more laborious to use. It could be used on all sightlines down to elevation angles near zero, but increasing care in the definition of the layer thickness was necessary. The curvature method became easier to use at zero elevation angles as a constant value for the refractive index or air temperature gradient could be used.

7. ACKNOWLEDGEMENTS

The author wishes to thank the Australian Department of Supply for permission to base this thesis on work arising in the course of the Author's normal duties at the Weapons Research Establishment, Salisbury.

APPENDIX I

FORTRAN PROGRAMME FOR COMPUTING TEMPERATURE INFORMATION

FLOW DIAGRAM

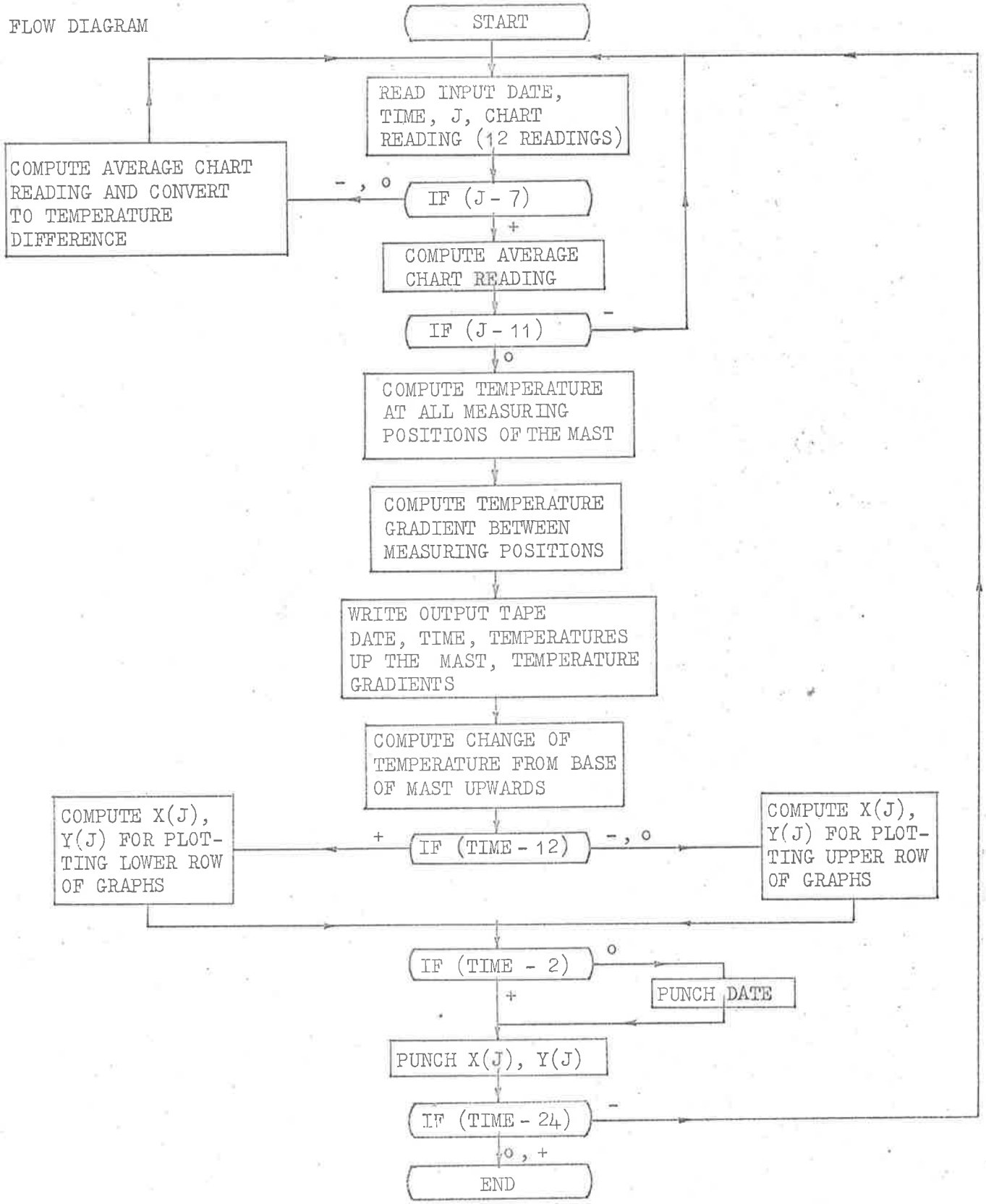

APPENDIX II

COMPUTATION OF REFRACTION ANGLE (CURVATURE METHOD)

FLOW DIAGRAM

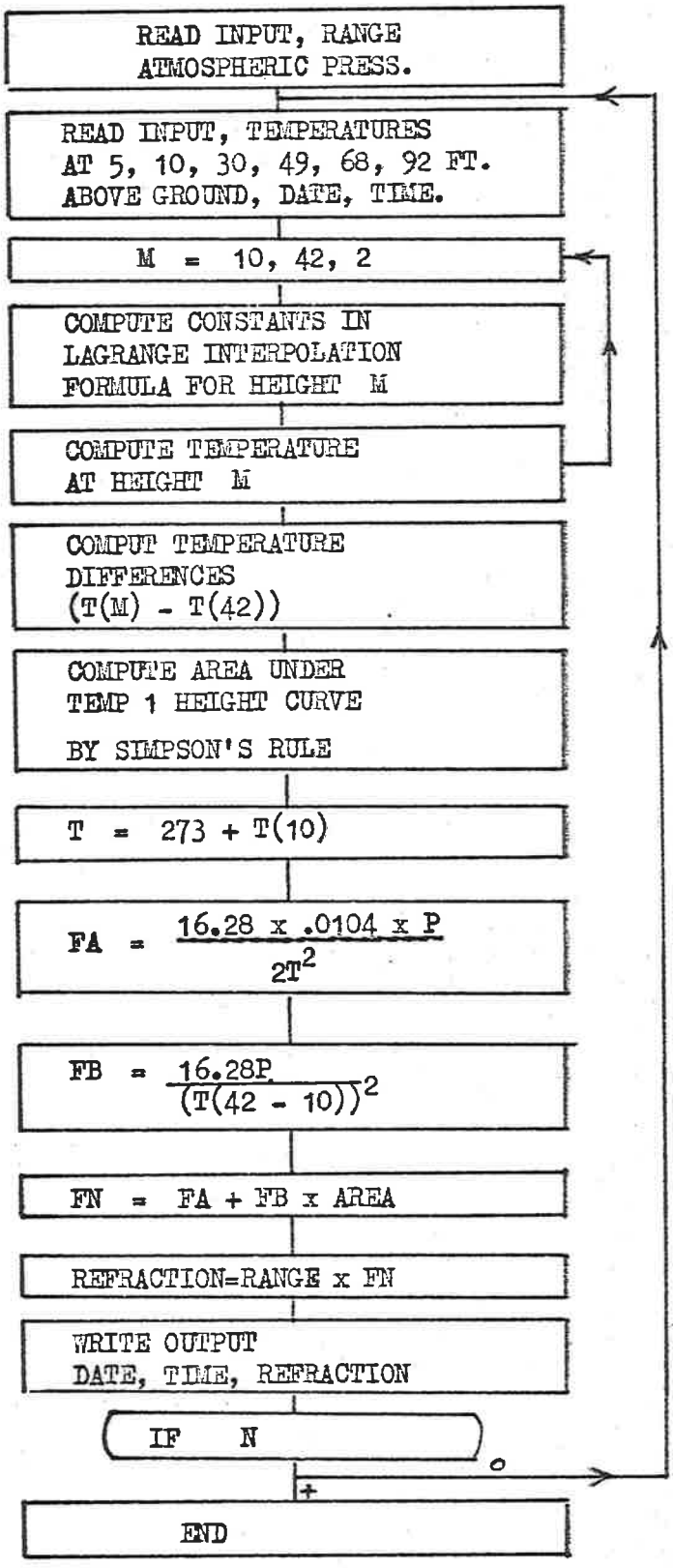

APPENDIX III

CALCULATION OF MONTHLY MEAN TEMPERATURE GRADIENT AND STANDARD DEVIATION

FLOW DIAGRAM

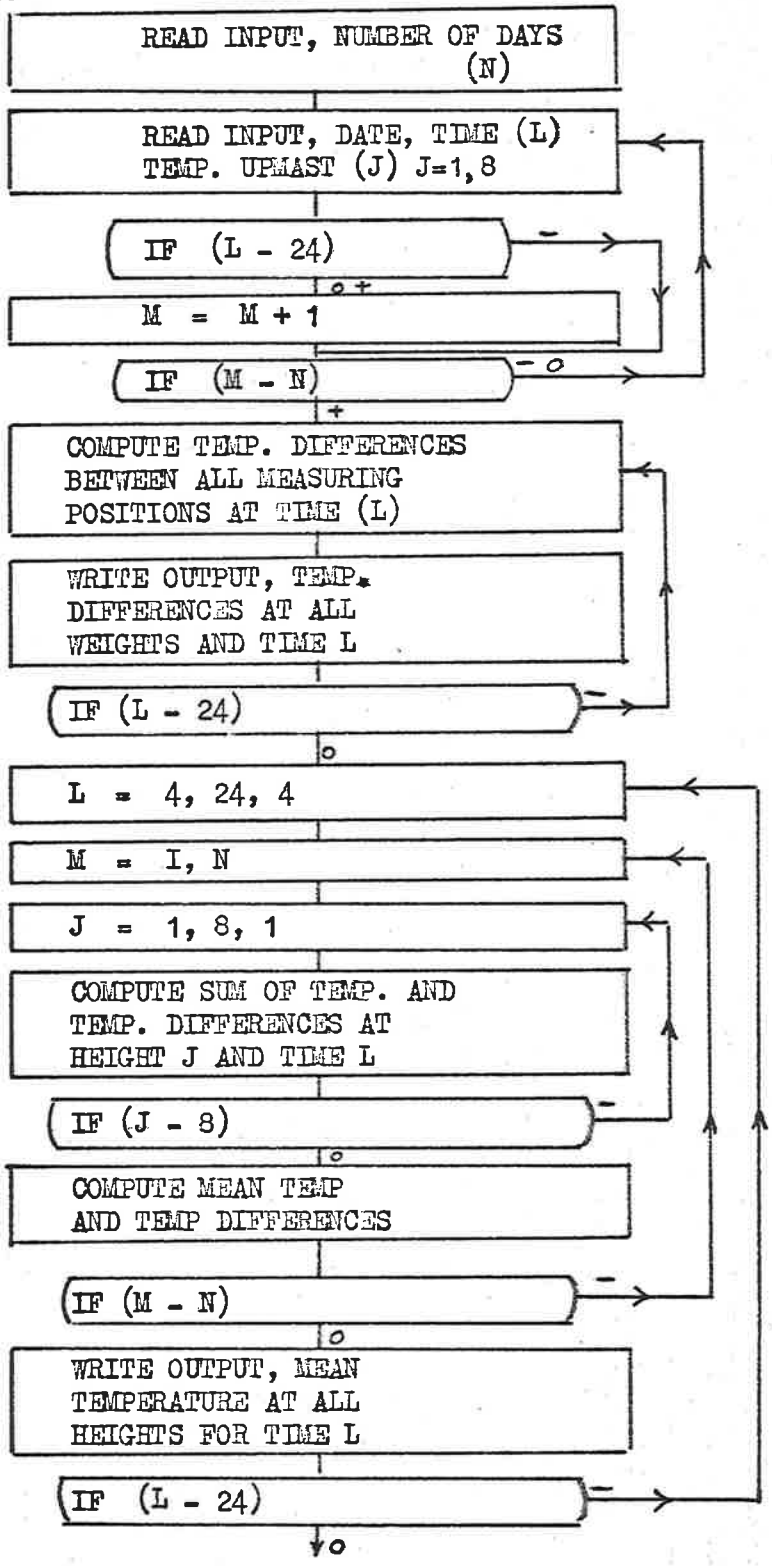

continued overleaf

APPENDIX III (continued)

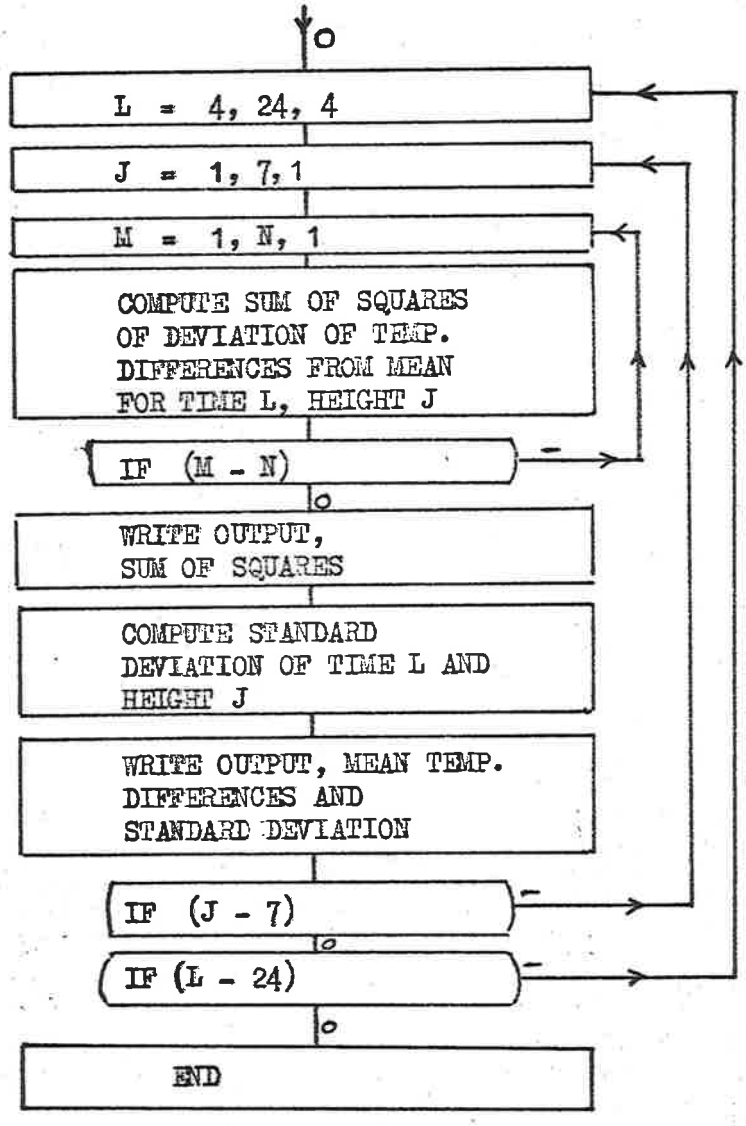

APPENDIX IV

RAY TRACE CALCULATION

FLOW DIAGRAM

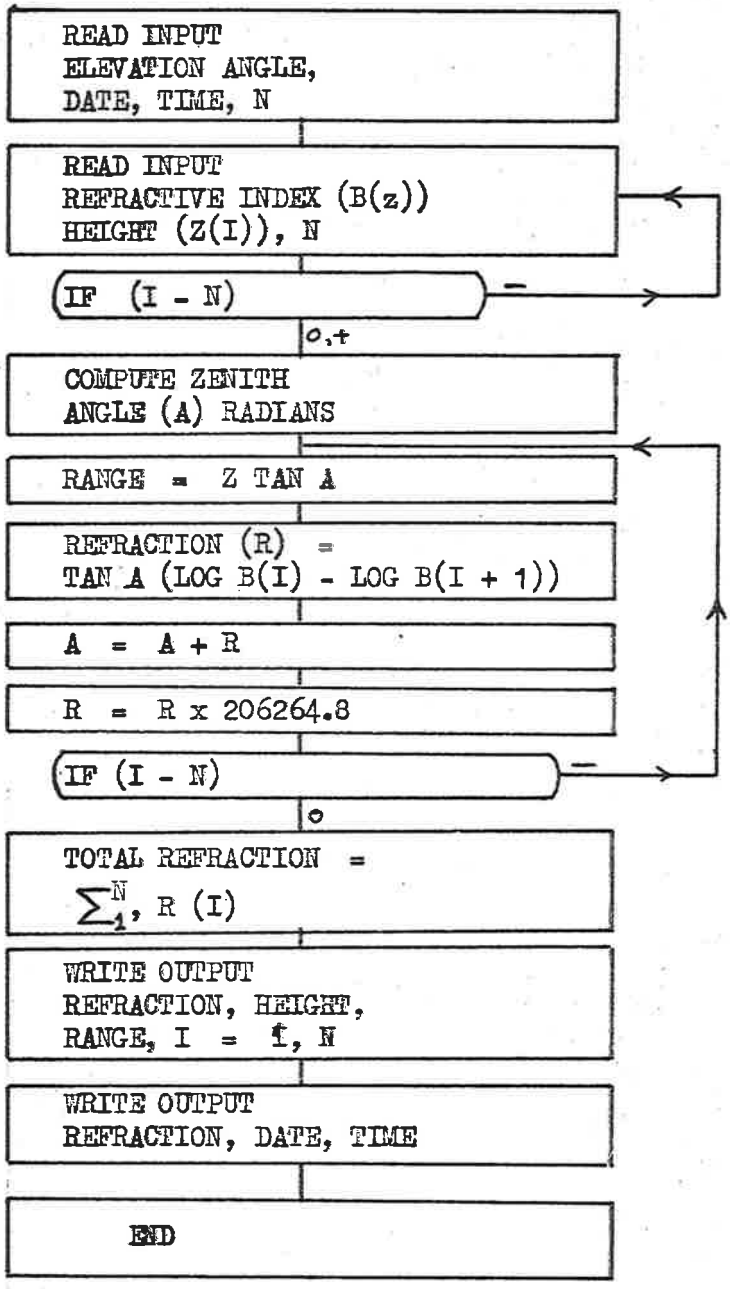

BIBLIOGRAPHY

No.	Author	Title
1.	Humphreys, W.J.	"Physics of the Air" (Dover Publications. New York 1964) Chapter V, PP 67 - 52.
2.	Geiger, R.	"The Climate Near the Ground". Havard University Press. 1950
3.	Coulman C.E. and Hall, D.N.B.	"Optical Effects of Thermal Structure in the Lower Atmosphere". Applied Optics Vol. 6 No. 3 March 1967
4.	Gladston & Dale	Philosophical Transactions of the Royal Society 1863, P317
5.	Bomford G.	Geodesy (Oxford University Press 1952) Chapter 4, section 4.05, PP 156 - 161
6.	Hanson F.	"Astronomical Refraction Errors for Optical Instrumentation - A Preliminary Report" White Sands Proving Ground. Tech. Memo. No. 104 October 1953.
7.	Angus-Leppan P.V.	"A Study of Refraction in the Lower Atmosphere". Survey Review Vol. 16 Nos. 120, 121, 122. 1963.
8.	Foulds, A.H. and Brock, R.H.	"Atmospheric refraction and its distortion of aerial photography." Photogrammetric Engineering Vol. XXX, No. 2 March 1964.

No.	Author	Title
9.	Longhurst, R.S.	"Geometrical & Physical Optics". (Longmans, Second impression 1960). Chapter XXI Section 21-2, PP 429-430.
10.	Raman, C.V.	"The Optics of Mirages" Current Science No. 8. August 1959.
11.	Little, R.E.	"Diurnal variations of the refraction error over a horizontal sightline." W.R.E. Technical Memorandum ISD 107 June 1966.
12.	Johnson, N.K. and Roberts, O.F.T.	"The measurement of the lapse rate of temperature by an optical method." Quarterly journal of the Royal Meteorological Society Vol. 51. PP 131-138 1925.
13.	Rogers, C.B.	"An experiment to gather seeing statistics' W.R.E. Tech. Memo. OID 60 July 1967.
14.	Rogers, C.B.	"A years survey of atmospheric seeing conditions at Woomera." W.R.E. Tech. Note ISD 40. July 1964.
15.	Johnson, N.K. and Heywood, A.S.P.	"An investigation of the lapse rate of temperature in the lowest hundred metres of the atmosphere". M.O.G.M. No. 77, HMSO 1938.

No.	Author	Title
16.	Flower, W.P.	"An investigation into the variation of the lapse rate of temperature at Ismailia, Egypt." M.O.G.M. No. 71, HMSO, 1937.
17.		"Analysis of Meteorological tower data April 1950 - March 1952". Brookhaven National Laboratory, BNL Report 461 (T-102) U.S. Atomic Energy Commission June 1957.
18.	Carnes, P.S.	"Temperature variations in the first 200 feet of the atmosphere in an arid region". ASMSA data report AD266802
19.	Angus-Leppan, P.V.	"A mathematical model for temperatures in the lower atmosphere and its applicatic in refraction calculations". Vienna March 1967.
20.	Kosters, W.	Interferenzdoppelprisma Fur Messzweeke," Reichspatentamt, Patentschrift NR 565211 (1931)
21.	Saunders, J.B.	"The Kosters Interferometer". Journal of Research of the National Bureau of Standards Vol 58, No. 1, January 1957.

No.	Author	Title
22.	Terrien, J.	"An Air Refractometer for Interference Length Metrology". Metrologia Vol. 1, No. 3 July 1965.
23.	Svensson, H.	"Some New Interferometric Techniques and Their Applications to Physico - Chemical Problems". Instruments and Measurements Conference Transactions, Stockholm, 1952.
24.	Saunders, J.B.	"Construction of a Kosters Double Image Prism". Journal of Research of the National Bureau of Standards Vol. 58, No. 1, January 1957.
25.	Saunders, J.B.	"Wave Front Shearing Prism Interferometer" Journal of Research of the National Bureau of Standards Vol. 68C, No. 3. September 1964.